MODELING OF A COMBINED ITM-POROUS OXYGEN TRANSPORT REACTOR: TOWARDS A SPATIALLY UNIFORM TEMPERATURE ITM

BY

SHAIK PERVEZ AHMED

A Thesis Presented to the

DEANSHIP OF GRADUATE STUDIES

KING FAHD UNIVERSITY OF PETROLEUM & MINERALS

DHAHRAN, SAUDI ARABIA

In Partial Fulfillment of the
Requirements for the Degree of

MASTER OF SCIENCE

In

MECHANICAL ENGINEERING

MAY 2012

KING FAHD UNIVERSITY OF PETROLEUM & MINERALS

DHAHRAN 31261, SAUDI ARABIA

DEANSHIP OF GRADUATE STUDIES

This thesis, written by Shaik Pervez Ahmed under the direction of his thesis advisor and approved by his thesis committee, has been presented to and accepted by the Dean of Graduate Studies, in partial fulfillment of the requirements for the degree of **MASTER OF SCIENCE in MECHANICAL ENGINEERING**.

Thesis Committee

Dr. Mohamed A. Habib (Advisor)

Dr. Rached Ben-Mansour (Member)

Dr. Hassan M. Badr (Member)

Dr. Amro M. Al- Qutub
Department Chairman

Dr. Salam A. Zummo
Dean of Graduate Studies

29/5/12
Date

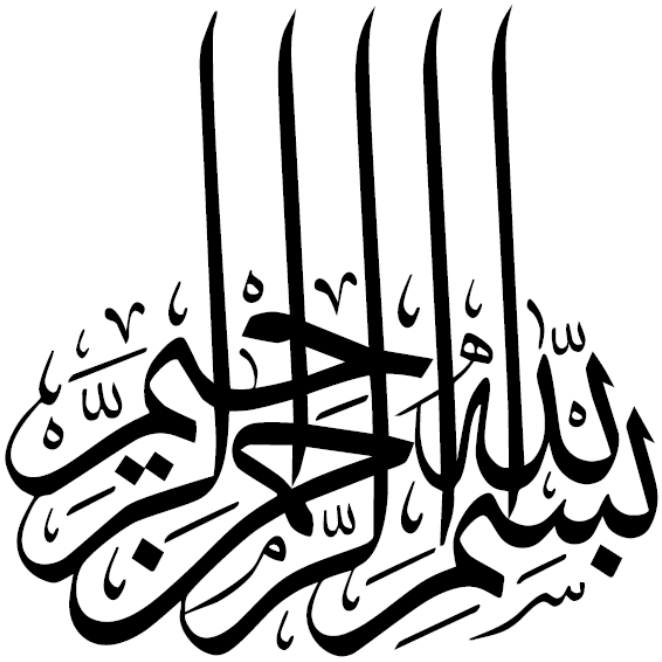

Dedicated to

My beloved parentsand sister for their duas and constant support and encouragement throughout my life

ACKNOWLEDGEMENT

"In the name of Allah, The Most Gracious and The Most Merciful"

All praise belongs to Almighty Allah (s.w.t.) for bestowing me with courage and perseverance to carry out this work sincerely. I thank Almighty Allah for giving me chance to do my M.S. successfully at King Fahd University of Petroleum and Minerals, Dhahran. I am happy to have had a chance to glorify His name in the sincerest way through this small accomplishment and ask Him to accept my efforts.

Acknowledgement is due to King Fahd University of Petroleum and Minerals for providing me financial support and good academic environment during the course of my M.S. Special thanks is also due to the Center of Clean Water and Clean Energy at MIT and KFUPM.

My deep gratitude and appreciation goes to my thesis advisor, my mentor Dr. MohamedA.Habib for his constant endeavor, guidance and motivation during the course of my study. His valuable and priceless suggestions made this work interesting and challenging for me. I also wish to express my deep appreciation to Dr.Rached Ben-Mansour and Dr. Hassan M.Badr for their help, guidance, and constant encouragement during my M.S.

I would also like to acknowledge all the Mechanical Engineering faculty members with whom I took courses during my M.S. who helped me a lot, guided me and encouraged me during my coursework and related research. I also owe thanks to all the graduate students and faculty with whom I interacted during my Masters program.

CONTENTS

LIST OF TABLES

LIST OF FIGURES

THESIS ABSTRACT (ENGLISH)

NAME: SHAIK PERVEZ AHMED

TITLE: MODELING OF A COMBINED ITM-POROUS OXYGEN TRANSPORT REACTOR: TOWARDS A SPATIALLY UNIFORM TEMPERATURE

MAJOR: MECHANICAL ENGINEERING

DATE: MAY2012

Almost all the fossil fuels, on combustion, emit CO_2 which is considered to be a greenhouse gas. Developing new power generation cycles that enables carbon-dioxide capture and sequestration are the limelight of current research. Present absorption technologies for carbon capture are energy-intensive and expensive. An alternative to these absorption technologies would be to combust fossil fuels in pure oxygen, whereinthe flue gas stream will have a much higher concentration of CO_2, reducing or eliminating the need for costly CO_2 capture. Oxy-fuel combustion is considered to be one of the new emerging technologiescapable of capturing and sequestrating CO_2. In oxy-fuel combustion, the fossil fuel is burned in an environment of pure oxygen instead of air and the flue gas mainly consists of CO_2 and H_2O that can be easily separated through condensation processes. Ion Transport Membranes (ITMs) offer promising oxygen production technology with high purity (upto 99%) without adversely affecting the efficiency of the oxy-fired plants. The separation rate of such ITMs can be increased by replacing the conventional inert sweep gas with a reactant/diluent mixture (e.g. CO_2, CH_4) as this reduces the permeate partial pressure on the permeate side of the membrane, which, along with the temperature, governs the permeation flux. The significant limitation of this approach is that an uncontrolled, exothermic consumption of the permeated specie, can lead to membrane damage, and thus limits the potential of ITMs using reactive sweep gases (i.e. ITM reactors). By using a multichannel ITM reactor, it is proposed to operate the ITM reactor at, or near to isothermal conditions (i.e. a spatially uniform temperature). This may be achieved by introducing a reactant

into the permeate stream uniformly across the entire ITM reactor length from an adjacent channel with porous walls.

The present work is aimed at predicting the oxy-combustion characteristics in an oxygen transport reactor with the objective of developing a nearly isothermal reactor. This is achieved by separation of oxygen from air through Ion Transport Membranes (ITM's) and by using a porous membrane, to achieve uniform stoichiometric ratio of fuel/O_2 in order to have uniform combustion all along the length of the membrane. A two-dimensional, computational fluid dynamics (CFD) model is solved to study the combustion characteristics. The simulations are based on the numerical solution of the conservation of mass, momentum, energy and species transport equations of two dimensional flows. For the CFD calculations, the commercial solver FLUENT has been used. The mass transfer of oxygen through the membrane is modeled by user defined functions (UDF's) and the mass transfer of fuel through the porous layer is modeled using a 1D porous jump model. The membrane (ITM) is modeled as a selective layer, which allows the permeation of oxygen as a function of temperature and the difference of partial pressures of oxygen in the feed side and the permeate side. The flux through the porous layer is a function of permeability and thickness of the medium in addition to the pressure difference. The models used have been validated against the experimental results found in the literature and are found to be in good agreement. Influence on the performance of oxygen separation through the ITM has been studied by varying the flow conditions at the permeate side. Results show that for a constant mass flow rate of fuel mixture, the permeation rate of oxygen through ITM increases with increase in CH_4/CO_2 ratio. It was found that the oxygen permeation rate increased by approximately 3 times with reaction taking place on the permeate side compared to the separation only case. An improved uniform temperature distribution along the membrane was obtained by the combined ITM-porous oxygen transport reactor.

MASTER OF SCIENCE DEGREE

KING FAHD UNIVERSITY OF PETROLEUM & MINERALS

Dhahran, Saudi Arabia

THESIS ABSTRACT (ARABIC)

اسم الطالب الكامل : شيخ برويز أحمد

عنوان الدراسة : تصميم مفاعل مكون من غشاء الانتقال الأيوني (ITM) وغشاء مسامي (Porous) لفصل الأوكسجين وتحقيقتوزيع حراري منتظم

التخصص الدراسي: الهندسة الميكانيكية

التاريخ: مايو 2012

ينبعث غاز ثاني أكسيد الكربون من احتراق جميع أنواع الوقود الأحفوري والذي يعتبر من الغازات الدفيئة. في هذا البحث سيتم تسليط الضوء على تطوير دورات توليد الطاقة بحيث يتم امتصاص غاز ثاني أكسيد الكربون والحد من انبعاثه. تعتبر التقنيات الحالية لامتصاص هذا الغاز مكلفة ومستهلكة للطاقة بشكل كبير. سيكون بديلا لهذه التقنيات الممتصة لغاز ثاني أكسيد الكربون هو حرق الوقود الأحفوري في الأوكسجين النقي ، بحيث أنه في تيار غاز الاحتراق يكون تركيز ثاني أكسيد الكربون عاليا وبالتالي حرق الوقود في أوكسجين نقي يقلل أو يلغي الحاجة إلى استخدام تقنيات مكلفة لالتقاط غاز ثاني أكسيد الكربون. إن تقنية احتراق الوقود في الأوكسجين تعتبر واحدة من التقنيات الناشئة والمستخدمة في امتصاص وتحجيم غاز ثاني أكسيد الكربون. في مثل هذا النوع من الاحتراق يتم احتراق الوقود الأحفوري في الأوكسجين النقي بدلا من الهواء العادي بالإضافة إلى أن غازات الاحتراق عادة مكونة من غاز ثاني أكسيد الكربون وجزيئات الماء والتي يمكن فصلها بسهولة باستخدام عمليات التبريد. تقدم أغشية نقل الأوكسجين (ITM) تقنية واعدة لإنتاج الأوكسجين بنسبة نقاء عالية تصل إلى 99% دون أن تؤثر سلبا على كفاءة محطات احتراق الأوكسجين. يمكن زيادة معدل فصل هذه التقنية (ITM) باستبدال غاز الاكتساح الخامل بخليط متفاعل ومخفف مثل (غاز ثاني أكسيد الكربون ، غاز الميثان) وهذه تقلل الضغط الجزئي على جانب الغشاء. من أهم مشاكل هذه المفاعلات هو الاستخدام الغير منضبط للوقود والذي يؤدي إلى عدم انتظام درجة حرارة الغشاء مما قد يؤدي إلى تلف الغشاء. في هذا البحث اقترحنا أن نستخدم مفاعل أغشية الانتقال الأيونية (ITM) بقنوات متعددة لنحصل على درجة حرارة متساوية تقريبا على طول الغشاء وذلك يتحقق بتوزيع غاز الأوكسجين باستخدام (ITM) إلى قناة الاحتراق ، و بتوزيع غاز الميثان عن طريق الغشاء المسامي إلى قناة الاحتراق أيضا مما يؤدي إلى احتراق متوزع على طول القناة فتصبح درجة الحرارة على طول الغشاء ثابتة.

الهدف الرئيسي من هذه الرسالة هو التمكن من التنبؤ بخصائص الاحتراق الأوكسجيني في مفاعل نقل أوكسجين بهدف جعل المفاعل ذو درجة حرارة ثابتة تقريبا وذلك من خلال فصل الأوكسجين من الهواء باستخدام أغشية

الانتقال الأيونية (ITM) وباستخدام أغشية مسامية لتحقيق نسبة موحدة القياس من الغاز إلى الأوكسجين من أجل أن يكون الاحتراق متوزع بالتساوي على طول الغشاء كاملاً. تم استخدام نموذج ثنائي الأبعاد لدراسة ديناميكا الموائع الحسابية (CFD) في دراسة خصائص الاحتراق. وتستند عمليات المحاكاة على الحل العددي لمعادلات حفظ الكتلة، والقوة الدافعة، والطاقة، ومعادلة الانتقال المتعدد. لأداء حسابات (CFD)تم استخدم البرنامج التجاري FLUENT. تم استخدام نموذج معرف إضافي (UD F) لحساب كتلة الأوكسجين المنتقلة من خلال غشاء (ITM) ونموذج مبني بداخل البرنامج (1D) لحساب كتلة غاز الميثان المنتقل خلال الغشاء المسامي .تم تصميم غشاء (ITM) على شكل طبقة انتقائية على أنها تسمح للأوكسجين بالانتقال من خلالها متأثرة بدرجة الحرارة وبالضغط الجزئي للأوكسجين في كلا الجانبين (الجانب المنتقل الأوكسجين منه والجانب المنتقل إليه)، أما بالنسبة لتدفق غاز الميثان من خلال الغشاء المسامي فهو يتأثر بمسامية الغشاء وبسماكة الغشاء المسامي. تم التحقق من النموذج المستخدم في هذا البحث مع تجربة سابقة تم أدائها في نفس مجال البحث وتم الحصول على اتفاق جيد في النتائج. تمت دراسة أداء غشاء (ITM) في فصل الأوكسجين عن الهواء بواسطة تغيير ظروف التدفق في جانب الاحتراق. توضح النتائج أنه عند تثبيت مستوى تدفق غاز الميثان يزداد معدل تغلغل الأوكسجين من خلال غشاء (ITM) بازدياد نسبة غاز الميثان إلى ثاني أكسيد الكربون وهذه الزيادة تصل إلى ثلاثة أضعاف عند الاحتراق مقارنة بالتغلغل دون حدوث هذا الاحتراق. باستخدام غشاء (ITM) مع الغشاء المسامي تم الحصول على توزيع منتظم للحرارة على طول مفاعل انتقال الأكسجين.

درجة الماجستير في العلوم

جامعة الملك فهد للبترول والمعادن

الظهران – المملكة العربية السعودية

مايو 2012 – جمادى الثاني 1433هـ

CHAPTER 1

INTRODUCTION

1.1 Research Background:

Most of the heating systemsrequire combustion of hydrocarbon fuels that emits CO_2 which is considered a greenhouse gas. Renewable energies are carbon neutral and so present a favorable solution to the problem of greenhouse gas emissions. Unfortunately, renewable energy technologies are currently not mature enough in comparison to fossil fuel based technologies. Much work is required before such energy sources can produce a major portion of our energy.

Fossil fuels will continue for decades to be the source of fuel to meet global energy demands [1]. Energy production from fossil fuel combustion results in the emission of greenhouse gases, the dominant contributor being CO_2 [2].These anthropogenic carbon dioxide (CO_2) emissions are contributing to global climate change. Therefore, it is critical to develop technologies to mitigate this problem [3]. Carbon dioxide is one of the species, whose emission cannot be avoided during combustion of the fuel containing carbon. In order to achieve storage of CO_2, this specie has to be separated from the flue gases,

whichcontain mainly nitrogen. Such process is very expensive. Carbon capture and sequestration (CCS) means capturing $CO_2$and trapping it away from the atmosphere. There are many methods of sequestering CO_2. One of the important methods is Enhanced Oil Recovery (EOR), which involves injecting CO_2 into partially depleted oil wells to increase the pressure and produce more oil. This is currently a common practice in many oil fields.

Many studies are being undertaken on sequestration, and many numerical simulations have been developed and tested [4, 5].Among the proposed methods of CO_2 capture, oxy-fuel combustion technology provides a promising option, which is applicable to power generation systems. This technology is based on combustion with pure oxygen (O_2) instead of air, resulting in a flue gas that consists mainly of CO_2 and water (H_2O), the latter can be separated easily via condensation, while removing other contaminants leaving pure CO_2 for storage. However, fuel combustion in pure O_2 results in intolerably high combustion temperatures. In order to provide the dilution effect of the absent nitrogen (N_2) and to moderate the furnace/combustor temperatures, part of the flue gas is recycled back into the combustion chamber. On the other hand an efficient source of O_2 is required to make oxy-combustion a competitive CO_2 capture technology. Conventional O_2 production utilizing the cryogenic distillation process is energetically expensive.

As an alternative to traditional air separation methods to provide on-site oxygen, Ion Transport Membranes (ITMs) can selectively transport oxygen at a particular temperature range and facilitate oxy-fuel combustion without an external oxygen supply system.The

oxygen partial pressure ratio across the membrane provides the driving force for the separation process. If the permeate can be consumed by a useful reaction, the partial pressure of permeate is reduced and the permeate flux can be increased. Integrating these membranes with combustion systems, such as boiler furnace can provide the requisite high temperature environment and many other advantages. Ceramic membranes made from mixed ion-electronic conducting oxides have received increasing attention because of their potential to mitigate the cost of O_2 production, thus helping to promote these clean energy technologies. Some effort has also been expended in using these membranes to improve the performance of the O_2 separation processes by combining air separation and high-temperature oxidation into a single chamber [6].

The development of mixed-ionic electronic-conducting materials, in particular with the perovskite material system such as LSCF and BSCF, has shown large enhancement in O_2 permeation flux and catalytic combustion. Next generation ITMs will require significantly higher permeation flux at reduced operating temperatures to lower the cost of the technology and increase the probability of commercialization success. The successful development of these new approaches for ITMs will make commercial O_2 separation systems a reality[6].

Oxy-fuel combustion, particularly using an integrated oxygen ion transport membrane (ITM), is a thermodynamically attractive concept that seeks to mitigate the penalties associated with CO_2 capture from power plants. Oxygen separation in an ITM system consists of many distinct physical processes, ranging from complex electrochemical and

thermo-chemical reactions, to conventional heat and mass transfer. The dependence of ITM performance on power cycle operating conditions and system integration schemes must be captured in order to conduct meaningful process flow and optimization studies where multiple degrees of freedom are considered[7].

1.2 Fundamentals of Hydrocarbon Combustion:

The kinetic mechanisms used to model hydrocarbon combustion are generally composed of a large number of elementary reactions in which the initial fuel and oxidizer combine to form the final products. The rates in which reactions proceed are primarily dictated by collisions of two molecules that may have the capability to react. Therefore, the most common elementary reactions used are bimolecular in which two species collide and react to form two new species. To illustrate, consider an arbitrary bimolecular second order reaction

$$A + B \rightarrow C + D \tag{1}$$

The rate at which such a reaction proceeds is proportional to the concentration of the reactant species,

$$\frac{d[A]}{dt} = -k[A][B] \tag{2}$$

The rate constant k is a function of temperature T and is the parameter used to describe each elementary reaction composing the entire kinetic mechanism. A reaction will only take place, however, if the colliding molecules possess an adequate amount of energy

called the activation energy E_A. Kinetic theory shows that the fraction of all collisions that possess energy greater than E_A is given by the Boltzmann factor

$$\exp\left(\frac{-E_A}{RT}\right) \tag{3}$$

Determination of reaction rates also requires that the frequency of molecular collisions be taken into account in the form of a pre-exponential factor *A*. The rate constant *k* is then typically expressed in a modified Arrhenius form as

$$k = AT^b \exp\left(\frac{-E_A}{RT}\right) \tag{4}$$

where *A*, *b*, and E_A are parameters determined experimentally and *R* is the universal gas constant. The exponent *b* becomes particularly important in systems where temperatures vary widely. Mechanism construction is accomplished by including all elementary reactions believed to contribute either directly or indirectly to the formation of products.

Most combustion processes are governed by chain reactions initiated via the production of unstable radicals from the dissociation of one of the reacting species. The radicals then initiate a relatively fast chain of steps reacting with other molecules. A simple chain propagating reaction involves the production of one radical for each consumed, however, in chain branching reactions two or more radicals are generated from the consumption of one. This leads to a rapid buildup of radical concentration and hence a very fast overall reaction explosive in character. The termination of the chain occurs when the reaction of two radicals or a radical reacting with another molecule form a stable species.

Termination can also be achieved with the formation of a radical with lower activity that cannot propagate the chain.

The oxidation of saturated hydrocarbons of the form C_nH_{2n+2} has been described by Fristrom and Westenberg [8]to occur in two thermal zones. In the primary reaction zone, fuel molecules are attacked and reduced to CO, H_2, H_2O, and various radicals (H, O, OH). It is also here that other intermediates are formed. In the secondary reaction zone, oxidation of CO and H_2 occurs. They suggest that in oxygen-rich saturated hydrocarbon flames, lower order hydrocarbons form according to equation(5)

$$OH + C_nH_{2n+2} \rightarrow H_2O + C_nH_{2n+1} \Rightarrow C_{n-1}H_{2n-2} + CH_3 \tag{5}$$

while in fuel-rich flames

$$H + C_nH_{2n+2} \rightarrow H_2 + C_nH_{2n+1} \tag{6}$$

equation(6) is the scheme. These characteristics have been confirmed by Dryer and westbrook[9] via high-temperature flow reactor studies which also revealed that the fuel is consumed prior to the majority of the energy release. This evidence led Glassman [10] to characterize the general oxidation of hydrocarbons into three steps: (1) following ignition, the primary fuel disappears with little or no energy release producing unsaturated hydrocarbons and H_2 with some hydrogen being oxidized to water; (2) the unsaturated hydrocarbons are further oxidized to CO and H_2, and essentially all hydrogen is simultaneously oxidized to water; and (3) finally, most of the heat from the overall reaction is released from the oxidization of CO to CO_2. For a more detailed discussion on

hydrocarbon oxidation, including characteristics unique to methane, higher order hydrocarbons, and alcohols, the reader is referred to Glassman [10].

1.3 Technologies: Carbon Capture and Sequestration (CCS):

Current CCS power cycles have efficiencies typically on the order of 35% [2], where the penalty incurred is in the range of 7-11 percentage points [11]. There are three promising methods for capturing CO_2 for low-emission coal-fired power generation. Figure 1 shows the block diagram of three different carbon capture technologies: post-combustion capture, pre-combustion capture, and oxy-fuel combustion.Post-combustion capture is the most conventional method, and it uses chemical absorption/desorption processes with amines to scrub CO_2 directly from the exhaust [2]. Since post-combustion capture units are installed as “add-on” units at the exit of the flue gas stack, the upstream power plant does not require significant modification. However, post-combustion capture is energy-intensive and expensive due to the low CO_2 concentration typical of hydrocarbon oxidation in air [12]. Pre-combustion capture is an alternative CCS technology that essentially removes carbon from the fuel prior to combustion via chemical processes such as steam reforming, partial oxidation, or auto-thermal reforming, and transfers part of the chemical bond energy stored in the original hydrocarbon into pure hydrogen [13]. This method requires complex process equipment and incurs exergetic losses for each conversion into another chemical form, thus making it both economically and thermodynamically expensive [2].Oxy-combustion is a promising CCS technology that has the potential to significantly reduce the penalty associated with the carbon dioxide separation process.

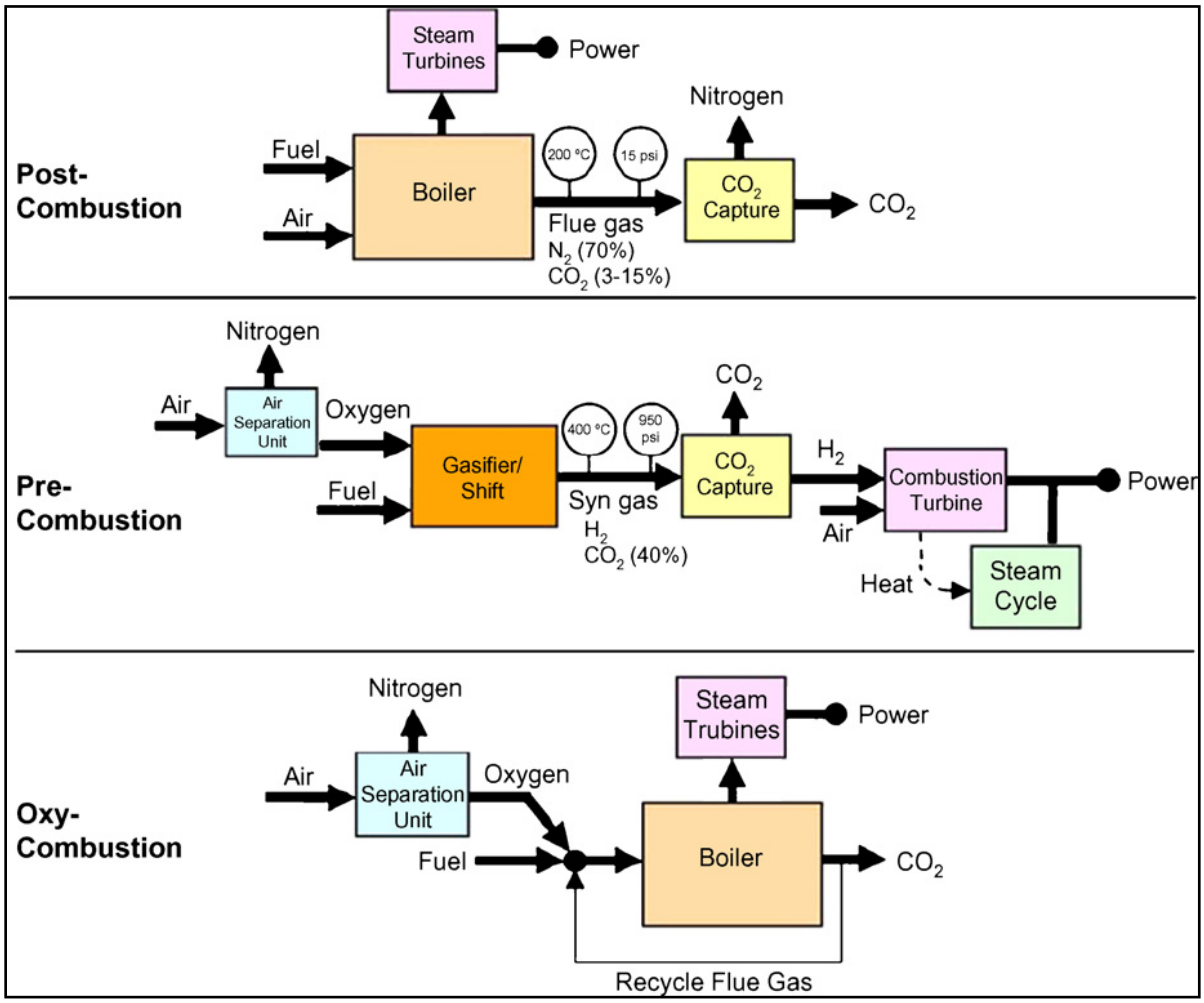

Figure 1: Block diagram illustrating the three systems (Ref : [3]**)**

In post-combustion capture, CO_2 is chemically washed out of flue gas. In pre-combustion capture, coal is first transformed into a gas called syngas; CO_2 is then removed from the syngas prior to combustion. In oxy-fuel combustion, coal is burned in pure oxygen instead of air, which results in a significantly higher concentration of CO_2 in the flue gas. The flue gas must then be scrubbed of its remaining components such as oxygen, sulfur dioxide, and nitrous oxides. Post-combustion capture is the only capture method that can be retrofitted onto existing power plants without significant modifications.

1.3.1 Post-combustion capture: (CO_2scrubbing)

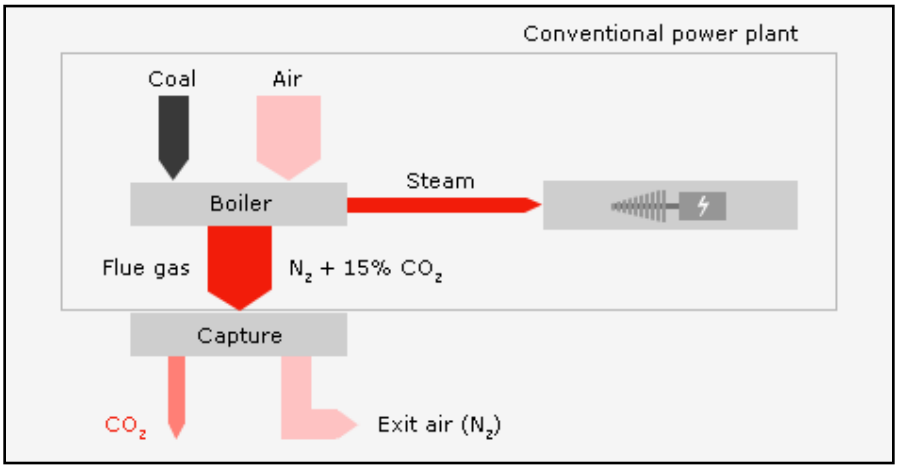

Figure 2: Post combustion capture cycle(Ref: http://www.eon.com)

Figure 2 shows the post combustion capture cycle. CO_2 accounts for about 15 percent, by volume, of the flue gas of a coal-fired power plant. To capture it, conventional flue-gas purification equipment, which has been in use for decades, is enhanced by an additional process in which the flue gas column is exposed to a solvent that absorbs CO_2. The CO_2-saturated solvent is piped into a second fractionating column and heated with steam until the CO_2 is separated and washed out. The regenerated solvent is recycled into the carbon-capture process, resulting in a closed scrubbing cycle.

The decisive advantage of post-combustion over other capture methods is that it can be easily retrofitted onto existing power plants. One prerequisite, of course, is that plants have enough room on site to install capture equipment.

1.3.2 Pre-combustion capture: (Turning coal into clean hydrogen)

Figure 3 shows the pre-combustion capture cycle. As the name suggests, pre-combustion capture involves capturing CO_2 before a fuel is burned. The first step of this process is to separate air into nitrogen and oxygen. The second step is to combust coal at high temperatures using insufficient oxygen and steam. This step, called coal gasification, creates syngas, which consists mainly of CO_2, carbon monoxide (CO), and hydrogen (H_2).

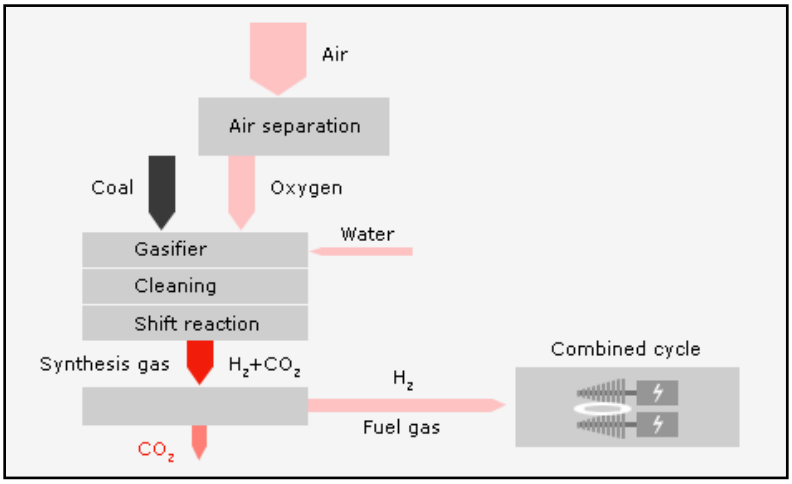

Figure 3: Pre-combustion capture cycle(Ref: http://www.eon.com)

Next, a catalytic converter uses steam to transform CO into a mixture of CO_2 and H_2. The CO_2 is then washed out of this gas mixture and pressurized for transport to a storage facility. The hydrogen that remains can be used to generate electricity in a combined-cycle gas turbine (CCGT), which operates at a high level of thermal efficiency.

1.3.3 Oxy-fuel combustion: (Using pure oxygen to produce pure CO_2)

Figure 4 shows the oxy-fuel combustion cycle. The oxy-fuel combustion concept, along with the pre-combustion and post-combustion capture options, is one of the main options

developed towards the implementation of CO_2 Capture and Storage (CCS) technologies for fossil fuel power plants. The main concept of the oxy-fuel combustion mode is the combustion air substitution with pure oxygen, supplied by an Air Separation Unit (ASU). The produced flue gas has a high CO_2 content and does not require extensive treatment, due to its mass reduction (owed to N_2 absence), before transportation and storage in appropriate geological formations.

In the oxy-fuel process, a fuel like coal is combusted with pure oxygen instead of air, with exhaust gas added to regulate the combustion temperature. The resulting flue gas consists of almost pure CO_2 along with some steam. Cooling the flue gas enables the CO_2 to be separated from the steam, which condenses to water at low temperatures. The CO_2-dense flue gas is then scrubbed using conventional equipment, which removes the minimal amounts of dust, sulfur dioxide, and nitrogen oxides it contains. The success of the oxy-fuel method depends to a considerable degree on determining how thoroughly these gases must be scrubbed from the CO_2 before it can be safely transported and stored.

It takes a lot of energy to produce the pure oxygen with which the fuel is combusted, but comparatively little to scrub the CO_2 after combustion. Another challenge is to improve control of the combustion process in the boiler. Innovative solutions to meet these challenges will be important milestones towards rolling out the oxy-fuel process on a utility scale.

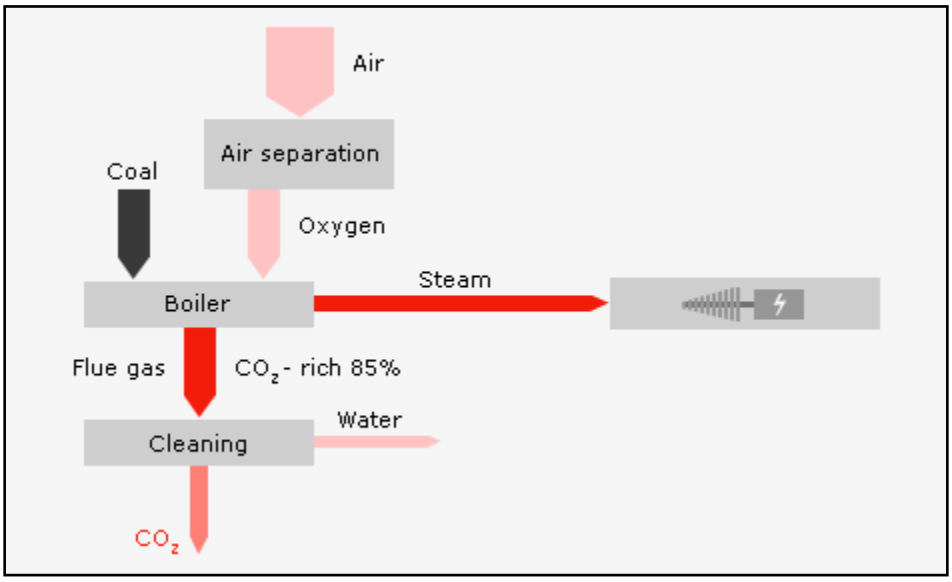

Figure 4: Oxy-fuel combustion cycle(Ref: http://www.eon.com)

1.3.4 Gas separation using membranes (CCS technologies):

Generally three types of membranes are currently available for gas separation applications and are considered for CO_2 capture:

- Organic porous polymer membranes.
- Inorganic porous membranes, amorphous or crystalline.
- Inorganic dense membranes, metallic or ceramic.

Organic polymeric membranes are excellent candidate for CO_2 separation from N_2 for the post-combustion process. These membranes can even separate the H_2/CO_2 in pre-combustion process but they have low thermal stability and are not suitable for high temperature and pressure applications [14]. On the other hand dense inorganic membranes are good in H_2/CO_2 and O_2/N_2 separation. Oxygen ion transport membranes (OTMs) are dense ceramic membranes which allow oxygen and only oxygen to pass

through the membrane. They have been the subject of much research in the past decade, and new materials are continually being created. They could be used to create a mixture of O_2 and another gas, e.g. CO_2, if air were on the feed side of the membrane and CO_2 on the permeate side. Alternatively, air could pass over the feed side, a mixture of fuel and CO_2 could pass over the permeate side, and combustion could take place in a chamber made of ceramic.

1.3.5 Mixed ionic and electronic conducting (MIEC) membranes for O_2/N_2separation

MIEC membranes are regarded as clean, cost effective technology and are good in separating oxygen from air. These membranes are dense in nature with no detectable pores which means that the molecular oxygen cannot pass through these membranes. These membranes have the capability of separating oxygen from air because of the oxygen vacancies in the crystal lattice which is created by doping of the material. Oxygen ions are transported from one side of the membrane to other by a mechanism called hopping. This mechanism is activated only if the oxygen anions have enough thermal energy to overcome the energy barrier to hop from one side of the crystal lattice to other which means that, for the membrane to operate high temperatures are required. The typical range for the membranes to activate the mechanism of oxygen transport is 700 ^{0}C to 1000 ^{0}C [15]. There will be a counter balancing electron transport to maintain electro-neutrality in the material and there is no need of any potential voltage for the oxygen transport. ITMs are composed of specific combinations of inorganic compounds with a particular crystal lattice structure such as the perovskite or fluorite configuration [16].

Perovskite membranes generally have a higher overall rate of oxygen flow through the membrane (oxygen flux) than fluorite membranes, but have a lower maximum operating temperature. ITM systems operate at relatively high temperatures, e.g., above 1000 K [17], and rely on a difference in O_2 chemical potential to drive the separation process [18]. However, other key physical aspects such as ion surface exchange electrochemical reactions, molecular diffusion through porous layers, and convective-diffusive mass transfer must be considered [19]. Most of the oxygen flux data are obtained under mixed-control of surface exchange kinetics and ion diffusion. BSCF, a relatively newer membrane material, appears to have the highest performance for separation-only applications [20], while LSGF-BSGF has been cited as one of the more promising for reactive applications due to its excellent stability under reducing conditions [21].

1.4 Objectives of Research:

The objectives of this research are

1. To develop a computational model of the isothermal ITM reactorcomprising of (a) ITM sub-model (for permeation of oxygen) (b) porous membrane sub-model (for uniform fuel injection) and flow, heat transfer and combustion sub-models for the purpose of achieving uniform combustion (temperature distribution) all along the length of the membrane (ITM).

2. To validatethe ITM and porous membrane sub-modelsusing the experimental data available from previous research.

3. To optimize the isothermal reactor model through parametric simulations and analyses for (a) Permeation (separation only) and

(b) Combustion operating modes.

4. To study the combustion characteristics in the model developed.

1.5 Thesis Outline:

The objective of this thesis is to design a novel methodology to study the transportation (permeation) of oxygen across the membrane based on the partial pressure of oxygen (across the membrane) and the activation energy required to ionize the oxygen molecules and to use the porous model in order to achieve uniform combustion all along the length of the membrane.

This thesis contains six chapters.

Chapter 1 introduces the fundamentals of hydrocarbon combustion. It also includes the subject of different combustion and sequestration techniques. It also discusses the challenges related to these techniques. The first chapter then discusses the possible solutions and defines the objectives of this thesis work.

Chapter 2 reviews the literature related to different perovskite membranes and porous membranes. Summary of literature review presents a gist of the previous work done in the area of ion transport membranes especially related to LSCF and BSCF membranes. It also discusses the different cycles incorporating ion transport membranes.

Chapter 3 describes the problem statement and methodology for modeling ITM's and porous membranes. It mentions the equations that are used for modeling ITM's and porous membranes.

Chapter 4 describes the numerical modeling of the oxygen transport reactor for the present study. It also presents the validation results for the models being used.

Chapter 5 includes the results and discussions of the oxygen transport reactor for the present study.

Chapter 6 includes the conclusions of the study and also presents the directions in which this study can be extended in future.

CHAPTER 2

LITERATURE REVIEW

2.1 Oxy-fuel Processes:

In oxy-fuel combustion process, the fuel (coal, methane, etc) is burnt in an oxygen-rich atmosphere to produce CO_2 enriched flue gases. The composition of the flue gases will be relatively clean comparedwith normal air-fuel combustion. This technology has been used in the glass and metal manufacturing industries. From the technical side, the oxy-fuel process can be applied to the existing coal-fired power plants and new one with only oxy-fuel combustion chambers can be built [22]. The new technology of membrane separation and combustion is not yet fully matured for application in large scale power production units. However, the efforts put by the researchers [23-26] show large potential to implement this membrane integration with oxy-rich fuel combustion. The significant scope is present to see several aspects of oxy-fuel process for the use in coal-fired power plants, e.g. boiler design, combustion reactions and chemistry of combustion, sealing issues for oxygen transport reactor (OTR) which has to be investigated to make this technology more viable. The idea of this oxy-fuel combustion can be extended to natural gas combustion or syngas production withmembrane integration in combustion chamber.

More work has to be done for clarification of combustion issues such as reaction kinetics, ignition in case of coal-fired, flame stability, sealing of membrane and the activation energy required, making these OTR active for separation of oxygen from air.

2.1.1 Oxy-fuel combustion:

The combustion oxidizer generally used for the oxy-fuel process should have a purity of more than 95% and rest being nitrogen [27, 28]. In coal-fired combustion there has to be excess oxygen supplied to the boiler which is necessary to obtain a stoichiometric and homogenous combustion. In the flue gas along with CO_2 there will be H_2O vapors with small concentration of NO_X, SO_X, etc. The boiler flue gas is sent to a clean-up process to remove acid gases and particulates. Then it is gain treated for NO_X removal in deNO_X treatment unit, this NO_X generation due to the air-leakage in boiler which accounts to be 8%-15% [28]. DeSO_X treatment is also necessary for the removal of sulphur inside the boiler [29, 30]. After complete dehumidification of the flue gas, it is estimated that we have high purity CO_2 ranging 85%-95% [31, 32] ready for compression and storage.

If the combustion is done with natural gas (mainly methane) with integration of oxygen transport reactor then the process of DeNO_X and DeSO_X treating can be avoided since with membranes we have very high purity of oxygen and the leakage is also negligible compared to boiler reactor. Since the oxygen flames gives higher temperatures (due to high heating value) which has to be controlled, because of the material melting temperature constraints, around 2/3 of the flue gas needs to be recycled [22]. The missing element of N_2 is replaced by recycled CO_2 which will carry away the heat and will

increase the concentration of CO_2 which is needed to separate it from the flue gas [30]. Moreover, the recycled CO_2 is used to sweep out the permeate side of the membrane thus lowering the oxygen partial pressure and allowing the gradient of partial pressure of oxygen to remain across the membrane. If the membrane is integrated with combustor then oxygen is removed due to combustion.

2.1.2 Flue gas composition:

In general oxy-fuel combustion process, in which oxygen is separated and used in the combustion chamber, is considering two mechanisms for the flue gas recirculation for sweeping the oxygen permeated from the membrane. The first mechanism, shown in Figure 5, is called “wet recycling”. In this process flue gas is recycled directly after the clean-up process that removes of particulates and acid gases. The swept gas will be mainly composed of water and CO_2. The second mechanism, shown in Figure 6, is “dry recycling”. In this process water is removed from the flue gas by condensation which doesn’t remove all but after condensation if we pass the flue gas through molecular sieves then we can eliminate the water completely [31].

In case of Oxygen transport reactor in which permeation and combustion takes place at the same time the recycled CO_2 will play a major role in controlling the temperature of the reactor and increasing the CO_2 concentration at the exit of the combustor to make it feasible to capture it.

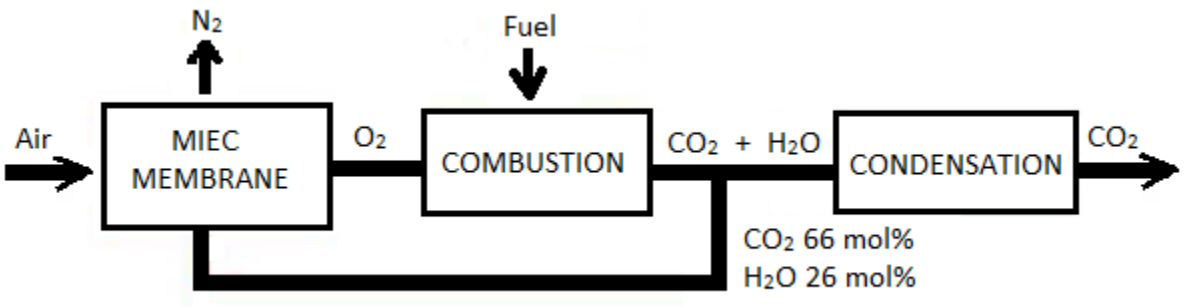

Figure 5:Oxy-fuel process with water condensation(Ref:[27])

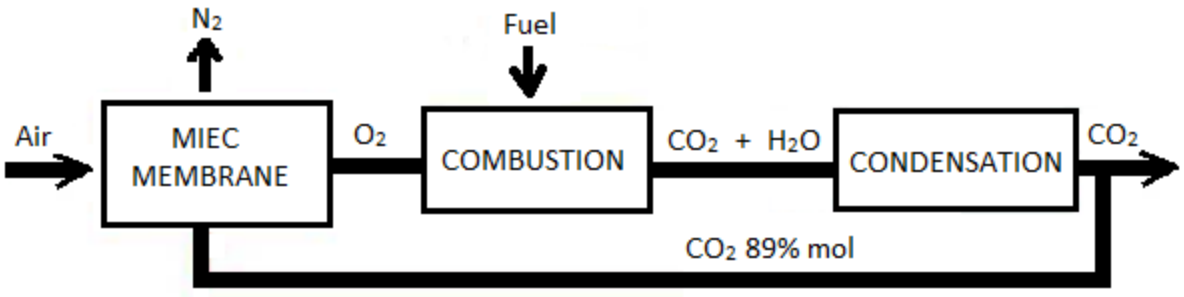

Figure 6 : Oxy-fuel process without water condensation (Ref:[31])

2.2 Ion Transport Membranes (ITM‘s):

2.2.1 Experimental studies:

Tan and Li[33] studied oxy-fuel combustion using a catalytic ceramic membrane reactor. In his experimental work Tan et al has used perovskite $La_{06}Sr_{0.4}Co_{0.2}Fe_{0.8}O_{3-\alpha}$ (LSCF-6428) hollow fiber oxygen-permeable membranes, for combustion in a hollow fiber membrane reactor (HFMR). The results showed that as the methane feed flow rate increases, more oxygen is converted and the oxygen conversion eventually approaches 100%. Furthermore no products other than carbon dioxide were observed during the experiments. It was concluded that the granular LSCF-6428 catalyst shows a high

catalytic activity to methane combustion. The oxygen concentration in the product stream was found to increase as the temperature was increased indicating that the oxygen permeation rate is higher than the oxygen consumption rate due to the reactions. The conversion for both methane and oxygen will increase as the reaction rate increases.

Haihui et al [34] has done oxygen permeation study in a tubular $Ba_{0.5}Sr_{0.5}Co_{0.8}Fe_{0.2}O_{3-\delta}$oxygen permeable membrane. Oxygen permeation flux was measured at different partial pressure on both side of the membrane for different membrane temperatures in the range of 700^0C and 900^oC. The results show that the oxygen permeation flux increases with increase of partial pressure of oxygen at shell side for a constant temperature. The increase of temperature also greatly affects the permeation flux along with the partial pressure of O_2 at the feed side. The analysis is done on two mechanism of transport of oxygen, one is surface exchange current model and other is bulk diffusion given by equations (7) and (8) respectively.

$$J_{O_2} = \frac{2\pi r_1 r_2 w C_i k_{io}}{S(r_1 + r_2)} \left(\sqrt{\frac{P'_{O_2}}{P^0_{O_2}}} - \sqrt{\frac{P''_{O_2}}{P^0_{O_2}}} \right) \tag{7}$$

$$J_{O_2} = \frac{\pi w C_i D_a}{2S \ln(r_1 / r_2)} \ln\left(\frac{P'^{0.5}_{O_2}}{P''^{0.5}_{O_2}} \right) \tag{8}$$

Guillodo et al [35] has done experimental analysis for oxygen permeation through dense $Bi_2V_{0.9}Cu_{0.1}O_{5.35}$ ceramic membranes. For the analysis oxygen permeation rate was schematically decomposed in three steps: bulk diffusion, surface exchange between oxygen and oxygen vacancies at feed side and surface exchange between oxygen and

oxygen vacancies at permeate side. The oxygen flux was modeled using Wagner theory assuming both surfaces of the membrane are in equilibrium with the imposed gas atmospheres. The oxygen permeation flux is correlated as equation(9).

$$J_{O_2} = \frac{RT}{4F^2L}\sigma_h^o\left(P_{O_2}^{'-1/4} - P_{O_2}^{''-1/4}\right) \tag{9}$$

The experiments are done on three cells and out of which two cells were coated with porous gold layer. The amount of oxygen permeation flux was calculated by varying the pressure at the feed side between $10^2$and 10^5 Pa. The results showed that permeation flux is proportional to the $\left(P_1^n - P_2^n\right)$ where the best fit value of n obtained to be 0.5. The maximum value of oxygen flux was 9.1×10^{-7} mol cm^{-1}min^{-1} for 923K and 10^5Pa.

Taheri et al [36] has compared the permeation of oxygen flux through three membranes SCF, LSCF-6482 and LSCF-8264 which was found to be a function of temperature and oxygen partial pressures for a particular thickness of membrane. The permeation of oxygen was assumed to predominant by bulk diffusion is given by equation(10).

$$J_{O_2} = \frac{RT}{16F^2L}\bar{\sigma}_i \ln\frac{P_{O_2}^{'}}{P_{O_2}^{''}} \tag{10}$$

The flux increased as LSCF-8264 < LSCF-6482 < SCF-82. The increase of flux was found to be linear to the ratio of natural log of partial pressure of oxygen at feed and permeate side. Zhu et al [37] has done experimental investigation of oxygen permeation through perovskite membrane under vacuum and elevated pressures. The maximum

permeation reported was 9.5 cm^3/cm^2-min at 925^oC and 7 atm pressure at feed site for 200 ml/min mass flow rate of air at feed.

2.2.2 Numerical studies:

Xuan et al [38] have done numerical modeling by integrating the chemical kinetics for auto-thermal reforming of biogas. The performance and characteristics of biogas for hydrogen production has been studied for two-dimensional model which is based on the integration of chemical kinetics with the computational fluid dynamics. The analysis was done for three physical models; one was the conventional ATR reformer and other two with hydrogen membrane reformer and oxygen membrane reformer. The results obtained from the numerical investigation were compared with the experimental data of auto-thermal reforming of methane and results were found to be in good agreement.

Mirella et al [39] has done numerical and experimental investigation to mass transfer performance of Pd-Ag Membrane Modules for Hydrogen separation. Numerical analysis carried out for different modules of configuration for H_2 and N_2 mixture and compared with the experimental results are found to be predictive, requiring only the permeability characteristics of the selected membrane. Shigeo Goto [40] has studied the effect of hydrogen permeation rate through composite palladium membrane. The analysis is done for increasing temperatures for two different mode, CP mode and PC mode. The numerical models are based on the combined resistances of both composite and palladium film. From the results it was clear that with increase of temperature permeation rate increases under CP mode.

M Coroneo et al [41] has done CFD modeling of inorganic membrane modules for gas mixture separation for laminar flow. In the study Coroneo derived the permeation coefficient, based on the transport mechanisms for the gas molecules across the membrane such as molecular diffusion, Knudsen diffusion and viscous (Poiseulle) flow, and implemented in the source term formulation in continuity and species transport equation on either side of the membrane and with the Pd-Ag support. The analysis showed the dependence of transport mechanism has great impact on the permeation rate and for Hydrogen permeation molecular diffusion is predominant mechanism for high pressure. The mole fraction and permeation rate of hydrogen increases with increase of working pressure and are in good agreement with the experimental results.

Oxygen transport in an ITM membrane is a physically complex process, and should be represented inside of a reduced-order ITM model without excessive computational expense. Mancini and Mitsos [7] developed a axially spatially-distributed, quasi two-dimensional model, a compromise between extremely detailed oxygen transport models as in Ref[42] and simplified models found in black-box analyses, based on fundamental conservation equations, semi-empirical oxygen transport equations obtained from the literature [19], and simplified fuel oxidation kinetic mechanisms. Equation(11) shows the flux expression developed by Mancini and Mitsos.

$$J_{O_2} = Ae^{(-B/T_M)}[(P_{O_2}^{'})^n - (P_{O_2}^{''})^n] \tag{11}$$

2.3 Porous Membranes:

A large number of studies have demonstrated the physics of flow through porous media, revealing that Darcy regime can predict the flow behavior properly when the flow velocity is sufficiently small, while Forchheimer regime, considering the inertial effects, is able to describe the flow pattern when the flow velocity becomes adequately large.

Zhong et al demonstrated the use of differentiated value ofpressure from the charge of air into an isothermal chamber todetermine the permeability coefficient, the inertia coefficient aswell, and represent the flow rate characteristics in terms of Darcyequation and Forchheimer equation. They verified the effectiveness of the proposedmethod experimentally [43]. Under steady state condition, within a small pressure drop ΔP ($\Delta P = P_1 - P_2$), the flow rate is approximately proportional to the pressure difference, indicating that the Darcy regime is applicable in the small pressure drop region.

In porous membranes, it is believed that Poiseulle flow is predominant only when Knudsen number (the ratio of gas mean free path to pore diameter) is less than 0.01. When the Knudsen number is greater than 10, on the other hand, Knudsen diffusion is predominant [44, 45]. Li-Zhi Zhang [46] proposed a fractal gas diffusion model for prediction of permeability through macro and micro porous membranes. His model clarifies the gas diffusion mechanisms in the membrane pores: when the Knudsen number is less than 0.01, the Poiseulle flow is dominant; and when the Knudsen number is greater than 10, the Knudsen flow is dominant; and when the Knudsen number is from 0.01 to 10, the two mechanisms coexist. His gas permeation model was validated numerically and experimentally.

Shelekhin et al [47] studied the gas permeability properties of He, H, CO_2, 0_2, N_2, and CH_4 in micro porous silica membranes as a function of temperatureand pressure. They concluded that the permeation rate of Helium in the micro porous membrane was comparable to that in industrially produced polymeric membranes.Sawly et al [48] presented a numerical method for the simulation of flow in porous. The method was proved to provide good results for both saturated and unsaturated porous media flow. From his results the Darcy law was confirmed for low drift velocities in a saturated medium, while non-linear behavior was observed for higher velocities.

Hou et al [49] presented a multi-scale approach to numerically simulate the gas flow in an Electrostatic precipitator (ESP) system with two parallel ESP units. The simplification of the perforated plates as porous jump boundaries was justified using a simple ESP experimental rig and it was found that the anisotropic porous media boundary has similar behavior while it is more convenient to control porosity distribution of the perforated plates. The consistency of the pressure drop through the PMs in the full system and the fitting curve in ESP unit study justified the simplification of the ESP unit as a uniform porous media.

2.4 Oxy-fired Power Plants Incorporating Oxygen Transport Membranes:

With cryogenic air separation there will be huge loss of efficiency of the oxy-fired cycles. However, OTMs offers promising oxygen production without such adverse effect on efficiency. Oxygen transport Membranes have been incorporated in power cycles and a well-developed example is Advanced Zero Emission Power (AZEP) cycle [50]as shown in Figure 7.In the cycle, after air is compressed it is split and part of it is used to heat

steam and air and part of it mixed with oxygen in OTM unit which is MCM in Figure 7and returns to the combustion chamber as oxidant. The membrane conducts oxygen to fuel side and heats the air side. The oxygen depleted turbine (main turbine) drives both air compressor and the electrical generator. The combustion products used to heat the Rankine cycle and are cooled to condense after boiler leaving only CO_2. The thermal efficiency of AZEP cycle is compared with conventional combined cycle power plant and it was found to be about 8.3% [51].

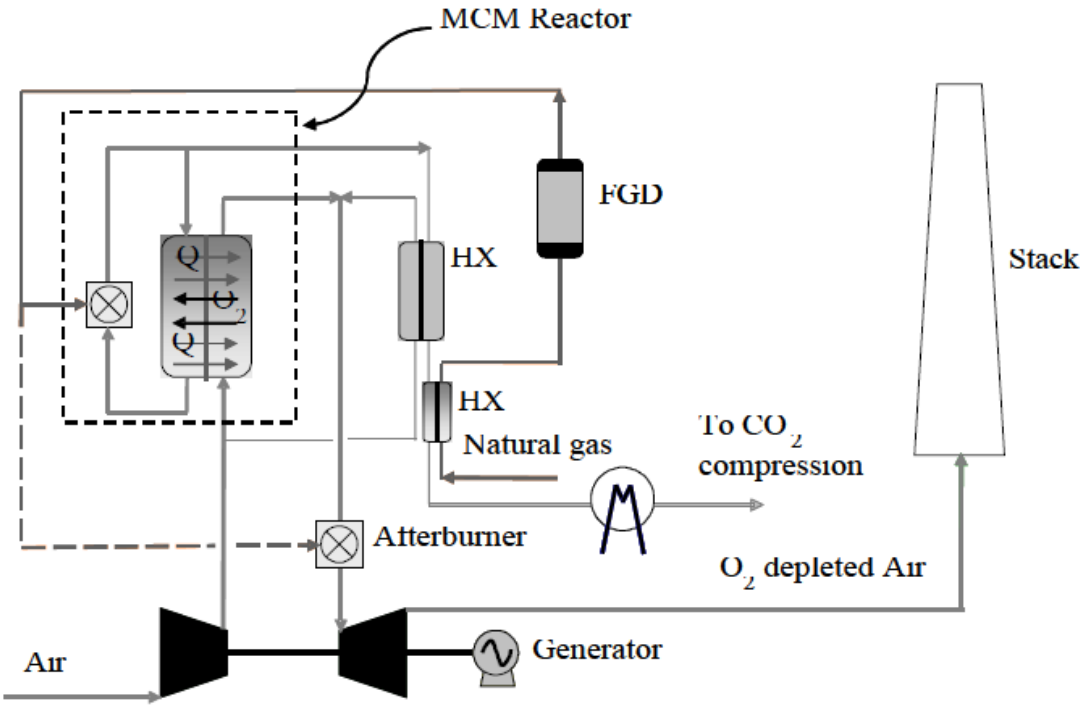

Figure 7 : AZEP Oxy-fired cycle incorporating OTM (Ref:[52])

The other cycle which was developed with OTM is Oxy-coal-AC cycle in Germany. The combustion products provide heat to air stream. In this air turbine drives the compressor and the power is generated in bottoming cycle only. The efficiency of the cycle was

reported 41.6% with 4-end concept and 39.7% with 3-end concept [53].The 4-end concept and 3-end concept is described in the following paragraphs.

Standler et al [54], has conducted analysis on Oxy-fuel coal combustion by efficient integration of Oxygen Transport Membranes, describes possible implementations of OTM into an Oxy-fuel process through three-end and four-end integration of membranes with a focus on overall cycle efficiency for different level of integration which includes low, medium, high integration, high integration with fogging and Co-firing.

The four-end concept, shown in Figure 8 (left),refers to the application of sweep stream on the low pressure side in order to remove the permeating component and thereby increasing the driving potential whereas in the three-end concept, shown in Figure 8(right), vacuum is applied at the permeate side.

Comparison of four end and three end concepts are shown in Figure 8. It is obvious through the experiments that the efficiency can be improved through optimization of membrane operation parameters such as oxygen separation degree, the partial pressure ratio and the total pressure ratio. It is found from the analysis that the oxygen concentration varies linearly with the separation degree and with 90% separation degree, 16.5 volume% concentrations of oxygen and with the partial pressure ratio of 26 the adiabatic flame temperature achieved was about 1500^{o}C.

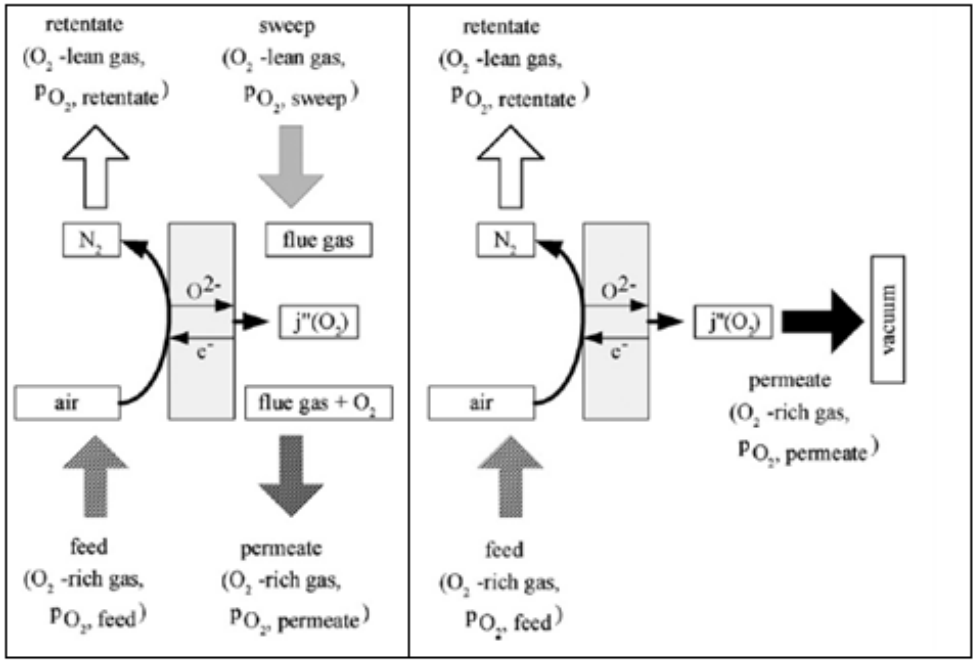

Figure 8 : Oxygen conduction in OTM in four-end design (left) and three-end design(right)(Ref: [54])

The concept developed by E Yantovski [55], for oxy-fired power plant with zero emission came up with a new cycle called ZEITMOP (Zero Emission Ion Transport Membrane Oxygen Power) cycle [55]. The cycle has three turbines, one for combustion products, second for depleted oxygen and third for CO_2 recirculation through the system.

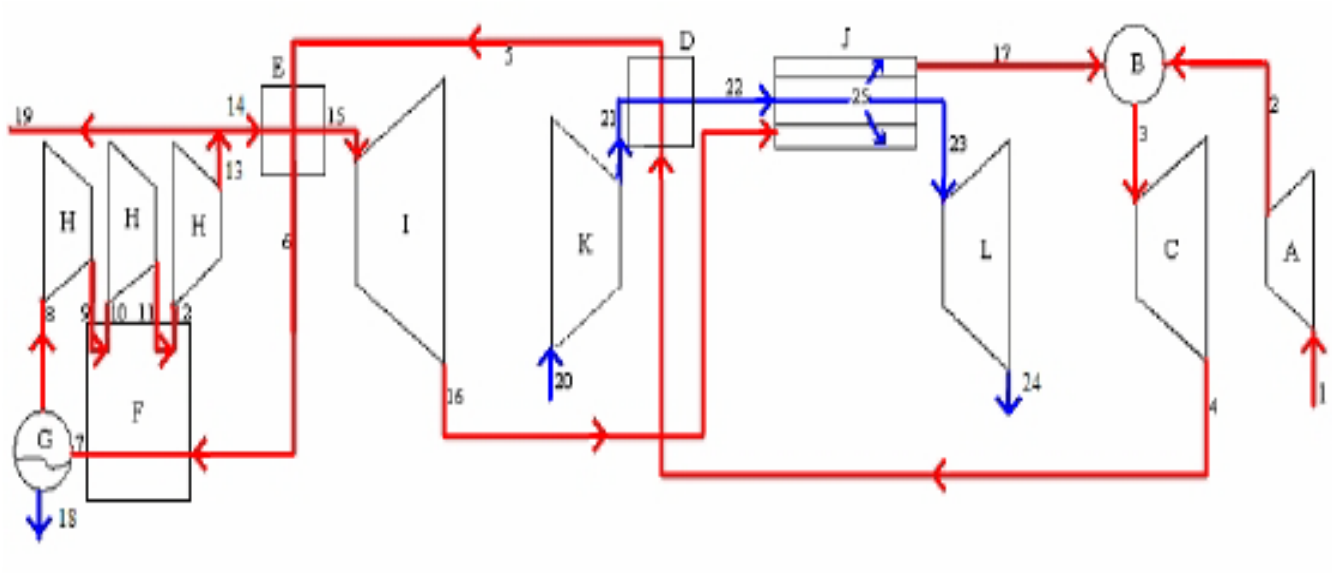

Figure 9: The ZEITMOP cycle where OTR is remote from combustion chamber (Ref: [55])

In the present case shown in ZEITMOP cycle (Figure 9), the OTM reactor is remote from the combustion chamber. The separation of oxygen take place in OTM reactor and then led it to burn in combustion chamber and from the products of combustion CO_2 is cooled, compressed and separated. To show the feasibility of ITMs, the numerical analysis of ZEITMOP power cycle with separate combustion and ITM reactor is done by Foy [56] using Aspen Plus for the combined OTR and combustion chamber in ZEITMOP cycle. For optimizing the thermal efficiency of the cycle many formats can be selected for CO_2 capture and improving the working performance of OTR. There is very wide potential of making hybrid power plants with OTR for carbon capture and clubbing the renewable energy sources like solar. The present work is focused on the study of combustion characteristics of OTR and the results can be used to optimize the total cycle efficiency.

2.5 Economic Feasibility:

The study of economic feasibility of these technologies is an important issue that has to be considered. Since the coal fired power plants generate high rate of flue gases but with low CO_2 concentration. There is huge capital investment needed to install the post combustion systems for massive volumes of flue gases in the present conventional power generation systems. Since most of the processes for CO_2 capture is energy intensive, pre-combustion and oxy-fuel process are viable processes which lies within in low investment.

The Air Separation units (ASU) which uses cryogenic fractionation process to separate oxygen from air may alone consume about 13% of the power plant output [15]. On the other hand gas separation membranes have relatively low energy consumption and their integration into membrane reactors is very promising. Therefore, they are excellent for gas separation in retrofitting coal-fired power plants and the oxy-fuel combustion power plant.

CHAPTER 3

PROBLEM STATEMENT AND SOLUTION METHODOLOGY

3.1 Problem Statement:

Ion Transport Membranes (ITMs) offer promising oxygen production technology with high purity (upto 99%) without adversely affecting the efficiency of the oxy-fired plants. The separation rate of such ITMs can be increased by replacing the conventional inert sweep gas with a reactant/diluent mixture (e.g. CO_2, CH_4) as this reduces the permeate partial pressure on the permeate side of the membrane, which, along with the temperature, governs the permeation flux. The significant limitation of this approach is that an uncontrolled, exothermic consumption of the permeated specie, can lead to membrane damage, and thus limits the potential of ITMs using reactive sweep gases (i.e. ITM reactors). To overcome the aforementioned problem, present oxygen transport reactor is modeled.

3.2 Present Oxygen Transport Reactor Modeling:

In order to overcome the limitations, stated in the previous section, the present oxygen transport reactor has been modeled. This model is believed to achieve uniform temperature (isothermal ITM) all along the length of the membrane. An investigation of combustion characteristics in the present reactor model is performed.

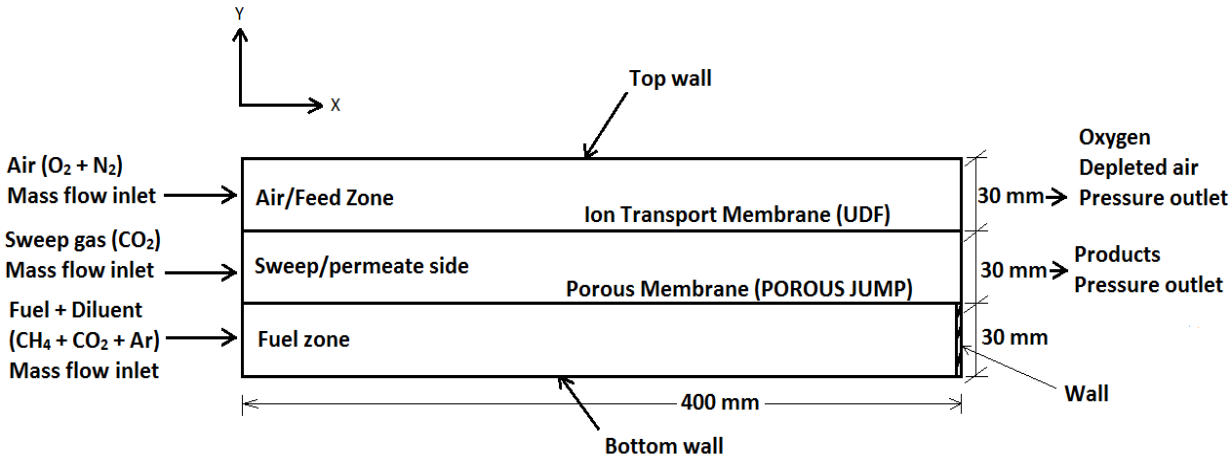

Figure 10: Schematic Diagram (with boundary conditions) of the oxygen transport reactor with ITM and porous membrane for oxygen separation and combustion

Figure 10 shows the schematic diagram of the oxygen transport reactor for the present study. It consists of an ITM and a porous membrane arrangement which divides the whole reactor into three channels. The thickness of ITM and porous membranes is taken as 1mm. The top channel is called the air zone (or feed zone), the middle channel called the sweep zone (or permeate zone) and the bottom channel as the fuel zone. The length of the reactor is 400mm and the height of each channel is 30mm. The total height of the reactor is 90mm. Air or other mixture from which a component is to be separated is passed through the top (feed) channel with one wall made of an ITM material. In the

adjacent (middle/permeate) channel, a sweep gas is passed through to remove the permeated specie. The bottom channel (fuel zone) consists of porous wall (given POROUS JUMP boundary condition), through which a mixture of reactants and diluent can pass through. The outlet of the bottom channel is closed with a wall in order to increase the pressure of the fuel mixture to pump it across the porous membrane. The top and the bottom walls are assumed to be adiabatic. To ensure uniform combustion all along the length of the membrane, uniform stoichiometric ratio has to be maintained all along the length. Since the oxygen flux along the length of the ITM varies, fuel mixture must be introduced accordingly to obtain uniform stoichiometric ratio to ensure uniform combustion. For this purpose the porous membrane is divided into four parts of equal length but with different porosities. The values of the porosities for these four porous membranes are discussed in the following chapter. By introducing the reactant uniformly across the length of the ITM reactor, isothermal operation can be achieved. The fraction of diluents in (fuel mixture) can range from 0-100%.

3.2.1 Boundary conditions and solution method:

The inlet conditions and the operating conditions are applied under steady-laminar flow conditions. The mass flow rate of air is kept constant at a value of 0.03 kg/s throughout the study. The mass flow rate of CO_2 through the sweep channel is also kept constant at a value of 1x10e-06 kg/s throughout the study. The discretization of the governing equations is done using a segregated compressible flow solver in which each governing equation is solved separately. The Semi-Implicit Method for Pressure-Linked Equations

(SIMPLE) formulation was used as a part of pressure-velocity coupling algorithm [57]. The convergence criteria for the continuity and velocity parameters were set to 10e-6 and species and energy equation were set to 10e-9 to offer sufficient iterations for complete convergence between the boundary and the interior mesh grid. To obtain the stable solution, the under relation factors, which limits the influence of previous iteration over the present which were fixed to 0.3 for pressure, 0.85 for density, 0.7 for momentum and 0.8 for species and energy. The values of these under relaxation factors were lowered to prevent the oscillating solutions [58].'Pressure Staggered Option' (PRESTO) scheme was used for pressure and 'First order upwind' discretization scheme was used for momentum, density, mass fraction and energy equation [57]. To enhance the convergence of solver 'Aggressive Advanced Multi-grid (AMG) scheme was used. The AMG cycle type for the coupled equations involving pressure, momentum, energy and species were set to fixed 'F-cycle' as a recursive process. To avoid the irregular convergence patterns 'Bi-conjugate Gradient Stabilized Method' (BCGSTAB) was employed.

3.2.2 User defined function (UDF):

Permeation of oxygen across the membrane is modeled using a series of user-defined functions that are written in VC++ and compiled and hooked in FLUENT software. The issue of hydraulic jump across the membrane was resolved by patching the cells from the upper and lower zones with two different values of initial partial pressures of species.

The three different Macros used in UDF were 'Define Initialize', 'Define Source' and 'Define Adjust'. These macros link the cell index across the membrane which allows the

addition and subtraction of the source term in continuity and species transport equation. Additionally, the UDF updates the solver data for each iteration with new parameter at membrane wall. The partial pressure given in the oxygen flux equation is calculated as concentration X_i (%wt) of oxygen.

3.3 Oxygen Transport Theory ofIon Transfer Membranes (ITMs):

MIEC compounds form dense ceramic membranes, which exhibit significant oxygen ionic and electronic conductivity at elevated temperatures. In turn, this process allows for the ionic transport of oxygen from air due to the differential partial pressure of oxygen across the membrane, providing the driving force for oxygen ion transport. As a result, defect-free synthesized membranes deliver 100% pure oxygen. Electrons involved in the electrochemical oxidation and reduction of oxygen ions and oxygen molecules respectively are transported in the opposite direction, thus ensuring overall electrical neutrality [16].

Oxygen transport through a dense mixed ionic–electronic conducting material (Figure 11) involves three progressive steps: (i) the surface-exchange reaction on interface I; (ii) the simultaneous bulk-diffusion of charged species and electron/electron holes in the bulk phase and (iii) the surface-exchange reaction on interface II [59] and [60].

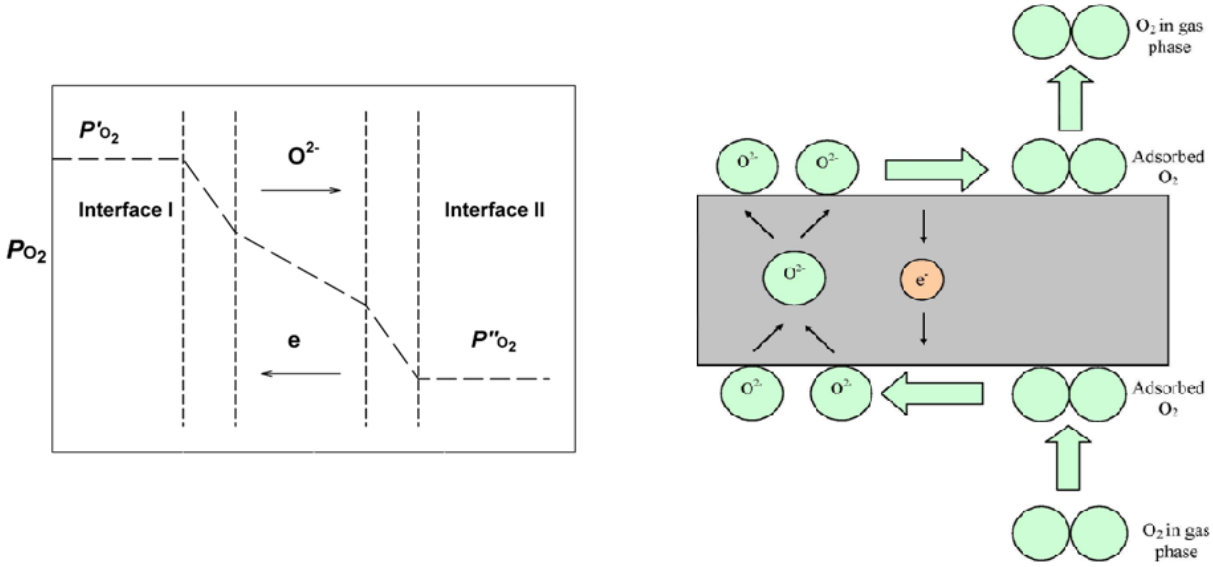

Figure 11 : Different processes involved in oxygen transport during oxygen permeation, (Ref [16])

The overall rate of oxygen permeation is expected to be limited by the slowest process or slowest moving species [59, 61, 62]. For example, in certain fluorite-based compounds, when the ionic conductivity is very high as compared to the electronic conductivity; the oxygen flux is mainly a function of the electronic conductivity, as seen for example in most bismuth oxide and zirconia-based compounds [59, 61-68]. However, as the membrane thickness is decreased, the controlling step will no longer be bulk-diffusion but surface-exchange reaction [59, 62, 68, 69]. Figure 12shows a typical variation of determining steps with membrane thickness.

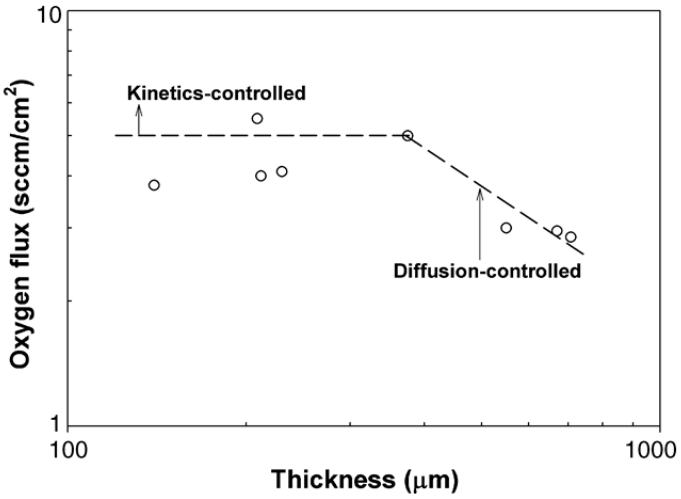

Figure 12 : Variation of regime from bulk-diffusion to surface-exchange reaction limited with decreasing membrane thickness (Ref: [69])

3.3.1 Determination of the characteristic membrane thickness L_c:

The "critical thickness," or "characteristic length," L_c is used to estimate the relative importance of each transport process [15]. L_c was introduced by Bouwmeester et al. in order to distinguish whether bulk diffusion or surface exchange govern the kinetics of oxygen permeation [70]. A characteristic thickness, L_c is defined as the membrane thickness at which the oxygen permeation is equally determined by the surface-exchange kinetics and bulk-diffusion.

$$L_C = \frac{D_i}{k} = \frac{D^*}{k} = \frac{1}{h} \tag{12}$$

where '*k*' is the surface exchange coefficient and '*D**' the tracer diffusion coefficient.

Here *k* expresses the exchange flux normalized by the molar concentration of oxygen anions at equilibrium, D_i is assumed to be identical to D^*, the tracer diffusion coefficient.

D^* and k values are available from the ^{18}O–^{16}O isotope exchange experiments. If the thickness of the membrane is greater than the characteristic thickness, then bulk transport dominate, if the thickness of the membrane is less than characteristic thickness then oxygen transport is equally limited by both surface exchange kinetics and the bulk diffusion.

When the thickness of the membrane is much lower than $2L_c$, the oxygen flux is independent of the thickness of the membrane. A value of 100μm is often quoted as the characteristic membrane thickness for perovskite structures although the L_c value can be much higher, up to 3000μm [70]. Calculations show that L_c can vary from the μm range to the mm range [15]. In general, ion diffusive transport is dominant for thick membranes operating at high temperatures under low partial pressure gradients, while surface exchange kinetics are necessary to model oxygen transport for thin membranes in the low temperature regime [16].

Different compounds of varying thicknesses tend to have different determining steps. Several limiting cases in which a different step becomes the controlling process for a certain material are discussed below.

3.3.2 Limitations of bulk diffusion:

The diffusion process for the thick membrane is commonly the slowest step. The Wagner theory can be used to describe the oxygen flux [60].

$$J_{O_2} = \frac{1}{16F^2L}\int_{\mu_{O_2}(II)}^{\mu_{O_2}(I)} t_i t_e \sigma_t d\mu_{O_2} \tag{13}$$

$$t_i = \frac{\sigma_i}{\sigma_e + \sigma_i} = \frac{\sigma_i}{\sigma_t} \tag{14}$$

The oxygen flux permeation equation is derived based on the assumption that local equilibrium exists between the two charged species such as oxygen ion and electron a hypothetical neutral species such as molecular oxygen in the bulk side. For consideration at least three species can contribute to the bulk-diffusion processes which are i) Oxygen vacancies, ii) electrons or iii) electron holes.

3.3.2. (a) Limitations of oxygen vacancies diffusion:

In the case of a mixed conductor where the electronic conductivity dominates, i.e., $\sigma_e >> \sigma_i$ and σ_i is a function of oxygen partial pressure only in the permeation flux equation.

The chemical potential in an ideal thermodynamic system is given by

$$d\mu_{o_2} = RTd\ln P_{O_2} \tag{15}$$

A more general expression for ionic conductivity is given by the Nernst–Einstein relation [71],

$$\sigma_i = \frac{4F^2 V_O^{\bullet\bullet} D_v}{RTV_m} \tag{16}$$

$$D_v = D_v^0 \exp\left(-\frac{E_a}{RT}\right) \tag{17}$$

For average value of σ_i and for small oxygen partial pressure gradient the oxygen permeation flux equation can be integrated as,

$$J_{O_2} = \frac{RT}{16F^2L}\bar{\sigma}_i \ln\frac{P_{O_2}^{'}}{P_{O_2}^{''}} \tag{18}$$

If the oxygen ionic conductivity, in general, can be correlated to oxygen partial pressure in a simplified manner as,

$$\sigma_i = \sigma_i^o P_{O_2}^{-n} \tag{19}$$

then the oxygen flux can be given as,

$$J_{O_2} = \frac{RT}{4F^2L}\sigma_i^o\left(P_{O_2}^{'-n} - P_{O_2}^{''-n}\right) \tag{20}$$

3.3.2. (b) Limitations of electrons diffusion:

For ideal thermodynamic systems, the electronic conductivity is a function of its electron concentration as

$$\sigma_e \approx n \approx KP_{O_2}^{-1/4} \tag{21}$$

The Wagner flux equation can therefore be manipulated as

$$J_{O_2} = \frac{RT}{16F^2L}\int_{P_{O_2}^{''}}^{P_{O_2}^{'}} \sigma_e d\ln P_{O_2} \tag{22}$$

The electronic defects could be properly assumed to proceed as

$$O_O^x \leftrightarrow \frac{1}{2}O_2 + V_O^{\bullet\bullet} + 2e \tag{23}$$

And by using the basic laws of chemicalreaction the value of ‘n’ can be derived as

$$n = \frac{K_{V_O^{\bullet\bullet}}^{1/2}[O_O^x]^{1/2}}{P_{O_2}^{1/4}[V_O^{\bullet\bullet}]^{1/2}} \tag{24}$$

If the concentration of all other species (oxygen vacancies and interstitials) is much higher, then the electron concentration is proportional to $P_{O_2}^{-1/4}$.

All assumptions above have led to the final dependence of oxygen flux on-$(1/4)^{th}$ order of oxygen partial pressure as given by equation(25).

$$J_{O_2} = \frac{RT}{4F^2L}\sigma_e^o\left(P_{O_2}^{'-1/4} - P_{O_2}^{''-1/4}\right) \tag{25}$$

3.3.2. (c) Limitations of electron holes diffusion:

The electron holes assumed to follow the equation

$$O_2 + 2V_O^{''} \leftrightarrow 2O_O^x + 4h \tag{26}$$

By same assumptions made as in electron diffusion, oxygen flux equation can be derived as

$$J_{O_2} = \frac{RT}{4F^2L}\sigma_h^o\left(P_{O_2}^{'-1/4} - P_{O_2}^{''-1/4}\right) \tag{27}$$

$$h = \frac{K_{O_O^x}^{1/2}P_{O_2}^{1/4}[V_O^{\bullet\bullet}]^{1/2}}{[O_O^x]^{1/2}} \tag{28}$$

where *h* is derived by using the basic laws of chemical reaction.

3.3.3 Limitations of surface exchange reactions:

If the oxygen transport resistance in the bulk phase becomes very small due to an increase in the ionic or electronic conductivity or decrease in the membrane thickness, the surface-exchange reaction rate would become the limiting step in the oxygen permeation. The Wagner equation is not applicable when surface reaction becomes rate limiting step foroxygen flux. Other mechanisms and relations have been proposed to explain the oxygen flux within this regime. Dou et al. [68] has proposed possible mechanisms to incorporate the surface reaction into bulk-diffusion and came up with the following flux equation(29).

$$J_{O^2} = \alpha(p_{O_2}^{'1/2} - p_{O_2}^{''1/2}) \tag{29}$$

This flux equation has been used successfully to describe the oxygen permeation in a calcia-stabilized zirconia system, $(ZrO_2)_{0.85}(CaO)_{0.15}$ when the thickness of the film reached less than 1.75 mm.

Kim et al [72] has derived an equation(30) which accounts for the surface exchange kinetics for tubular perovskite membranes which was used to fit the oxygen permeation data for $SrCo_{0.8}Fe_{0.2}O_{3-\delta}$ and $Sm_{0.5}Sr_{0.5}CoO_{3-\delta}$.

$$J_{O_2} = \frac{2\pi r_1 r_2 w C_i k_{io}}{S(r_1 + r_2)} \left(\sqrt{\frac{P_{O_2}^{'}}{P_{O_2}^{0}}} - \sqrt{\frac{P_{O_2}^{''}}{P_{O_2}^{0}}} \right) \tag{30}$$

3.3.4 Generalized transport equations:

Several research groups [19, 73, 74] demonstrated the possibility to incorporate all the limiting cases of transport as discussed above into a single explicit equation with the following assumptions [16].

i. The oxygen permeation rate across the membrane is governed by the flux of oxygen vacancies as the electronic conductivity in perovskite is much greater than its ionic conductivity.

ii. A steady-state electric field gradient is negligible due to fast movement of electron holes (electronic holes is assumed to dominate the electronic conductivity).

iii. Ideal gas behavior is applied to the gas phase.

iv. The radial diffusion is neglected while the diffusion coefficient of oxygen vacancies D_v is assumed to be constant.

v. Surface-exchange reaction in the feed side is governed by equation(31) while the reverse of equation applies to the permeate side, both with the rate constant k_f and k_r that is equal for both sides.

$$O_2 + 2V_O^{"} \leftrightarrow 2O_O^x + 4h \tag{31}$$

vi. Concentration of electron holes is considered constant at both sides of the membrane while the law of mass action is applied for other components.

Equation(32) has been derived specifically for disk-shaped membranes and has been shown to fit the oxygen flux for LSCFO for temperature range of 750^{o}C-950^{o}C and for 0.21-1.0atm oxygen partial pressure at the feed side and 4.64e-04 – 2.3e-02atm on the permeate side. In the equation, each term in the denominator represents resistance in the feed, bulk membrane and permeates side respectively.

$$J_{O_2} = \frac{(k_r / k_f)(1/P_{O_2}^{"0.5} - 1/P_{O_2}^{'0.5})}{(1/k_f P_{O_2}^{"0.5}) + (2L/D_v) + (1/k_r P_{O_2}^{'0.5})} \tag{32}$$

Xu et al [19] has developed an explicit steady state oxygen permeation flux model for ion-conducting membranes (LCSF-6428) with a high ratio of electronic to ionic conductivity, to correlate the permeation flux to directly measurable variables. Surface exchange kinetics at each side of the membrane was emphasized and their resistance to oxygen permeation has been quantitatively distinguished from the bulk diffusion resistance.

$$J_{O_2} = \frac{D_v k_r \left[(P_{O_2}^{'})^{0.5} - (P_{O_2}^{"})^{0.5} \right]}{2Lk_f (P_{O_2}^{"})^{0.5} (P_{O_2}^{'})^{0.5} + ((P_{O_2}^{'})^{0.5} + (P_{O_2}^{"})^{0.5}) D_v} \tag{33}$$

Where D_v, k_f, k_r are functions of temperature and specific properties of the membrane and can be obtained by fitting experimental oxygen flux data as a function of temperature and oxygen partial pressure gradients.

Equation(33) can be rewritten in form as,

$$J_{O_2} = \frac{\Delta P_{O_2}}{R_t} \tag{34}$$

$$\Delta P_{O_2} = (k_r / k_f)(1/P_{O_2}^{"0.5} - 1/P_{O_2}^{'0.5}) \quad (35)$$

$$R_t = R_{ex}^{'} + R_{diff} + R_{ex}^{"} \quad (36)$$

Where equation(35) is the oxygen pressure driving force across the membrane and equation(36) is the total resistance to permeation.

$$R_{ex}^{'} = (1/k_r (P_{O_2}^{'})^{0.5}) \quad (37)$$

$$R_{diff} = (2L/D_v) \quad (38)$$

$$R_{ex}^{"} = (1/k_f (P_{O_2}^{"})^{0.5}) \quad (39)$$

If any one step is limiting then its resistance dominates the total pressure, so the permeation flux based on the single step can be given as follows

Bulk diffusion:

$$J_{diff} = \frac{\Delta P_{O_2}}{R_{diff}} = \frac{k_r D_v (1/P_{O_2}^{"0.5} - 1/P_{O_2}^{'0.5})}{2Lk_f} \quad (40)$$

Surface exchange: oxygen-rich side :

$$J_{ex}^{'} = \frac{\Delta P_{O_2}}{R_{ex}^{'}} = k_r (P_{O_2}^{'0.5} / P_{O_2}^{"0.5} - 1) \quad (41)$$

Surface exchange: oxygen-lean side :

$$J_{ex}^{"} = \frac{\Delta P_{O_2}}{R_{ex}^{"}} = k_r (1 - P_{O_2}^{"0.5} / P_{O_2}^{'0.5}) \quad (42)$$

The value of D_v, k_f, k_r can be obtained by the following expressions.

$$D_v = D_v^0 \exp\left(\frac{-E_D}{RT}\right) \tag{43}$$

$$k_f = k_f^0 \exp\left(\frac{-E_f}{RT}\right) \tag{44}$$

$$k_r = K_r^0 \exp\left(\frac{-E_r}{RT}\right) \tag{45}$$

Where E_r, E_D, E_f are the activation energies (kJ/mol) and k_r^0, D_v^0, k_f^0 are pre-exponential coefficients for reverse, bulk and forward reaction rate constants respectively.

From the literature it has been concluded that BSCF membranes offer high oxygen permeation flux than LSCF membranes at particular temperature and partial pressure range. But the former are less stable at high temperatures than the later. Hence inorder to have reasonable oxygen fluxes along with the stability of membranes at high combustion temperatures, LSCF membrane model has been used to study the present oxygen transport reactor. The equations to model this membrane are taken from Xu et al [19], which have been explained earlier.

3.4 Theory of Flow Through Porous Media:

A porous media consists of some particulate phase, contained within a vessel, or a control volume, as illustrated in the Figure 13. The fluid flow rate through the bed cross-sectional area is A (m^2). Thus the superficial (or empty tube) velocity U_0 is the total flow rate divided by the cross sectional area. The existence of the particles within the bed will reduce the area available for fluid flow i.e. to preserve fluid continuity. With the entering superficial flow the fluid has to squeeze through a small area; hence the velocity within

the bed (U – interstitial velocity) will be greater than the superficial. The volume fraction of solids present (i.e. volume solids in bed divided by total bed volume) is usually referred to simply as the volume concentration, or solids fraction, and the remaining fraction is that of the voids.

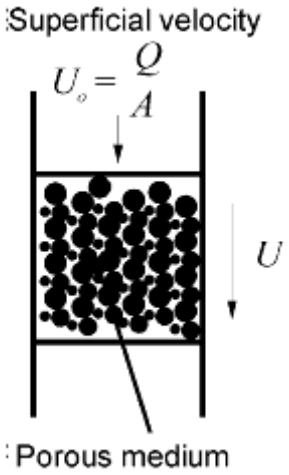

Figure 13 : Flow through porous media

The void fraction is called the voidage or the bed porosity. The porosity is usually an isotropic property (i.e. the same in all directions) hence the interstitial velocity is simply related to the superficial velocity by equation(46), which comes from a consideration of fluid continuity.

$$U = \frac{U_0}{\varepsilon} \tag{46}$$

When the bed is full of solids (porosity is zero –possible with cubic particles placed carefully within the bed) the resistance is infinite. When no solids are present and the porosity is unity, the interstitial velocity will be same as the superficial velocity. The resistance to the fluid flow gives rise to a pressure drop in the fluid (ΔP).

Due to the complexity of flowing through porous media, the following assumptions are made to enable a theoretical derivation[43].

(1) Inner geometry of the porous media is isotropic and homogeneous, thus, the fraction of void area to total area of a typical cross-section is normally equal to the porosity.

(2) Pressures on the same cross-section are consistent, as well as the velocities.

(3) Air flowing through the porous media remains isothermal (room temperature). This can be explained as that there exists a considerably large interface between air and internal particle so that heat exchange is rather fast and easily to be fully completed.

The mean flow velocity, which changes with the air density along the length direction, is written in the following form:

$$V = \frac{G}{\rho A \phi} \tag{47}$$

where V is the flow velocity, G is the mass flow rate, ρ is the density, A is the cross-sectional area and ϕ is the porosity. Assuming that the air is a perfect gas, density ρ is expressed as

$$\rho = \frac{P}{R\theta} \tag{48}$$

where p is the pressure, R is the gas constant and θ is the temperature. Two cases of flow regimes, Darcy regime and Forchheimer regime, are considered to characterize the flow pattern, respectively. When the flow velocity is sufficiently small, it is greatly affected by viscous effects and proportional to the gradient of pressure, as governed by Darcy regime

$$-\frac{dp}{dx} = \frac{\mu V}{k} \tag{49}$$

where $\mu$is the air viscosity, x is the displacement along length direction and k is the permeability coefficient denoting the fundamental characteristic of porous media.On the other hand, for high velocity flow, inertial effects prevail over the viscous effects and become dominant. Forchheimer regime, which takes into account the inertial effects by adding a quadratic term on the basis of Darcy regime, describes the flow pattern as shown in equation(50).

$$-\frac{dp}{dx}=\frac{\mu V}{k}+\beta\frac{\rho v^2}{k^{1/2}} \tag{50}$$

where β is a dimensionless coefficient called inertia coefficient[43].

CHAPTER 4

NUMERICAL MODELING

Numerical modeling of the present Oxygen Transport Reactor using ion transport membrane and the porous membrane has been accomplished using the control volume approach FLUENT. The velocities, are determined midway between the grid points while the remaining variables are computed at each grid point. A staggered grid arrangement is used in the present study, which links the pressure through the continuity equation and is known as SIMPLE algorithm [88].The permeation of oxygen through the membranes and combustionis solved as a two dimensional axis-symmetric problem using the double-precision solver. To ensure convergence, the temperature, mass fraction of CO_2 and H_2O (in case of combustion) at the outlet of the fuel zone is monitored using surface monitors along with the scaled residuals. Discretization of momentum and energy equations has been done using second order upwind schemes.

The mechanism of oxygen transport through the dense perovskite LSCF 1991membrane is shown in Figure 14. At feed side oxygen molecules are absorbed on the membrane surface and converted to oxygen ions. These oxygen ions then migrate to permeate side

through the bulk via the oxygen vacancies and then it gets recombine with the holes to form oxygen molecules.

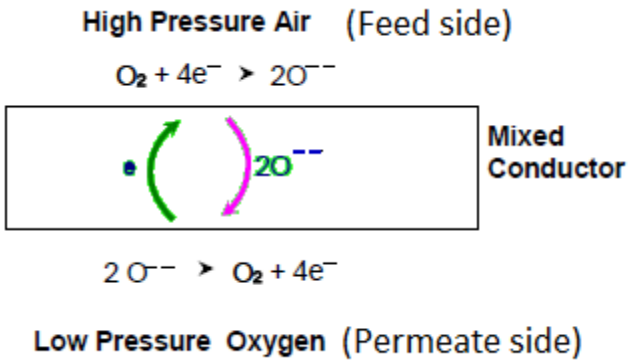

Figure 14 : Mechanism of oxygen transport through dense ion transport membrane by considering surface exchange mechanism

The CFD methods have been applied to the simulation of separation of gas from the gas mixture only in few cases [39-41, 75]. So far the CFD application to these membranes modeling study gives promising results, thus adopting CFD methodology for design and optimization of ion transport membranes for Oxy-fuel combustion power generation technologies. This work is aimed at presenting a CFD model and its applicability to the prediction of the separation behavior of a perovskite membrane for oxygen separation and also to study the combustion characteristics to achieve uniform temperature distribution along the length of the ITM by introducing fuel using a porous membrane. Simulations were run under different partial pressures and the predictive capability of the model is shown.

4.1 CFD Methodology and Numerical Solutions:

4.1.1 Scope of CFD:

Computational Fluid Dynamics modeling for gas transport could be considered as a powerful tool to study the separation of a gas (O_2) from a gas mixture (air).The objective is to visualize the flow and gas mixing inside the reactor. The current CFD model can predict the mass flow through the membrane, coupling the species transport with the defined mechanism of permeation. The permeation flux, local composition of the mass fractions within the gas mixture can be predicted using the governing equations as presented in the next section.

4.1.2 Governing equations:

The numerical simulations are based on the CFD methodology developed by Coroneo et al [41] which was developed in the realm of a finite volume method. The velocity and the pressure fields of the gas mixture are obtained from the numerical solution of the mass, momentum, energy equations, while the species concentration distribution and the fluxes at the permeate and the feed side are obtained by the scalar convection-diffusion equation including source term to account the mass flow of the species across the membrane.

The steady state equations for conservation of mass, momentum, and energy and species equation for Newtonian fluids were considered:

$$\nabla.(\rho U) = S_i \tag{51}$$

$$\nabla.(\rho UU) = -\nabla p + \mu\nabla^2 U \tag{52}$$

$$(\rho C_p)_f U \cdot \nabla T = \nabla\bullet(k_f \nabla T) \tag{53}$$

$$\nabla \cdot (\rho U Y_i) - \nabla \cdot (\rho D_{i,m} \nabla Y_i) = S_i \tag{54}$$

Where U it the velocity vector, ρ is the fluid density, p is the pressure, μ is the dynamic viscosity, S_i is the source or sink term. The source S_m is the mass added to the continuous phase. The S_i source/sink term accounts for the mass flow of species across the membrane. At the membrane boundary cells the species are allowed to disappear from one of the membrane sides through a sink term and to come out on the other through a source term. To apply this methodology the preliminary knowledge of the permeability characteristic of the membrane is required to formulate the source term. The diffusion coefficient was determined by specifying $D_{i,j}$, the binary mass diffusion coefficient of the component *i* in the component *j*. The corresponding diffusion coefficient in the mixture, $D_{i,m}$, is computed as [58].

$$D_{i,m} = \frac{1 - X_i}{\sum_{j, j \neq i} \left(\frac{X_i}{D_{i,j}} \right)} \tag{55}$$

Where X_i is the mole fraction of species i. The binary mass diffusion coefficient, $D_{i,j}$ are calculated by Chapman-Enskog formula using kinetic theory [76].

In the present work, the source term takes in account of only oxygen permeation across the ion transport membrane as given by the following expression.

$$S_i = \begin{cases} + \dfrac{J_{O_2} \cdot A_{cell}}{\mathrm{V}_{\mathrm{cell}}} & \text{At permeate side} \\ - \dfrac{J_{O_2} \cdot A_{cell}}{\mathrm{V}_{\mathrm{cell}}} & \text{At feed side} \end{cases}$$

Special source terms are applied in continuity and species transport equations on the computational cells adjacent to the membrane, in order to couple the equations to the volumetric-basis. It is worth observing that the driving force in the source term is evaluated adopting local values, thus removing the assumption of lumped parameter models.

Porous jump condition [58] is used to model thin "Porous membrane" that has known velocity (pressure-drop) characteristics. It is essentially a 1D simplification of the porous media model available for cell zones. This simpler model is used (instead of the full porous media model) because the results obtained using this condition are in good agreement with the experimental results (validated against the experimental results of Zhong et al[43]) and also it is more robust and yields better convergence.

The porous medium has a finite thickness over which the pressure change is defined as a combination of Darcy's Law and an additional inertial loss term:

$$\Delta p = -(\frac{\mu}{\alpha} \upsilon + C_2 \frac{1}{2} \rho \upsilon^2) \Delta m \qquad (56)$$

where ‘ μ ’ is the laminar fluid viscosity, ‘$\propto$’ is the permeability of the medium, ‘C_2’ is the pressure-jump coefficient, ‘ν’ is the velocity normal to the porous face, and ‘Δm’ is the thickness of the medium.

4.1.3 Radiation model:

In order to include the effects of radiation on the present oxygen transport reactor "Discrete Ordinates" radiation model has been used.The discrete ordinates (DO) radiation model solves the radiative transfer equation (RTE) for a finite number of discrete solid angles, each associated with a vector direction $\vec{s}$ fixed in the global Cartesian system (x,y,z)[58].

The DO model considers the radiative transfer equation (RTE) in the direction $\vec{s}$ as a

$$\nabla \cdot (I(\vec{r},\vec{s})\vec{s}) + (a+\sigma_s)I(\vec{r},\vec{s}) = an^2\frac{\sigma T^4}{\pi} + \frac{\sigma_s}{4\pi}\int_0^{4\pi} I(\vec{r},\vec{s}')\Phi(\vec{s}\cdot\vec{s}')\,d\Omega' \quad \text{.....(57)}$$

Here 'n' is the refractive index and is taken as unity. The absorption coefficient (1/m) of the gases is modeled using weighted sum of gray gases model (WSGGM). It is a reasonable compromise between the oversimplified gray gas model and a complete model which takes into account particular absorption bands. The internal emissivity of all the walls and membranes is taken as 0.8.

4.1.4 Geometry and domain generation (For validation):

The grid for simulations was generated by using the meshing software GAMBIT. Validation for ITM and porous Jump model has been done individually;therefore two separate grids have been prepared. The dimensions of the computational domain were identical with that of experimental setup for ITM model (used by Kusaba et al[77]) as well as Porous Jump model (used by Zhong et al [43]). The membrane cell computational geometry for ITM model validation, as show in Figure 15, consisted of

mass flow inlet, boundary for introducing the feed in two fluid zones i. e, Air feed and Sweep(N_2) feed and two pressure outlets for retentate and permeate flows. The membrane in the domain was defined as shadowed wall, while all other edges represented the barriers of the remaining cell geometry. The computational grid consisted of axis-symmetric 2D dimensional domain. Effect of gravity is neglected.

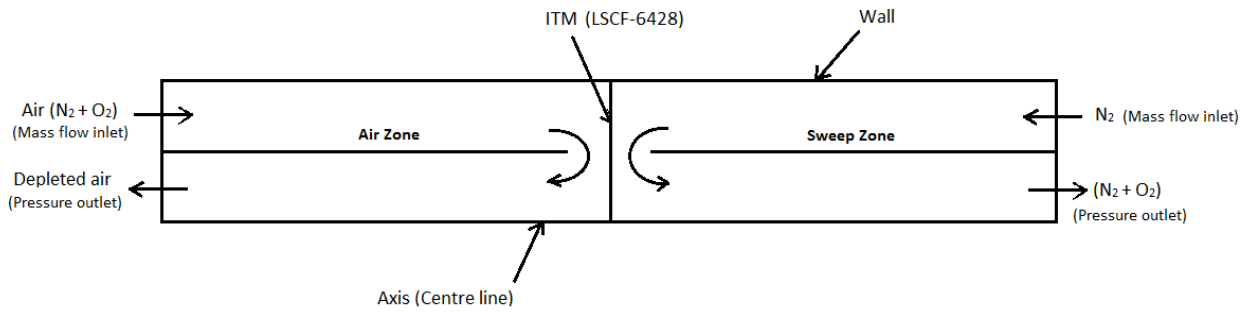

Figure 15 : ITM disc membrane model used for validation (Ref: [19])

The 2D axi-symmetric computational domain for Porous membrane model validation, is shown in Figure 16, consists of mass flow inlet boundary for introducing fluid at the inlet and one pressure outlet boundary condition at the outlet. The porous membrane in the domain was defined as POROUS JUMP boundary condition, while all other edges represented the barriers of the remaining cell geometry.

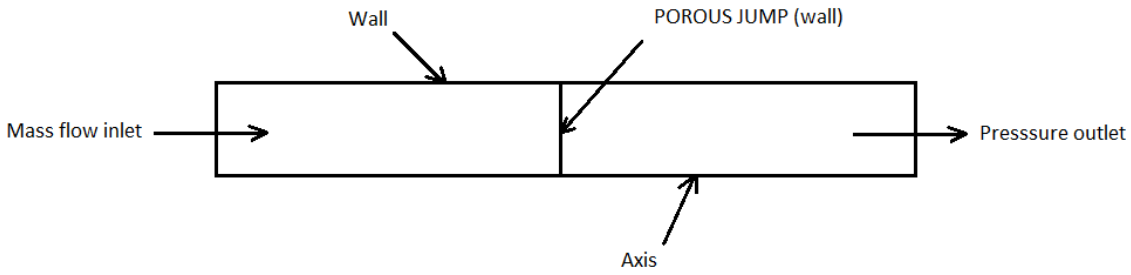

Figure 16: 2D Axi-symmetric model for porous jump (Boundary condition) validation(Ref: [43])

4.2 Validation:

There are two models used for the present study. The first one is the user defined function (UDF) used to model ITM and the second one is the POROUS JUMP boundary condition used to model the porous membrane. The validation for these models with experimental results are done individually choosing the geometry and physical properties of kusaba et al[77]and Zhong et al[43] respectively (shown in Figure 15, Figure 16 respectively).

4.2.1 ITM (UDF) validation:

Xu et al [19] reported studies on oxygen separation using LSCF membranes for different partial pressures of air for increasing temperature conditions and has come up with expressions for the same. The experimental conditions were maintained at steady state with laminar flow. The validation for the UDF, used to model the ITM in the present study, is done against the experimental results of kusaba et al[77] using the flux equation(58) given by Xu et al[19].

$$J_{O_2} = \frac{D_v k_r \left[(P'_{O_2})^{0.5} - (P''_{O_2})^{0.5} \right]}{2Lk_f (P''_{O_2})^{0.5} (P'_{O_2})^{0.5} + ((P'_{O_2})^{0.5} + (P''_{O_2})^{0.5}) D_v} \quad (58)$$

The values of the pre-exponential coefficients(D_v, K_r, K_f) and activation energies have been fitted to the experimental results of kusaba et al[77](LSCF 1991). The values of D_v, K_r, K_f for LSCF 1991 are given in **Table 1**.

Table 1 : D_v, K_f, K_r values for present calculations

Expression	Pre-Exponential coefficients		Activation Energy (kJ/mol)
	Unit	Value	
$D_v = D_{v0}\, e^{(-E_D/RT)}$	cm^2/s	1.58×10^{-1}	73.6
$K_f = k_{f0}\, e^{(-E_f/RT)}$	$cm/atm^{0.5}.s$	1.11×10^{12}	226.9
$K_r = k_{r0}\, e^{(-E_r/RT)}$	$mol/cm^2.s$	3.85×10^{7}	241.3

Figures 17-19shows the comparison of oxygen permeation fluxes, for three different thicknesses of the membranes (0.8mm, 1mm, 2mm respectively), obtained in the present calculations with that of the experimental results.

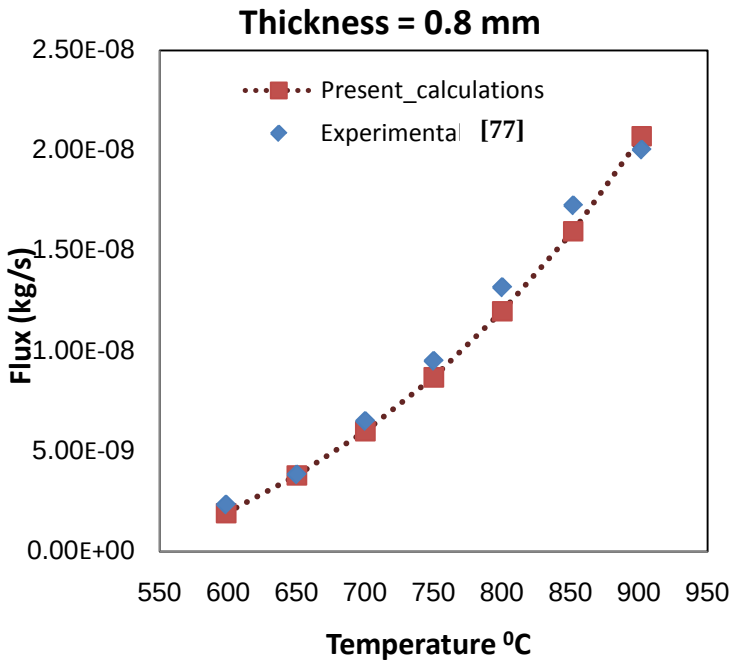

Figure 17: Variation ofoxygen flux with increasing membrane temperature for a membrane thickness of 0.8mm

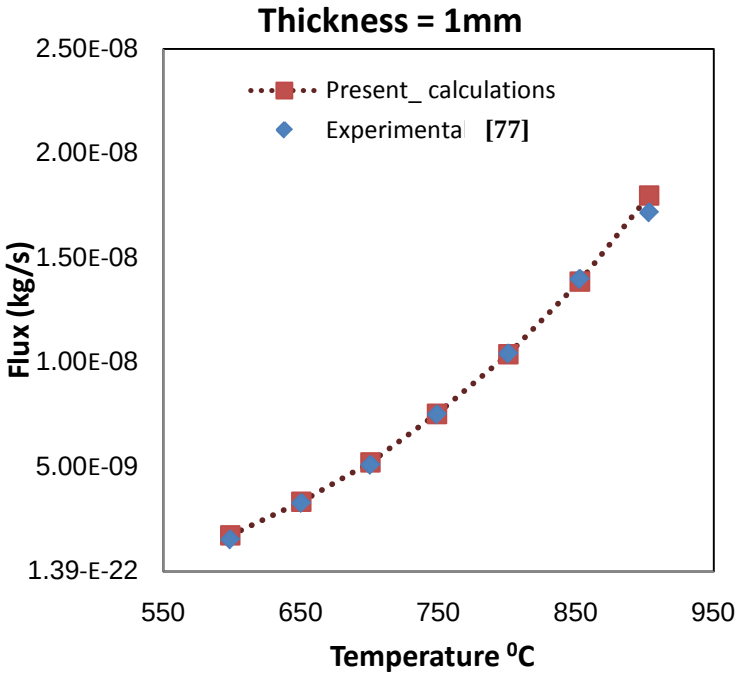

Figure 18: Variation ofoxygen flux with increasing membrane temperature for a membrane thickness of 1mm

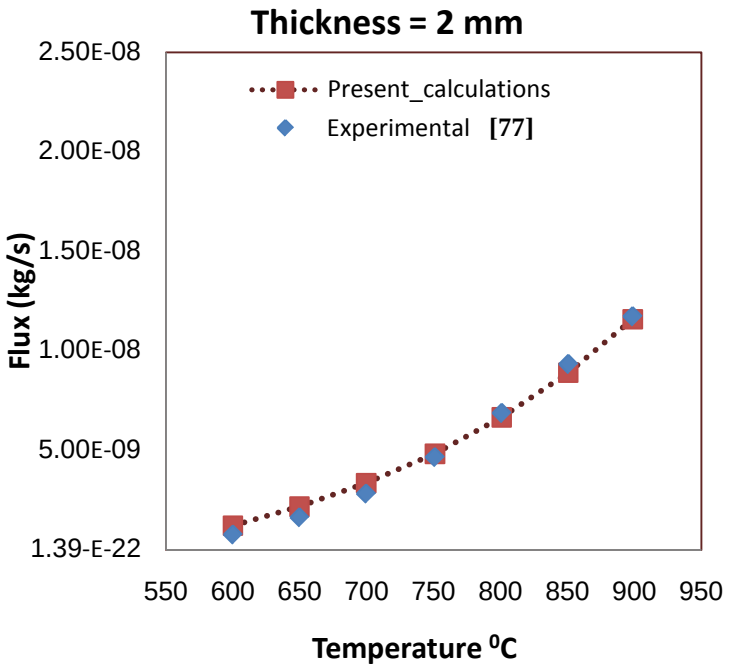

Figure 19: Variation ofoxygen flux with increasing membrane temperature for a membrane thickness of 2mm

The results show that the present model for ITM is in good agreement with the experimental results. The percentage error between the present numerical results and that of the experiments is found out to be less than 25 which is well in the acceptable range. Since the present calculations are very close to the experimental results obtained with 1mm thickness membrane, therefore 1mm thick ITM is considered to model the present oxygen transport reactor (isothermal reactor) under study.

4.2.2 Porous membrane validation:

The porous membrane is modeled using the POROUS JUMP boundary condition as described in the earlier sections. Darcy's law, given by equation(59), is used to model the porous membrane.

$$\Delta p = -(\frac{\mu}{\alpha}\upsilon + C_2 \frac{1}{2}\rho\upsilon^2)\Delta m \tag{59}$$

This model is validated against the experimental results of Zhong et al[43] for four porous membranes of different diameters and thicknesses. Figure 20 shows the comparison of the experimental results of Zhong et al[43] and the present numerical simulations for four porous membranes of different diameters and thicknesses. The percentage error is found out to be less than 3, which shows that the current model used for porous membrane is reliable and can better capture the results with less computational time and effort.

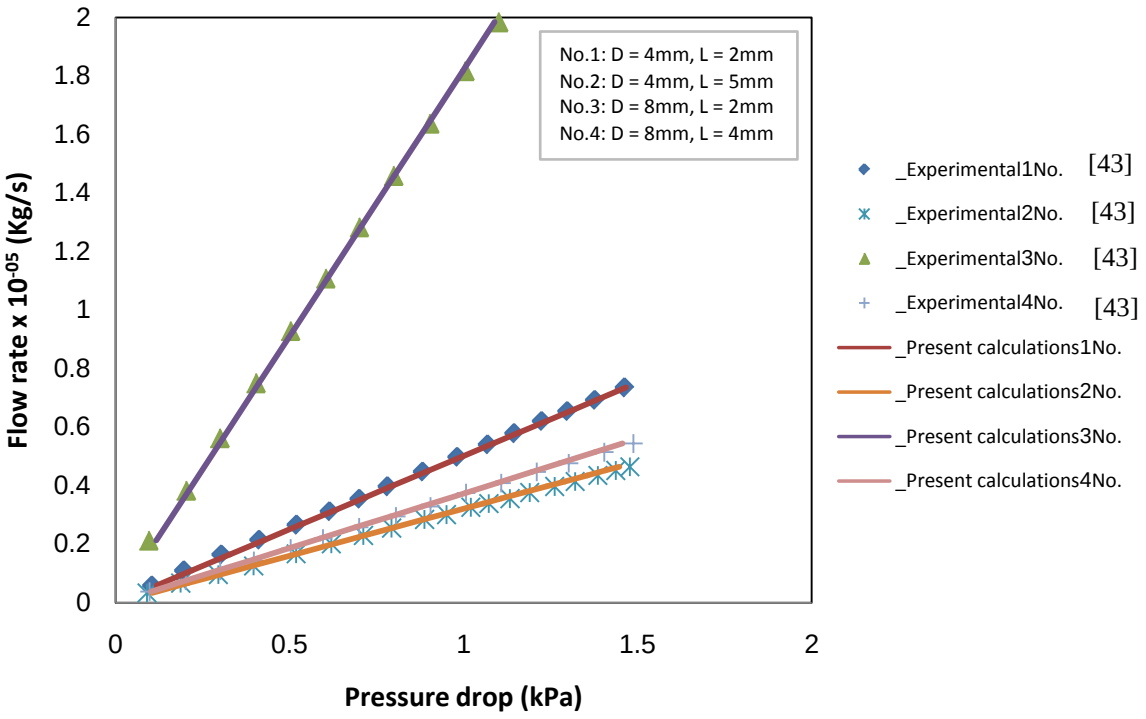

Figure 20: Pressure drop for different flow rates for four different porous membranes

4.3 Grid Independent Test:

4.3.1 Computational grid details:

GAMBIT software was used to generate the grid. Figure 21 shows the computational grid for the model being studied. The reactor is divided into three zones;the top zone for the inlet of air, the middle zone for sweep inlet and the bottom zone for fuel mixture inlet. UDF is used to model ITM and a POROUS JUMP boundary condition is used to model the porous media. The grid was made fine near to the ITM and the porous walls. An aspect ratio of less than 2 is used for the grid.

4.3.2 Grid independency test results:

In order to ensure grid independence, a grid independence test must be performed to choose a suitable grid. Figure 21 shows the computational grid for modeling the reactor under study. It can be seen that the grid is made fine near to the ITM and porous membrane in order to capture the gradients accurately. Three different grids with nodal densities 10000, 15000, 20000 were used for this test. Grids with nodes more than 20000 were also used for the grid independency test. It showed no obvious advantage but rather increased the computational effort and time.

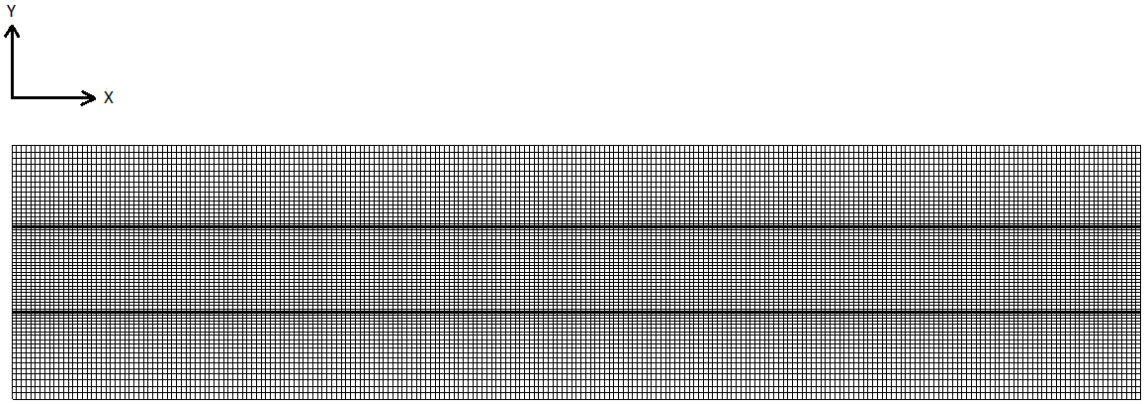

Figure 21: Computational grid for the present study of oxygen transport reactor

Mass flow rate of the air and sweep gas (CO_2)is taken as 0.3 kg/s and 1×10^{-06} kg/s respectively. Mass flow rate of the fuel mixture is taken as 0.00075 kg/s, where the mass fraction ratio of CH_4/CO_2 used is 0.2/0.8. Figure 22 shows the temperature on the permeate side of the ITM for three grids mentioned above. It is clear from the figure that the grid with nodes 10000 could not capture accurate results whereas grids with nodes 15000 and 20000 overlap. Similar results are found for the mass fraction distribution of CH_4 along the centre line of the reactor, shown in Figure 23. These observations show that the accuracy of the solution with the 15000 nodes grid is deemed to be satisfactory for the present simulations and gives better visualization of flow parameters.

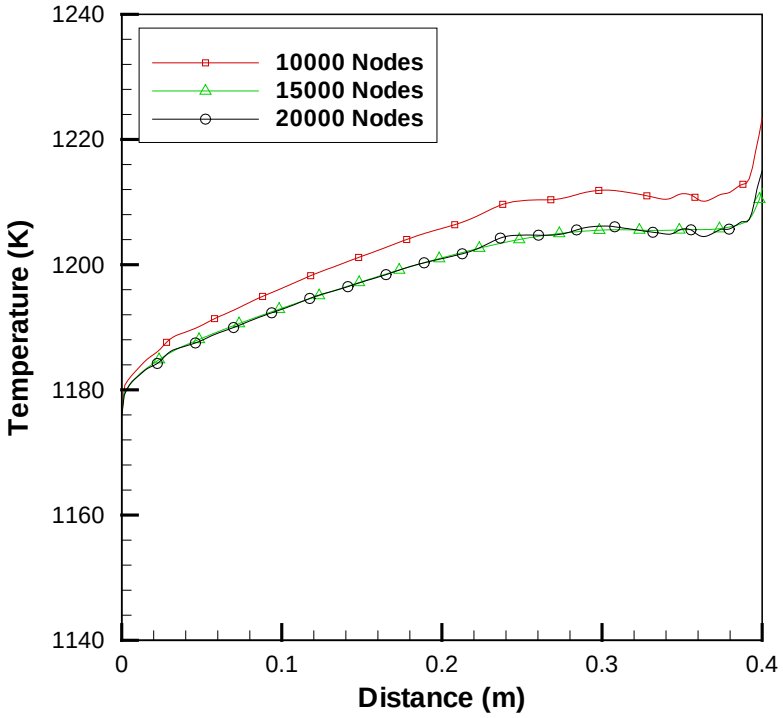

Figure 22: Grid Independency test: Temperatures on the permeate side of the ITM

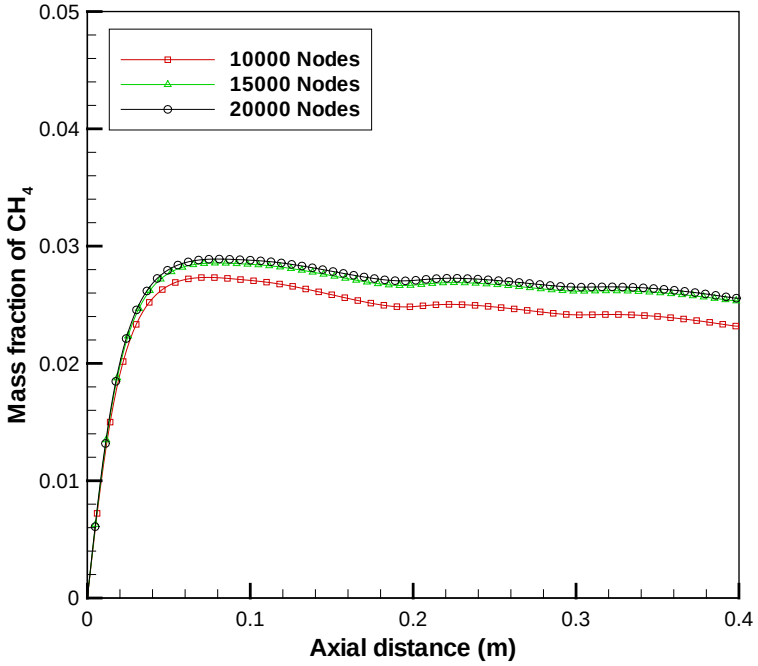

Figure 23: Grid Independency test: Mass fraction of CH4 at the centre line of the oxygen transport reactor

Table 2 presents the maximum temperature obtained using four different grids and the error has been calculated. The percentage error has been calculated with reference to the maximum temperature obtained using the grid with nodes 25000. It has been observed that error with 15000 nodes grid is less than 1%. With grids more than 15000 nodes does not show any obvious advantage. Hence for further case studies the grid with 15000 nodes has been used.

Table 2: Grid independency test:

No. of Nodes	Maximum temperature (K)	Percentage error (%)
10000	1209	2.9 > 1
15000	1245.1	0.13 < 1
20000	1246.67	0.025 < 1
25000	1246.8	---

CHAPTER 5

RESULTS AND DISCUSSIONS

In the present study a two dimensional model is used to simulate the combustion characteristics in an oxy-fuel reactor.This chapter consists of three sections. In the first section, results depicting the fluid flow and oxygen permeation fluxof non-reactive (separation only)cases are discussed. In the second section results of reactive (separation and combustion) cases i.e. the fluid flow, oxygen permeation flux and combustion characteristics are discussed. Finally in the third section the advantages of the present model reactor under investigation over the conventional co-feed reactor are presented.

5.1 SeparationOnlyMode (Non-reactive cases)

In this work the performance of an oxygen transport reactor using ITM-LSCF membrane [$La_{0.1}Sr_{0.9}Co_{0.9}Fe_{0.1}O_{3-\delta}$] with the dimensions given in Figure 10 was investigated. The study focuses on the effect of partial pressures of oxygen on both the feed side and the permeate side of the ITM membrane. The composition of the gas mixture on the permeate side, while the reactor is operating at 1 atm, has also been studied. The mass flow rate of air on the feed side of the ITM is kept constant, a value of 0.03kg/s, throughout the study. Air is assumed to consist of N_2 (77% by mass) and O_2 (23% by

mass). The mass flow rate of sweep gas (CO_2) in the middle channel (i.e. sweep channel) is also kept constant; a value of 1×10^{-06}, throughout the study. The flow considered is laminar and steady in nature. The inlet temperature of all the gases is kept constant at 1173K throughout the study. The temperature is so chosen as it is believed to give the maximum oxygen permeation fluxes for particular LSCF membranes [77] and is well in the operating range of ITM's for stability purpose [78]. As discussed in the earlier section, the porous membrane is divided into four equal parts and is assigned ascending order porosities from inlet to the exit of the reactor. The four porous membranes are designated as P1, P2, P3, and P4 and are given their respective face permeabilities as 1.47×10^{-20} m^2, 3.47×10^{-13} m^2, 1.47×10^{-12} m^2, 2.47×10^{-12} m^2. These values are selected randomly to obtain the desired uniform stoichiometric ratio all along the length in the middle channel. The CO_2 gas is used in the fuel mixture not only to control the flame temperature but also to make up the volume of the missing N_2. Argon gas is used in the fuel mixture in order to increase the fuel flow rate to ensure that there is enough gas to carry CH_4/CO_2 mixture all through the length to the other side of the porous membrane. The mass fraction of Argon gas in the fuel mixture is kept constant at 0.75 throughout the study. The remaining mass fraction of fuel mixture i.e. 0.25 comprises of CH_4 and CO_2.The mass fraction of this fuel mixture ($CH_4+CO_2 = 0.25$) has been varied. The variations of CH_4/CO_2 in this fuel mixture are presented in terms of their relative percentages. Table 3shows the relative percentages of CH_4 and CO_2in the fuel mixture.

Table 3: Relative percentages of CH_4 and CO_2 in the fuel mixture(On mass basis)

Case	*Massfractions in fuel mixture*			Re*lative percentages of* CH_4 *and* CO_2	
	Y_{Ar}	Y_{CH_4}	Y_{CO_2}	CH_4	CO_2
1	0.75	0.0025	0.2475	1%	99%
2	0.75	0.01	0.24	4%	96%
3	0.75	0.02	0.23	8%	92%
4	0.75	0.05	0.2	20%	80%
5	0.75	0.15	0.1	60%	40%
6	0.75	0.25	0	100%	0%

Thermal conductivity of perovskite membranes such as LSCF, $BaCeO_3$, $BaZrO_3$ ranges from 5-12 W/m/K for temperature operation in the range 500-1000 ^oC [79, 80]. In the present simulation the thermal conductivity of LSCF is assumed 4 W/m/K.To study the ITM characteristics and the composition of gas mixture on the permeate side of the ITM the numerical simulations are carried out with the conditions shown in Table 4.

Table 4: List of parameters and their values

Parameter	Value
$\dot{m}_{air}$	0.03 Kg/s
$\dot{m}_{sweep,\ CO_2}$	1×10^{-6} Kg/s
$\dot{m}_{fuel,\ (CH_4+CO_2+Ar)}$	0.00075kg / s
$T_{inlet,air}$	1173 K
$T_{inlet,sweep}$	1173 K
$T_{inlet,fuel}$	1173 K
$CH_{4,fuel\ mixture}$	4%
$CO_{2,fuel\ mixture}$	96%
ρ_{ITM}	6000 Kg/m^3
λ_{ITM}	4 W/m/K

The partial pressure on the feed and permeate sides along with the oxygen flux for a constant mass flow rate of fuel mixture is presented in Figure 24. Figure 24(a) shows the partial pressure of oxygen on the feed side and permeate sides of the ITM. The corresponding flux of oxygen is shown in Figure 24(b). It is observed that the partial pressure of oxygen on the permeate side of the ITM is zero at the inlet as there is no oxygen. It increases gradually as the oxygen starts permeating and then becomes constant. On the other hand the partial pressure of oxygen on the feed side is 0.21 bar at the inlet and then reduces slightly, because of the permeation of oxygen to the permeate side, and remains constant all along the length. The oxygen flux shows a very high value at the inlet and then reduces suddenly until it reaches a constant value. This can be explained from the zero partial pressure value at the inlet. The zero partial pressure at the inlet causes Δp across the ITM to reach a maximum value. As flux is a primary function

of Δp across the ITM membrane, the increase in Δp causes the oxygen permeation flux to increase. Therefore the oxygen flux starts with a maximum value at the inlet. When the oxygen molecules starts migrating to the permeate side, i.e. when desorption of oxygen ions takes place on the permeate side, the partial pressure on the permeate starts building up causing Δp to reduce along the length of the ITM and then becomes constant. As a result, the oxygen flux also becomes stable attaining almost a constant value all along the length of the ITM.

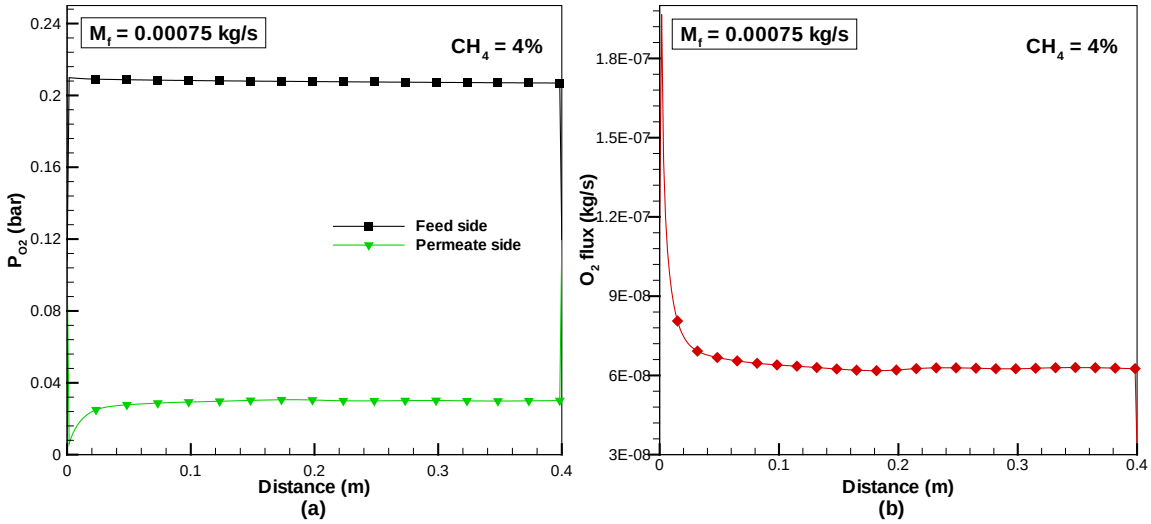

Figure 24: (a) Partial pressure of O_2 on the feed and permeate side of the ITM; (b) Flux of O_2 for a constant mass flow rate of fuel mixture

Figure 25(a) shows the mass fraction distribution of species along the centre line of the reactor. The corresponding ratio of O_2/CH_4 (approximately uniform) along the centre line is presented in Figure 25(b). It is observed that the mass fraction of CH_4 and O_2 along the centre line of the reactor for the case considered is same and therefore they overlap with each other. The mass fraction of CO_2 starts at 1 and then decreases until it becomes

constant. The high mass fraction value of CO_2 at the inlet is because of the introduction of some amount of CO_2 in the middle/sweep channel. It is evident from Figure 25(b) that the present reactor model can deliver the desired uniform O_2/CH_4 ratio throughout the length of the reactor and may be used to obtain uniform temperature all along the length of the ITM membrane.

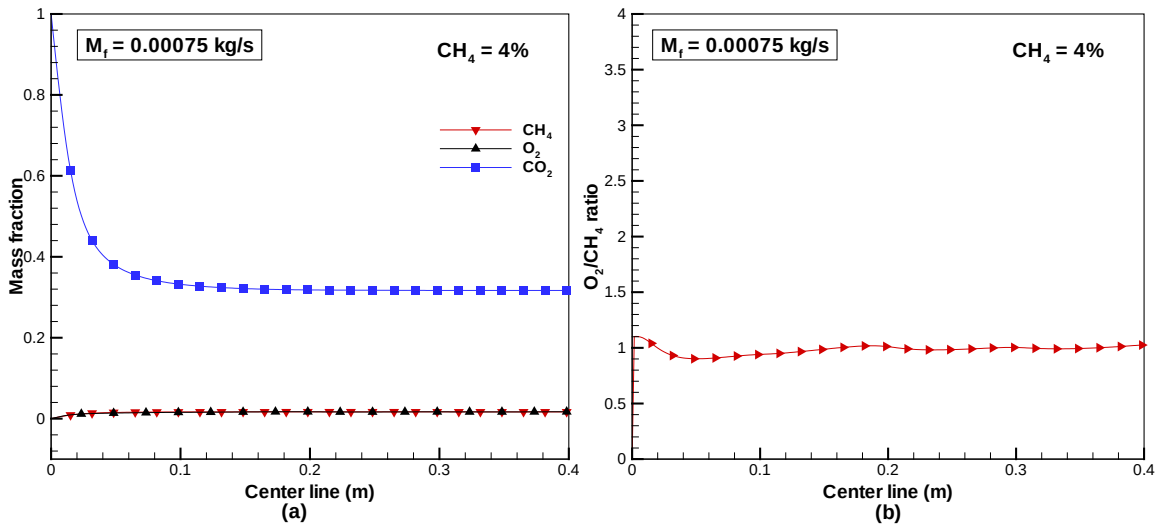

Figure 25: (a)Mass fraction (b)O_2/CH_4 ratio for mass flow rate of 0.00075kg/s

5.1.1 Effect of variation of CH_4/CO_2 ratio in the fuel mixture on oxygen permeation flux for non-reactive cases:

The effect of CO_2 concentration in the fuel gas mixture on the permeation flux of oxygen through the ion transport membrane (LSCF) has been investigated for non-reactive cases.Themass fraction of CO_2 in the fuel mixture has been varied for a constant mass flow rate of 0.00075 kg/s.Six CH_4/CO_2 mixtureswith different CH_4 concentrations, ranging from 1% (relative percentage of CH_4/CO_2 in fuel mixture) of CH_4 (remaining is CO_2) to 100% CH_4,were considered. Figure 26 shows the partial pressure on the feed and

permeates side, next to the surface of the ITM, for increasing percentage of CH_4 (the remaining is CO_2) in the fuel mixture.It was observed that with the increasing percentage of CH_4in the fuel mixture, the partial pressure of oxygen on the permeate side changed while on the feed side remained almost unaffected.

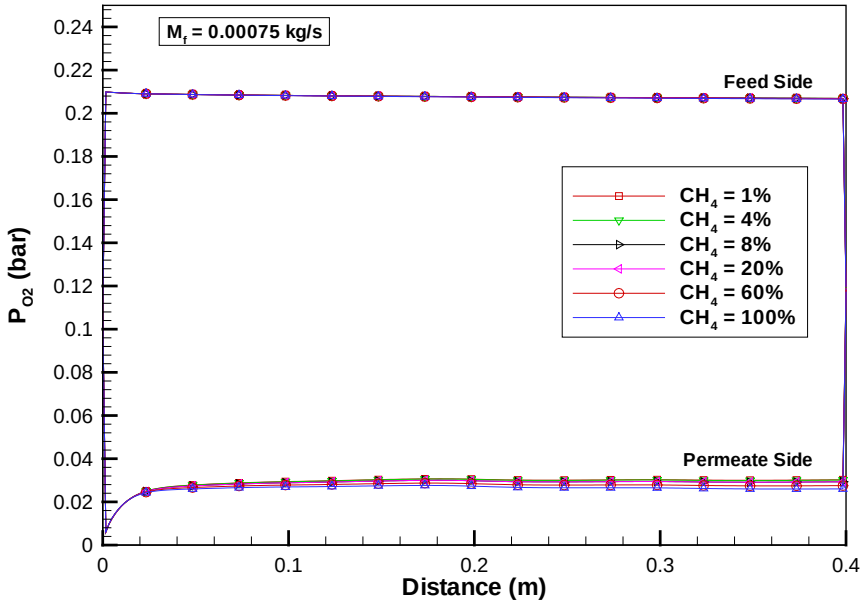

Figure 26: Partial pressures of O_2on feed and permeate side of the ITMwithvarying CH_4 percentage for a constant mass flow rate of 0.00075kg/s

In order to analyze the differences clearly, the partial pressure of oxygen on the permeate side for different CH_4% are presented in Figure 27. The corresponding flux of O_2 is shown in Figure 28.It has been observed that with decrease in the percentage of CO_2(or increase in the percentage of CH_4) in the fuel mixture the partial pressure of oxygen on the permeate side decreases and the corresponding oxygen flux increases. This may be attributed to the higher molecular weight (44) and lower mass diffusivity of CO_2. Due to

the higher molecular weight of CO_2, with decrease in the percentage of CO_2 the density of the mixture (shown in Figure 29) decreases. This decrease in density of fuel mixture is consistent with the increase in volume flow rate, which is shown in Figure 30, of the gases. Thus, for the same mass flow rate,with decrease in the concentration of CO_2 the volume flow rate of the gases increases. These observations are confirmed by the flame sizes of the oxy-fuel and air–fuel cases obtained in the study by Habib et al[81]. This increase in volume flow rate of gases sweeps away the permeated oxygen quickly causing the partial pressure of oxygen on the permeate side to decrease leading to a higher oxygen permeation driving force. This may be attributed to the purging of permeated oxygen on the permeate side. On the other hand lower mass diffusivity of CO_2(since the mean free path is inversely proportional to the density of the gas) also contributes to the increase in volume flow rate with decrease in CO_2 mass fraction in the mixture.Therefore it is evident that with decrease in the concentration of CO_2 (or increase in the concentration of CH_4), for a constant mass flow rate, the permeation flux of oxygen increases.

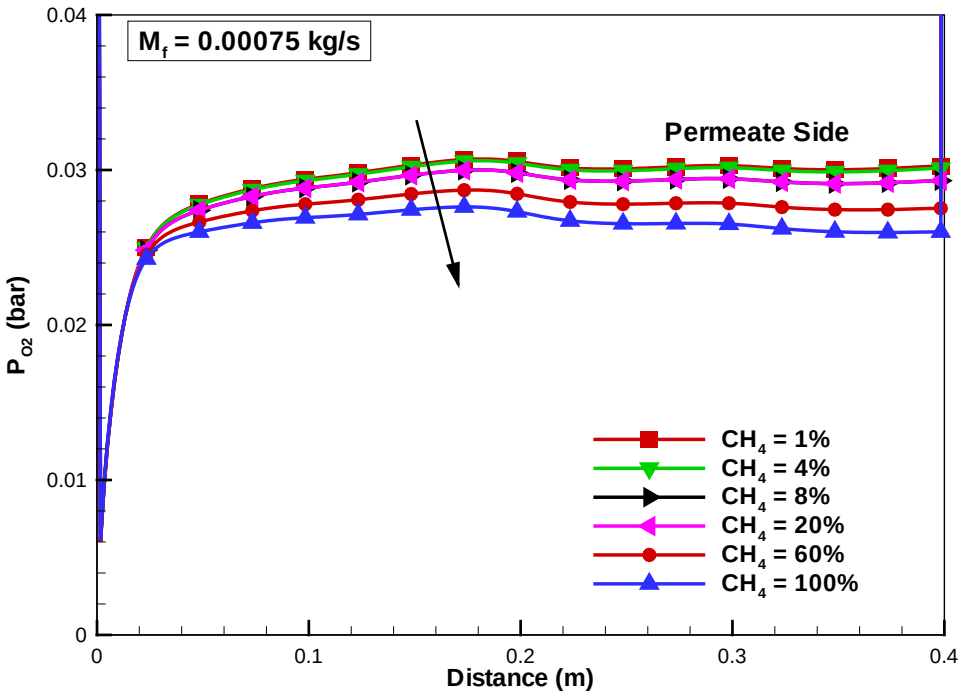

Figure 27: Partial pressure of O_2 on the permeate side of ITMwith varying CH_4 percentage for a constant mass flow rate of 0.00075kg/s

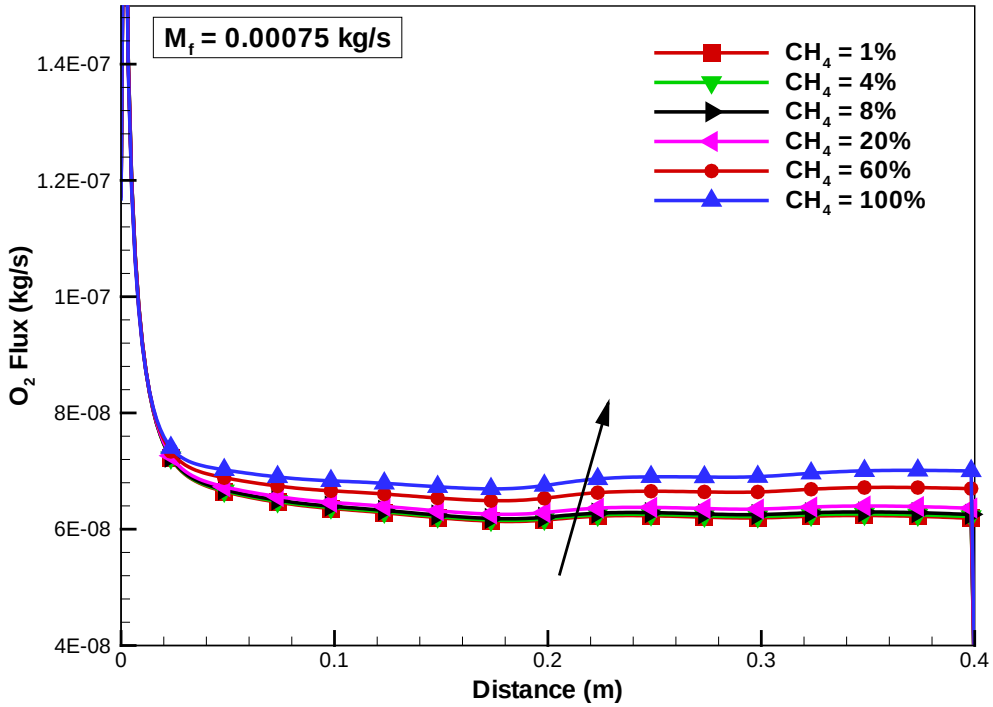

Figure 28: Oxygen flux on the permeate side of the ITMwith varying CH_4 percentage for a constant mass flow rate of 0.00075kg/s

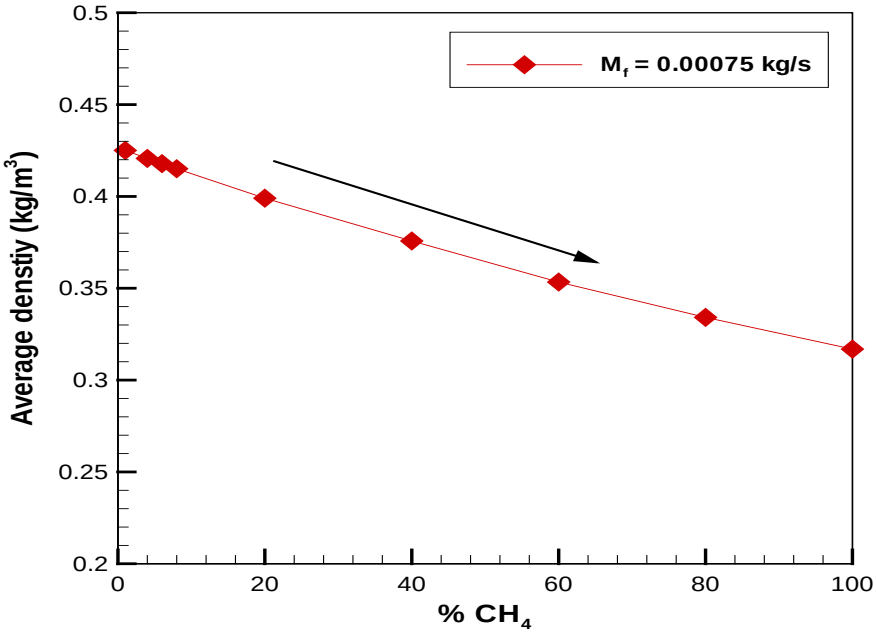

Figure 29: Averagedensity of gas mixtureat the exit of the reactor with increasing CH_4 percentage for a constant mass flow rate of 0.00075kg/s

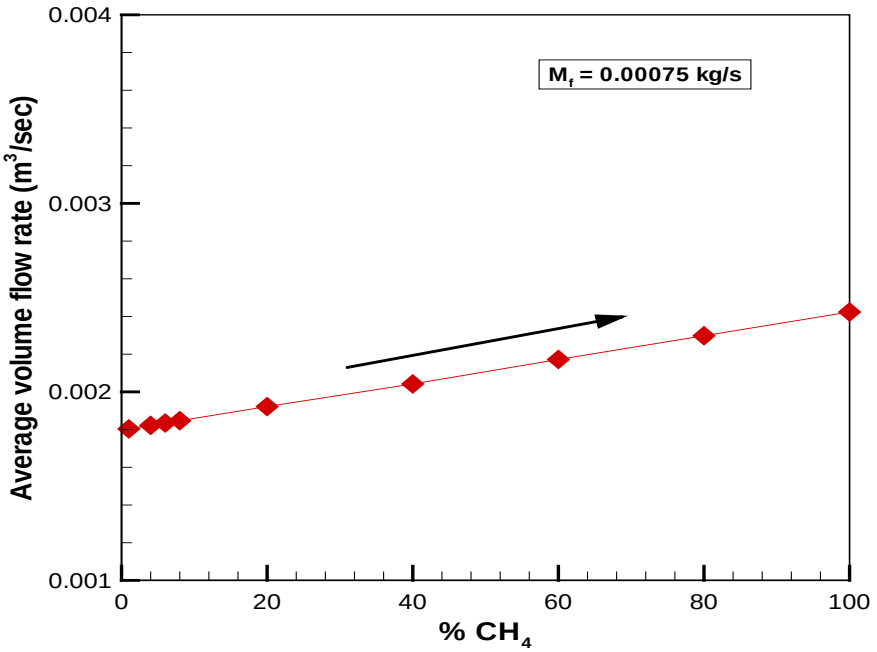

Figure 30: Average volume flow rate of the gas mixture at the exit of the reactor with increasing CH_4 percentage for a constant mass flow rate of 0.00075kg/s

Figure 31shows the mass fraction of CH_4 along the centre line of the reactor for the fuel mixture mass flow rate of 0.00075 kg/s for increasing percentage of CH_4 in the fuel mixture. In the region near to the inlet i.e. for approximately 0.1m the mass fraction of CH_4 increases gradually and then becomes constant. This is because of very low permeability of the porous membrane near to the entrance of the reactor. Figure 32 shows the corresponding mass fraction of O_2 along the centre line for the same mass flow rate of 0.00075 kg/s. It is observed that with increase in the mass fraction of CH_4 in the fuel mixture the mass fraction of oxygen also increases. As explained earlier that with increase in mass fraction of CH_4, for a constant mass flow rate of fuel mixture, the density decreases and hence the volume flow rate increases and this was attributed to the purging of permeated oxygen.

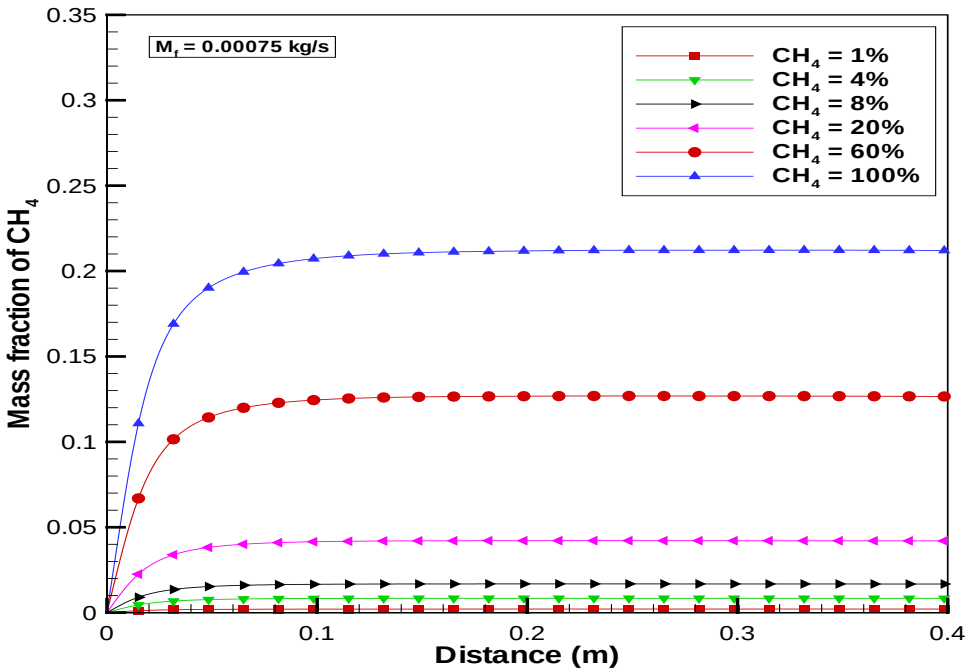

Figure 31: Mass fraction of CH_4 along the center line of the reactor with varying CH_4 percentage for a constant mass flow rate of 0.00075kg/s

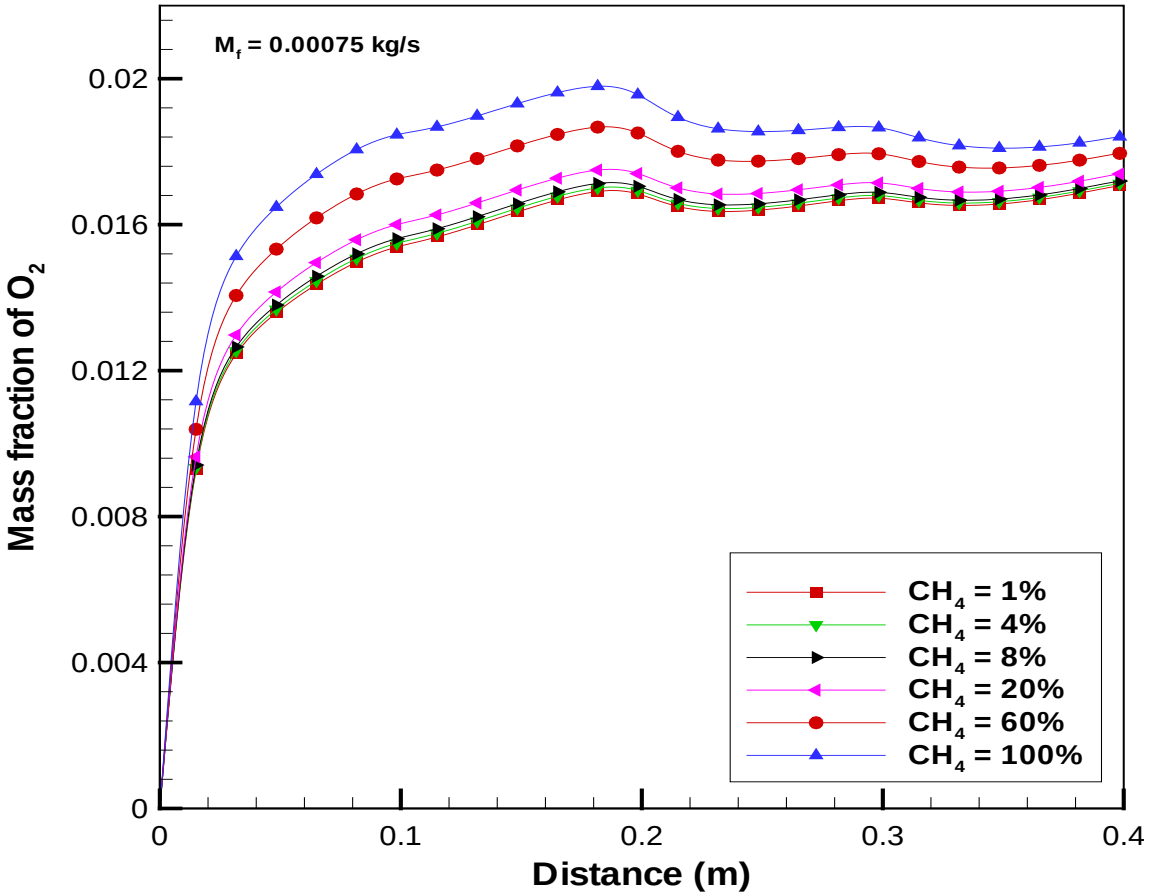

Figure 32: Mass fraction of O_2 along the center line of the reactor with varying CH_4 percentage for a constant mass flow rate of 0.00075kg/s

Figure 33 and Figure 34 show the normal profiles of mass fraction of CH_4 and $O_2$for increasing CH_4 percentage at a distance of 200mm from the entrance at a constant mass flow rate of 0.00075 kg/s. It has been observed that the diffusion of CH_4 decreases slightly from the porous membrane towards ITM. On the other hand the diffusion of O_2 decreases significantly as we move from ITM towards the porous membrane due to the resistance of the incoming CH_4/CO_2 mixture.

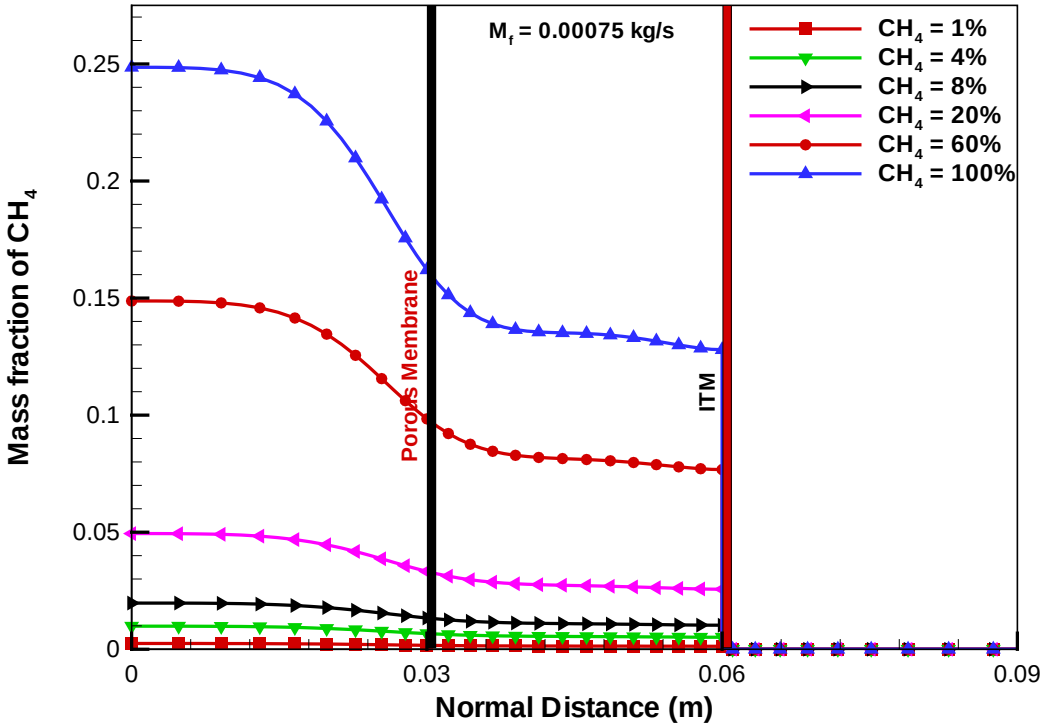

Figure 33: Normal profiles of mass fraction of CH_4 at a distance of 200 from the entrance of the reactor with varying CH_4 percentage for a constant mass flow rate of 0.00075kg/s

It is observed, from Figure 34, that small mass fractions of O_2 appear in the bottom channel (0. 2 to 0.3 m in Figure 34) even though the pressure in the bottom channel is higher than the middle channel (0.03 to 0.06 m in Figure 34). This may be because of the diffusion of O_2 due to partial pressure difference in both these channels. However in case of the reactive casesit becomes almost negligible. The results of the reactive cases are presented in the next section.

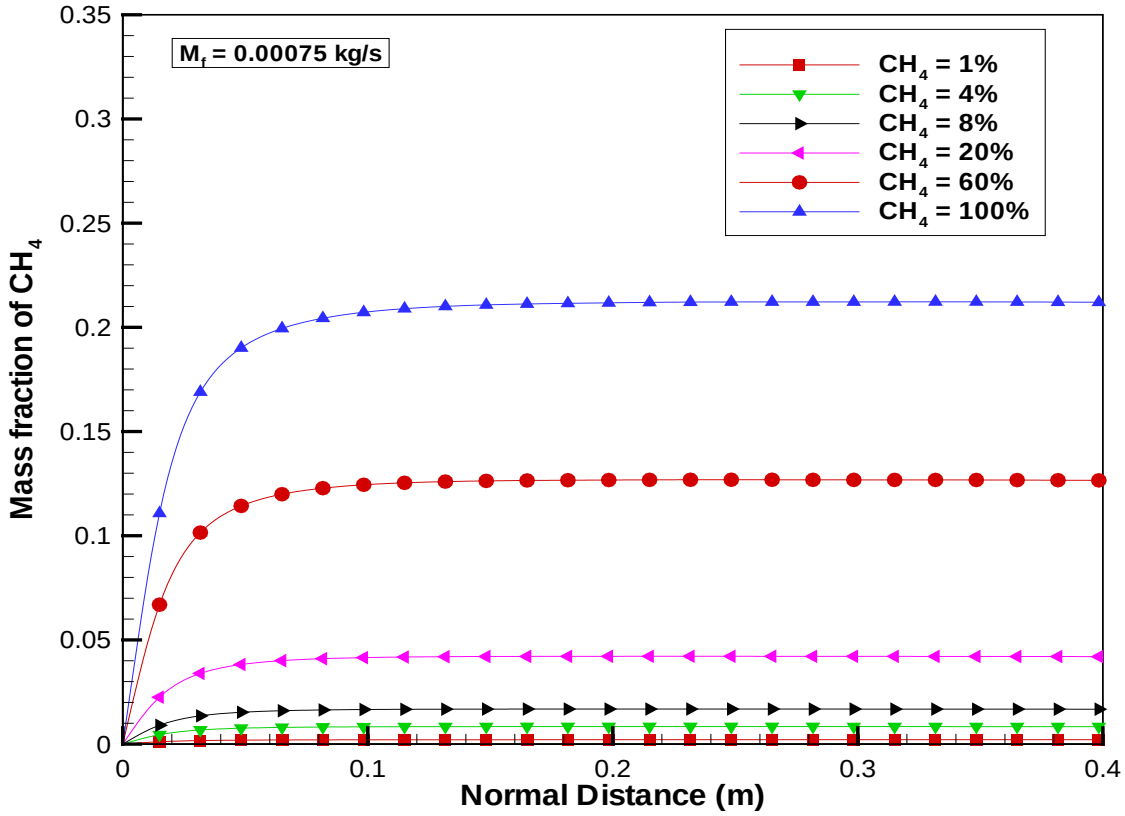

Figure 34: Normal profiles of mass fraction of O_2 at a distance of 200 from the entrance of the reactor with varying CH_4 percentage for a constant mass flow rate of 0.00075kg/s

In order to have a clear understanding of the distribution of species in the reactor, contours of CH_4 and O_2 for the non-reactive cases has been presented in Figure 35and Figure 36 respectively. It is important to mention that all the contours levels of species of CH_4 and O_2 presented are different and the color bar is adjusted in each figure to highlight the mass fraction variations. Figure 35shows that CH_4 is introduced into the bottom/fuel channel. As the outlet of this channel is blocked with a wall, the whole CH_4 is forced to move into the middle/sweep channel through the porous membranes. It is clear that from a distance of X/L = 0.25 uniform mass fraction of CH_4 is obtained in the middle/sweep channel.

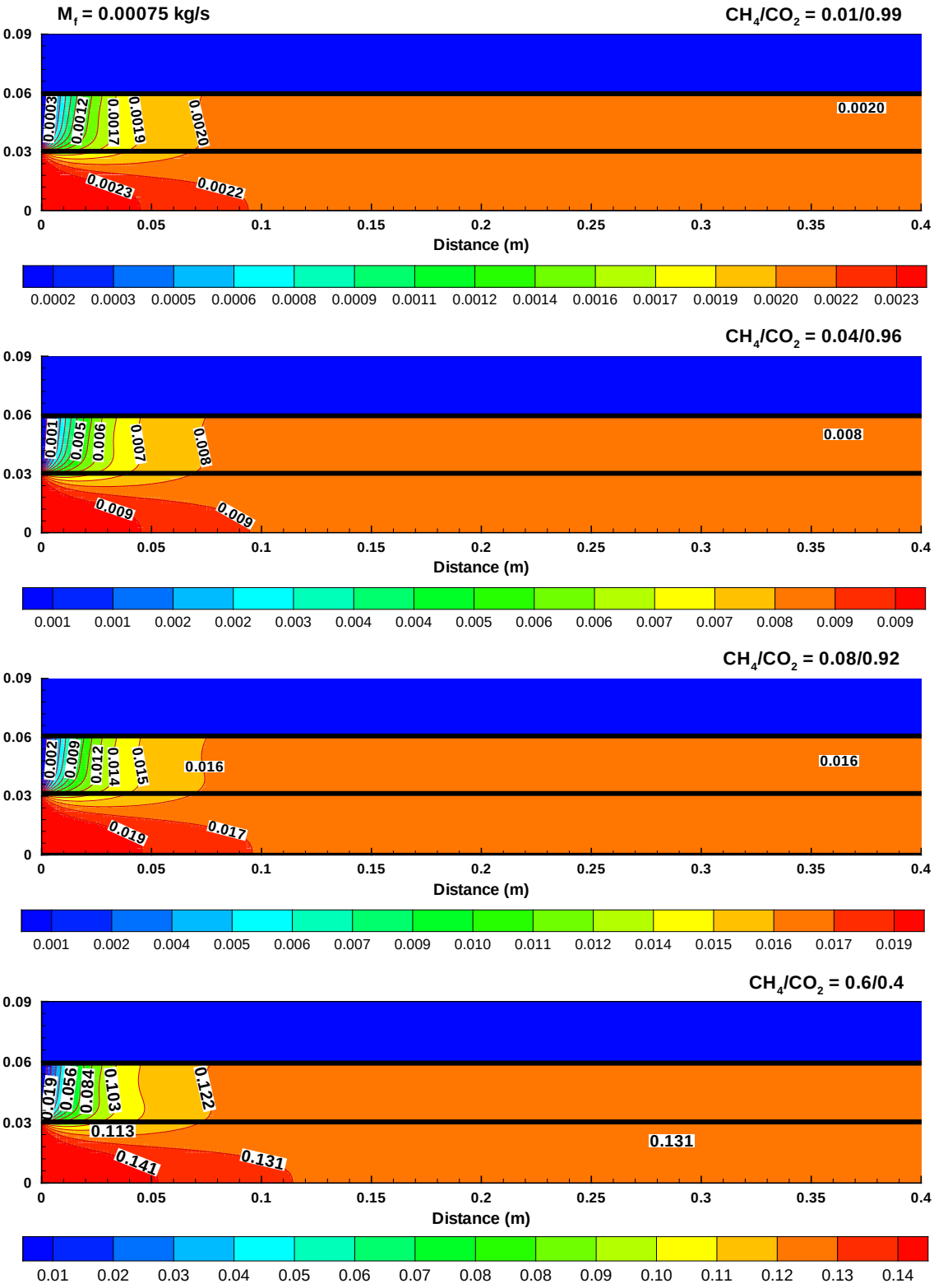

Figure 35: Mass fraction of CH_4 for increasing CH_4/CO_2 ratio (separation only)

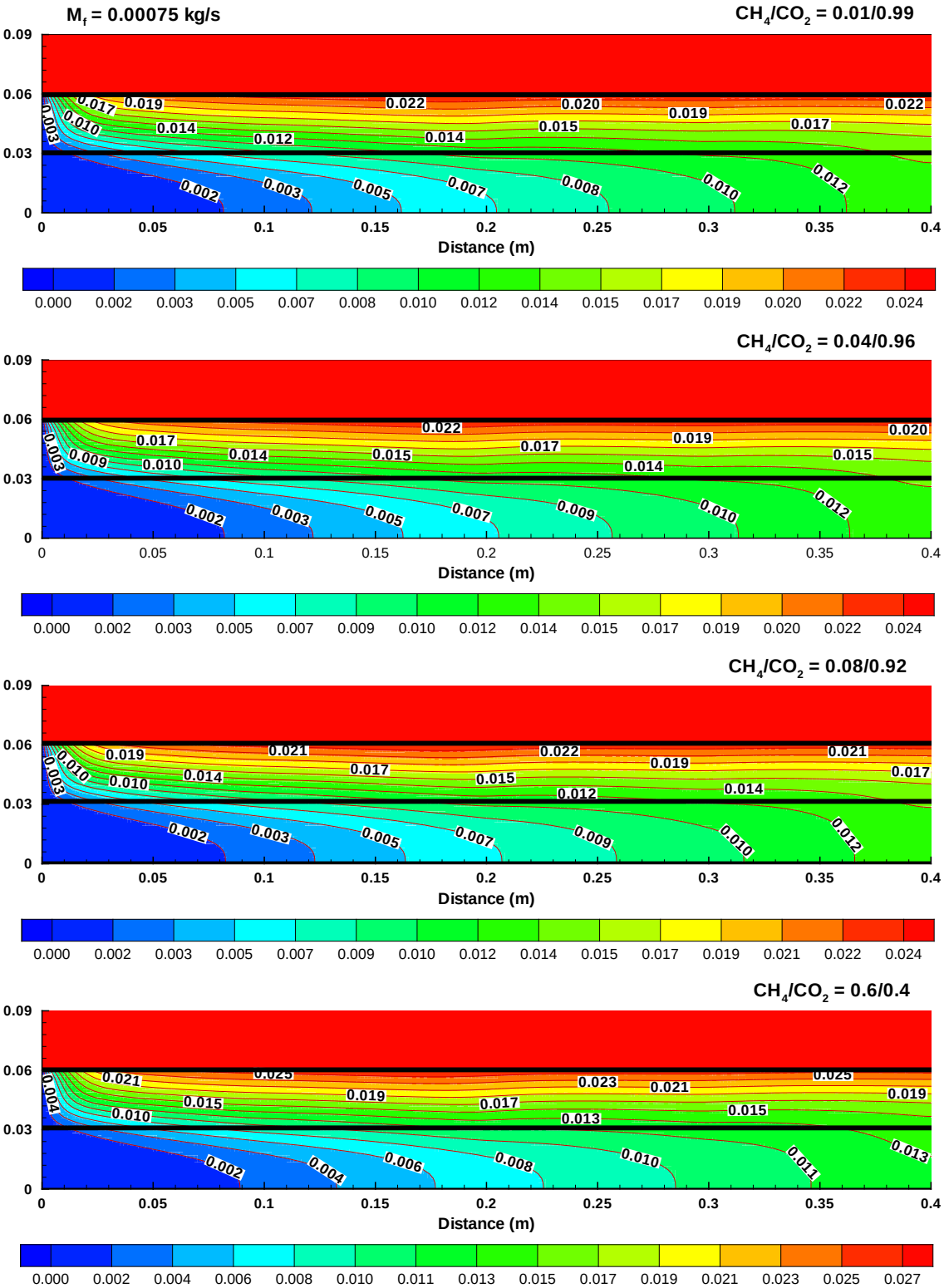

Figure 36: Mass fraction of O_2 for increasing CH_4/CO_2 ratio (separation only)

In order to investigate the permeation characteristics of ITM and the composition of different gases in the current reactor for different mass flow rates of fuel mixture with varying CH_4/CO_2 concentration, a parametric study is conducted for the conditions mentioned in Table 5.

Table 5 : List of operating conditions for the parametric study

Case	P_{1,O_2} (bar)	$\%CH_4$	$\%CO_2$	$\dot{m}_{feed,\ inlet}$ (Kg/s)	$\dot{m}_{sweep,\ inlet}$ (Kg/s)	$\dot{m}_{fuel,\ inlet}$ (Kg/s)
1	0.21	1	99	0.03	1×10^{-6}	0.00075
2		4	96			
3		8	92			
4		20	80			
5		60	40			
6		100	0			
1	0.21	1	99	0.03	1×10^{-6}	0.001
2		4	96			
3		8	92			
4		20	80			
5		60	40			
6		100	0			
1	0.21	1	99	0.03	1×10^{-6}	0.00125
2		4	96			
3		8	92			
4		20	80			
5		60	40			
6		100	0			

5.1.2 Effect of mass flow rate of fuel mixture on the oxygen permeation rates:

The effect on oxygen permeation rates for three different mass flow rates of the fuel mixturewith increasing percentage of CH_4 (or decreasing percentage of CO_2)are presented in Figure 37. It is observed that with the increase in mass flow rate of fuel mixture the oxygen permeation rate increases. As the mass flow rate of gases increases the oxygen on the permeate side is diluted and is driven away quickly. This dilution of O_2 gives rise to a lower partial pressure which leads to a higher oxygen permeation driving force.These results are confirmed from the work done by Wei et al[82]. In their observations when pure CO_2 was used as the sweep gas, the oxygen permeation fluxes increased. This was attributed to the higher flow rate sweep gas that dilutes the permeated oxygen concentration and lowers the oxygen partial pressure on the core side, leading to a higher oxygen permeation driving force. On the other hand, for a constant mass flow rates of fuel, as the mass fraction of CH_4 increases(or mass fraction of CO_2 decreases) the oxygen permeation flux increases. This can be attributed to theincrease in volume flow rate of the gases, as shown in Figure 38.The Figure 38 provides the influence of CH_4% on average volume at different mass flow rates.The influence ofincrease in volume flow rate has already been explained in the previous section. It is shown that a increment of approximately 6.0% of the oxygen permeation flux is observed as %CH_4 varies from 1 to 100 percent (or %CO_2 varies from 99 to 0).

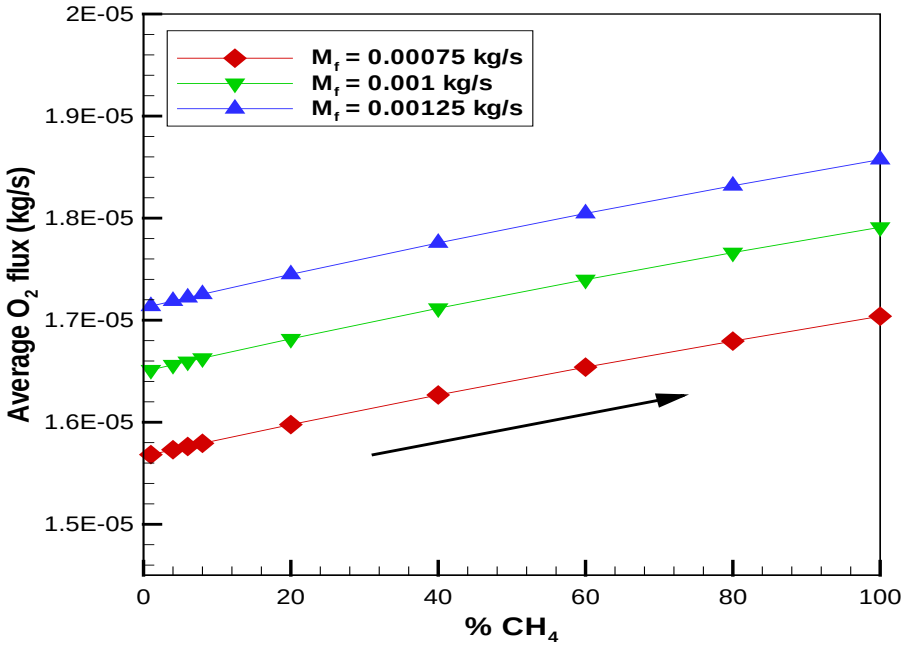

Figure 37: Effect of mass flow rate of fuel on the oxygen permeation flux with increasing percentage of CH_4 for non-reactive cases

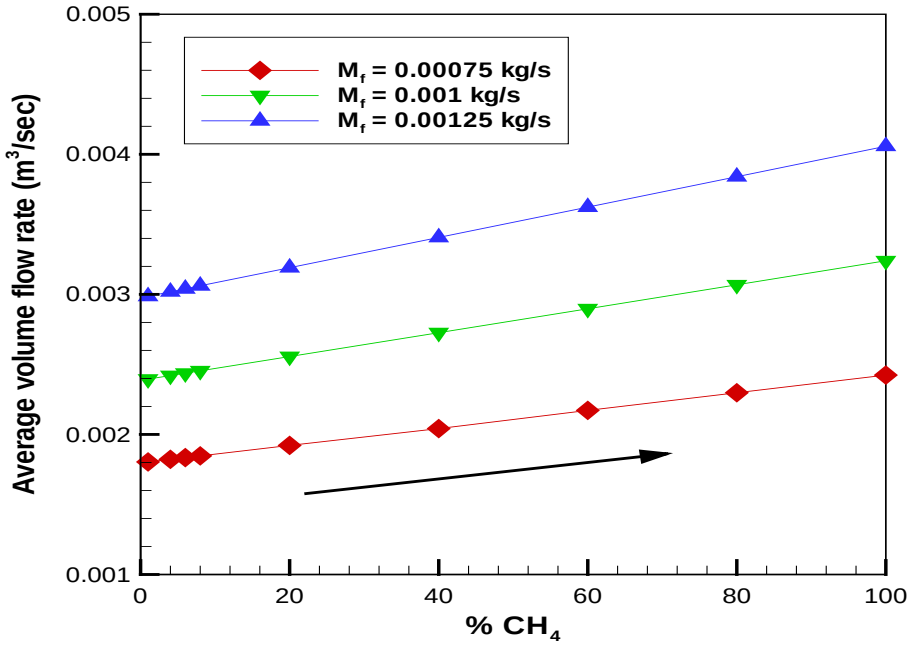

Figure 38: Average volume flow rate for three different mass flow rates of fuel mixture with varying mass fraction of CO_2 for non-reactive cases

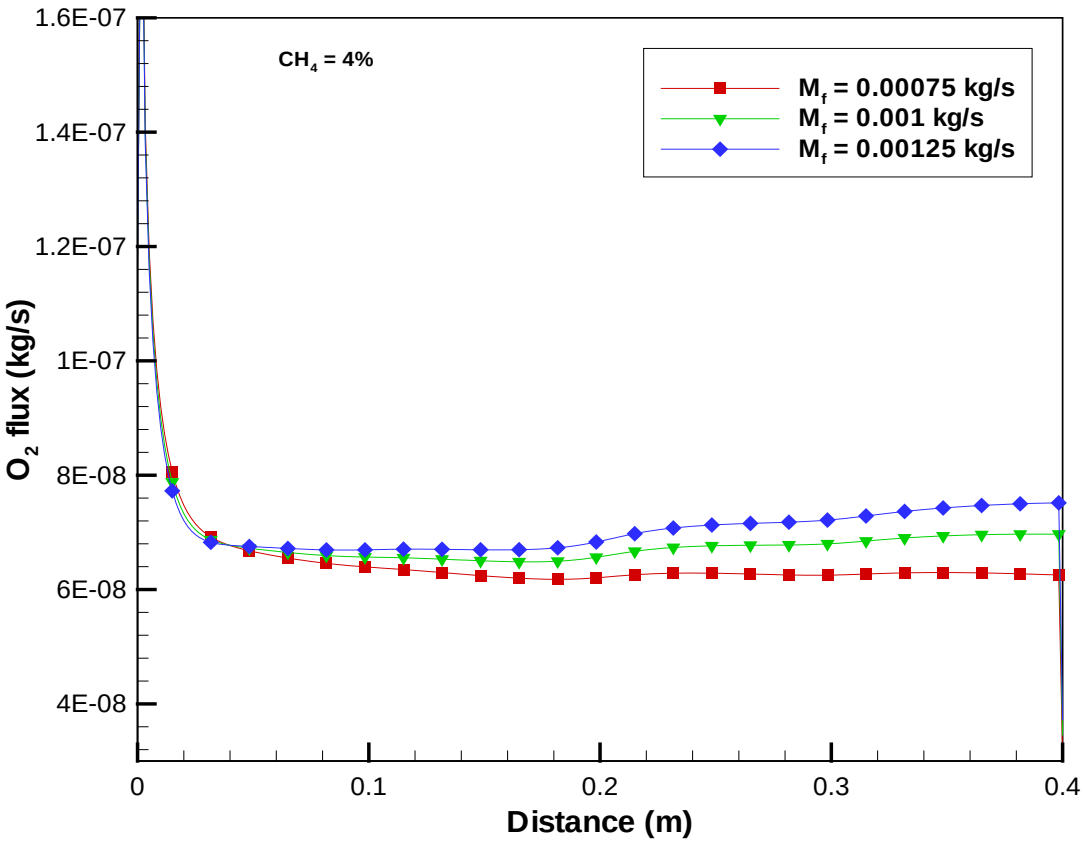

Figure 39: O_2 permeation flux for three different mass flow rates of fuel mixture

Figure 39 shows the comparison of oxygen permeation fluxes at the surface on the permeate side of the ITM for three different mass flow rates of the fuel mixture. For comparison, the cases with same concentrations of CH_4(4%) and CO_2(96%) have been considered. It is evident that the mass flow rate has a considerable effect on the permeation fluxes of oxygen. With increase in the mass flow rate of the fuel mixture the flow rate of the sweep gases increases thereby increasing the fluxes. Figure 40 shows the oxygen permeation fluxes for all the cases mentioned in Table 5.

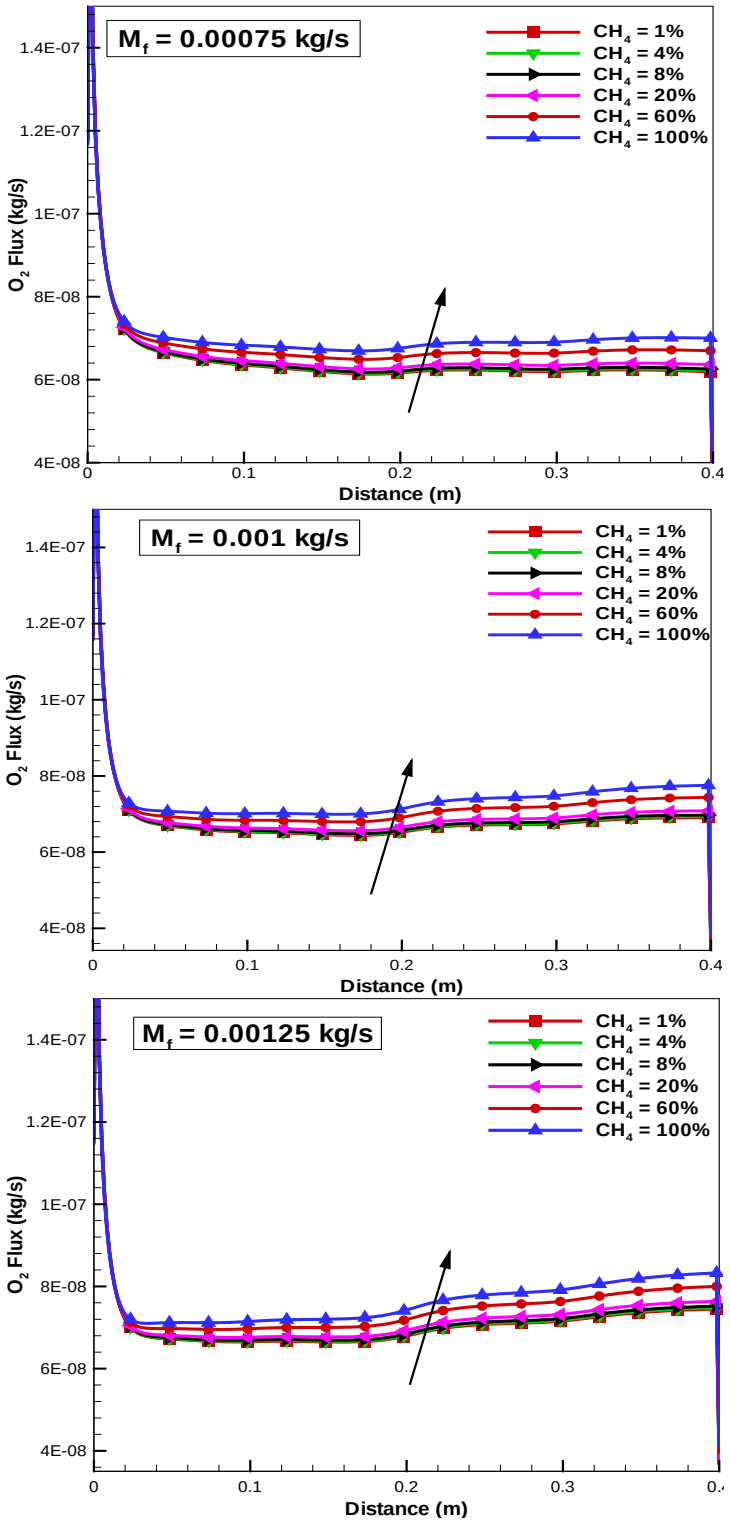

Figure 40: Oxygen permeation flux on the permeate side of the ITM with varying CH_4 percentage for three mass flow rate of fuel mixture

5.1.3 Effects of mass flow rate on the partial pressure of O_2 at permeate side of ITM

Figure 41 shows the partial pressure of oxygen next to the surface on the permeate side of the ITM for three different mass flow rates of fuel mixture. The partial pressure on the feed side of the ITM is kept constant at 0.21bar.

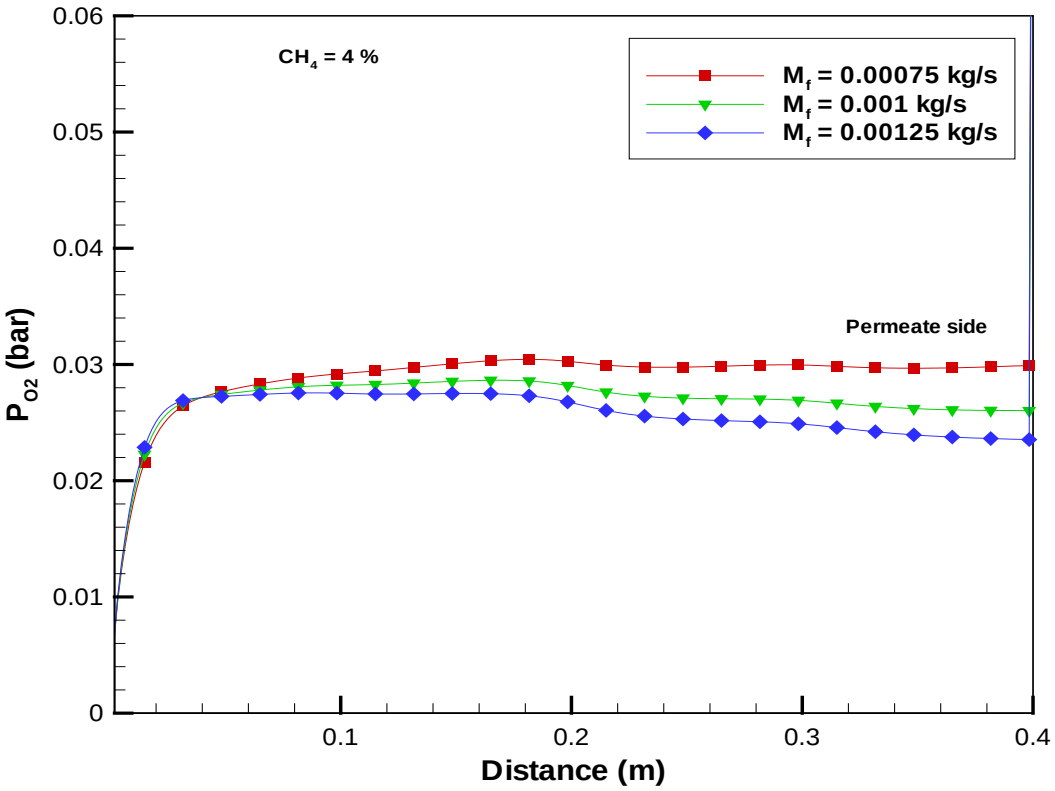

Figure 41: O_2 partial pressure profiles for different mass flow rates along the length

For comparison, the cases with same concentrations of CH_4 (4%) and CO_2 (96%) have been considered. It is clear that increase in the mass flow rate of the decreases the partial pressure of oxygen on the permeate side of the ITM. This indicates that the partial pressure on the permeate side is inversely proportional to the mass flow rates of the sweep gases. Since the permeabilities of the porous membranes P3 and P4 are high

compared to P1 and P2, higher sweep rates are expected in the section from X/L = 0.5 to X/L = 1 of the reactor (i.e. 0.2m to 0.4m). Therefore the partial pressure of O_2 in the second half section of the reactor exhibits more variation with increasing mass flow rates of the fuel mixture than the first half. Partial pressures of O_2 on the permeate side of ITM with varying CH_4 percentage for three different mass flow rates of fuel mixture are presented in Figure 42.

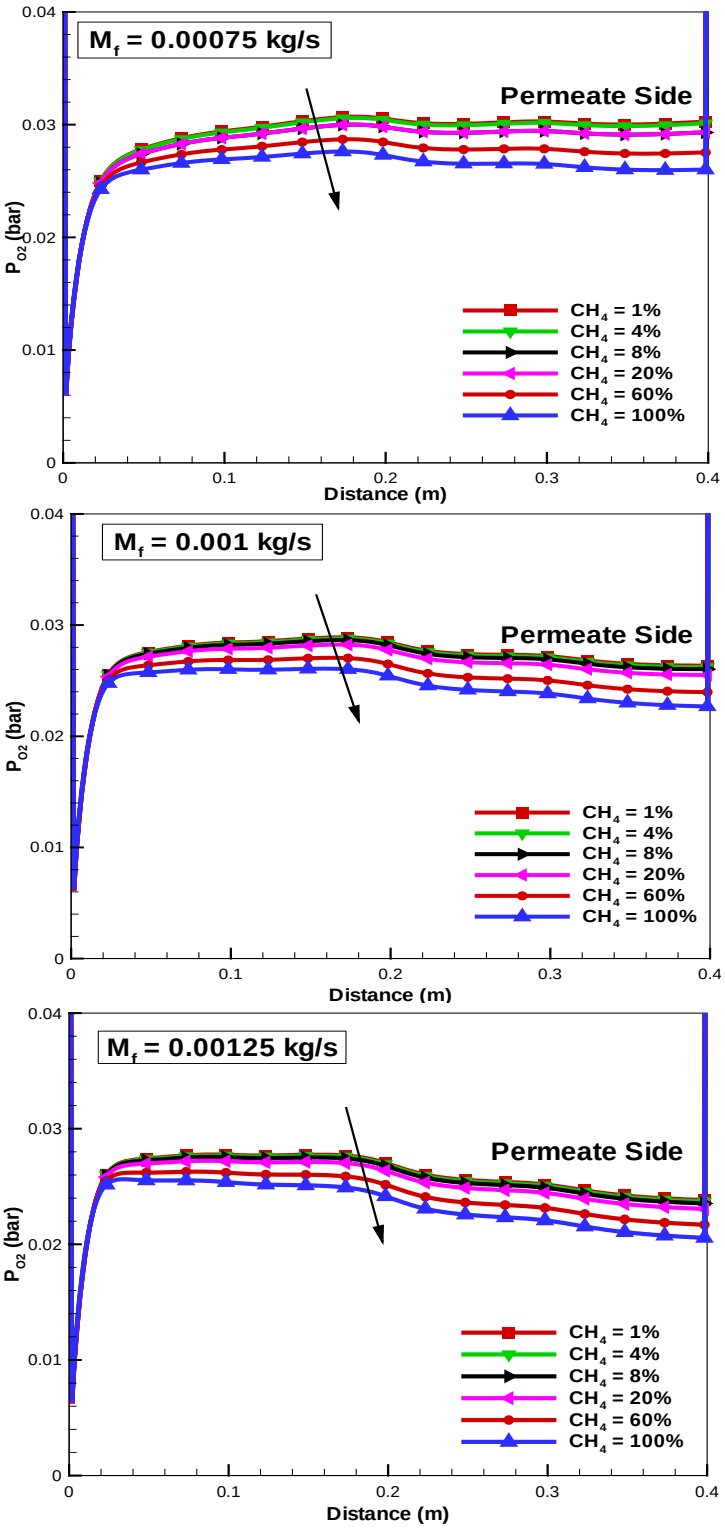

Figure 42: Partial pressure of O_2 on the permeate side of ITM with varying CH_4 percentage for three different mass flow rates of fuel mixture

5.2 Separationand Combustion (Reactive Cases)

A reactive ITM combines the separation of oxygen from air and oxidation of methane in order to reduce the overall size of the reactor and number of equipments in cycle. The chemical reaction at the permeate side produces high partial pressure difference along the membrane which in turn increases the oxygen permeation flux significantly. If the fuel combustion kinetics are significantly faster than the rate at which oxygen is getting permeated through the ITM membrane, the partial pressure of oxygen at permeate side will be very low enhancing the oxygen fluxsignificantly. In this section, the investigation has been extended to include from mixing of CH_4 and CO_2 with O_2 to create combustion with single-step chemistry. Density of LSCF membrane is taken as 6000 kg/m^3[83, 84]. The flow considered is laminar and steady in nature. Buoyancy effects are neglected.The top and bottom walls of the reactor are assumed to be adiabatic. The same listsof parametric values, as presented in Table 4, are used to study the ITM and combustioncharacteristics of reactive cases.

Centre line profiles of temperature and rate of reaction along with the corresponding mass fraction of species for the simulations conditions shown inTable 4 are presented in Figure 43. Figure 43(a) shows the temperature and kinetic rate of reaction. The centre line temperature within the reactor increases and reaches a maximum of 1219 K at the outlet while the reaction occurs all throught the length of the reactor. Rate of reaction drops as the methane is consumed. The fluctuations in the rate of reaction and the corresponding mass fraction of CH_4 is due to the stepwise porosities assigned to the four porous plate membranes.

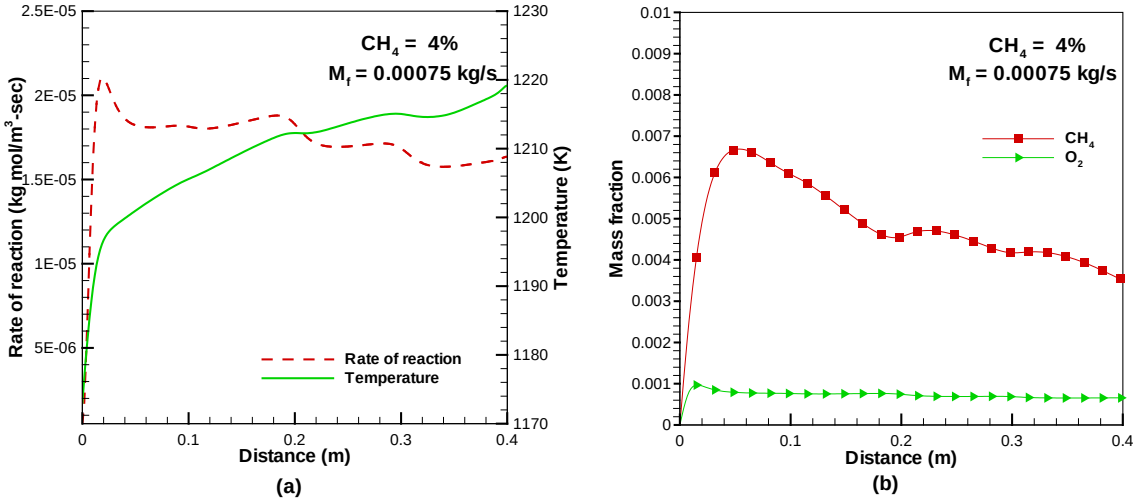

Figure 43: (a) Temperature and reaction rate plot (b) Mass fractions of CH_4 and O_2 at the centre line of the reactor

Figure 43(b) shows the composition profiles which indicates clearly the process of fuel consumption and reduction of the mass fraction of O_2downstream. The mass fracton of O_2 first increases as the rate of reaction increases then deceases as the methane is consumed. The increase in O_2 is due to the comsumption of fuel. For the given fuel mass fraction and mass flow rate in Table 4, the amount of O_2 permeated through the ITM is 3.05×10^{-05}kg/s which constitutes of O_2/CH_4ratio of 4.066.

Figure 44 shows the oxygen permeation flux and the corresponding rate of reaction for the same case considered in Table 4.The amount of CH_4 in the fuel mixture is 4%. It is observed that the flux of oxygen, shown in Figure 44, predicts a very high value at the inlet and then reduces suddenly. This can be attributed to the zero partial pressure value at the inlet of the channel. The zero partial pressure at the inlet causes Δp across the ITM to reach a maximum value. As flux across an ITM is a primary function of Δp across the membrane, the increase in Δp causes the oxygen permeation flux to increase. Thus the

oxygen flux starts with a maximum value at the inlet. The flux of oxygen starts decreasing from a maximum value to a minimum value. This is because of no reaction at the inlet. As the reaction starts the flux of oxygen also starts to increase. The flux increases to a considerable value and becomes constant as the reaction rate becomes stable.

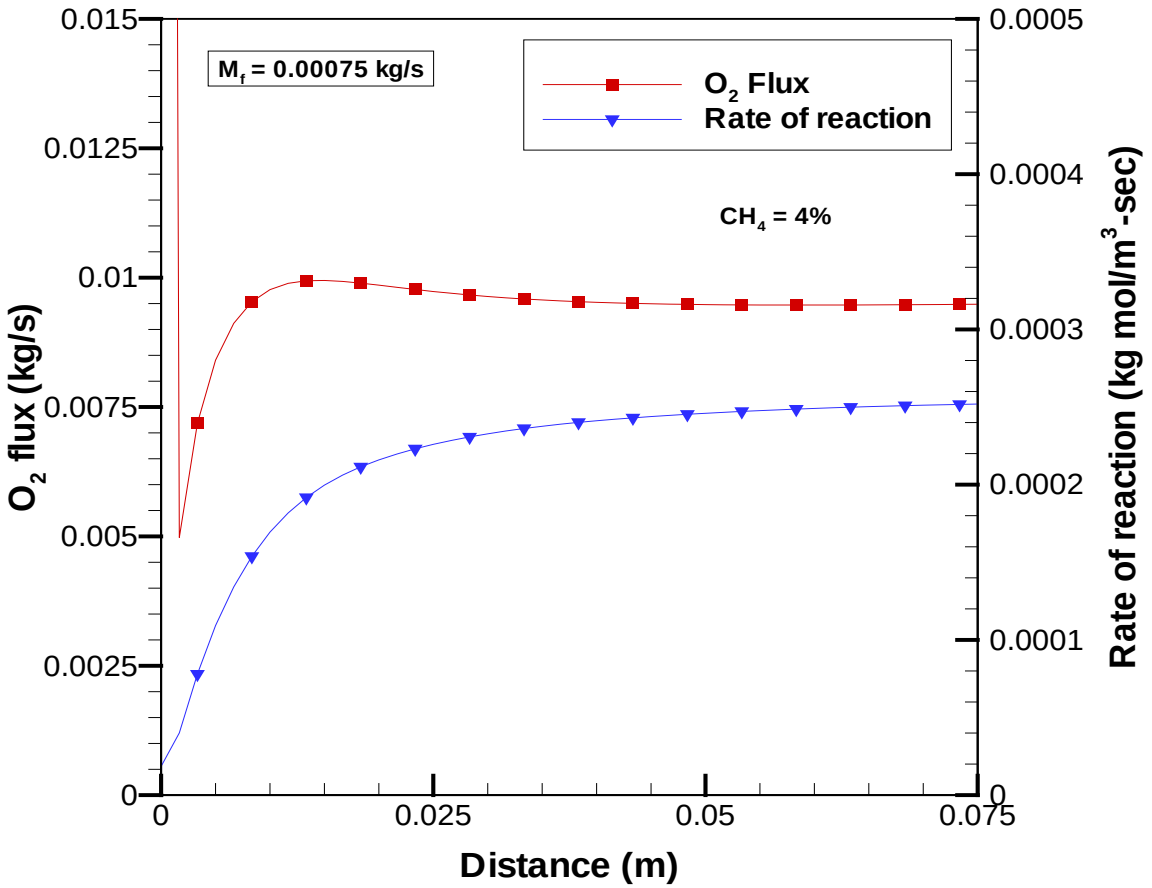

Figure 44: Oxygen flux and rate of reaction for the case of 4% CH_4 for a constant mass flow rate of 0.00075 kg/s

In order to explain the influence of reactivity on the different permeation characteristics, a comparison of results of reactive and non-reactive cases are presented in Figure 45.

Figure 45(a) shows the comparison of partial pressures of O_2on feed and permeates side of the ITM for both non-reactive (separation only) and reactive cases. It is observed that the partial pressure of oxygen on the permeate side of the ITM is zero at the inlet as there is no oxygen. It increases gradually as the oxygen starts permeating and then becomes constant. On the other hand the partial pressure of oxygen on the feed side is 0.21 bar at the inlet and then reduces all along the length, because of the migration of oxygen to the permeate side. It can be seen that the partial pressure of oxygen on the permeate side for reactive cases reduces significantly when compared to the non-reactive mode.

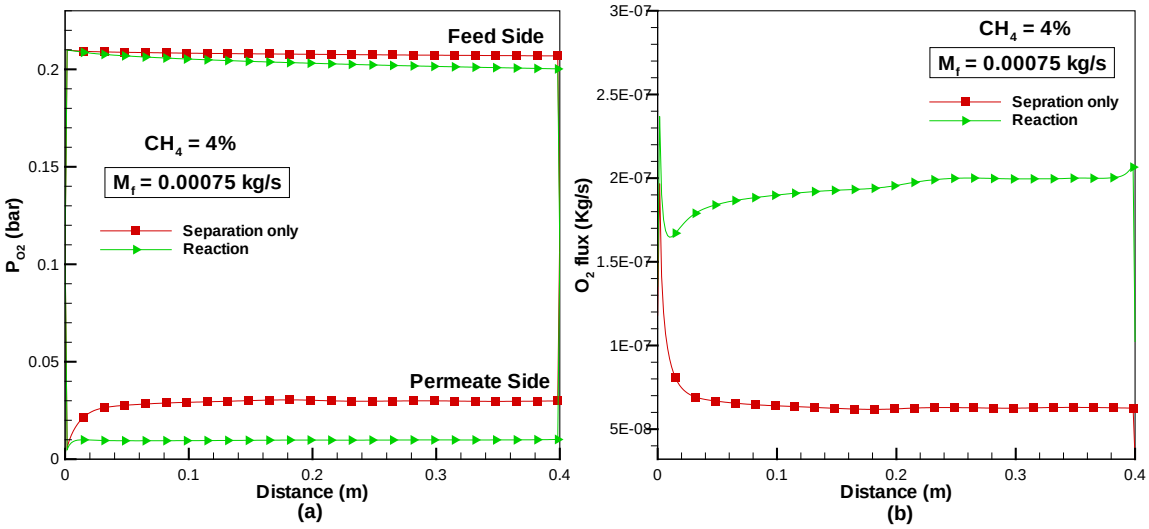

Figure 45:(a) Partial pressures of O_2 on both feed and permeate sides for non-reactive (separation only) and reactive cases (b) O_2 flux for non-reactive (separation only) and reactive cases

Figure 45(b) shows the comparison of oxygen permeation flux with the same amount CH_4 in the fuel mixture for both non-reactive (separation only) and reactive cases. It is clear that for the reactive case, the O_2 permeation flux decreases till the reaction starts then increases till the rate of reaction is maximum and then remains almost constant. It

has been observed that the oxygen flux has increased approximately 3 times from an average constant value of 7 x 10^{-08} kg/s (for non-reactive cases) to 2 x 10^{-07} kg/s (for reactive cases). The results of increase in O_2 flux with reaction are confirmed with the experimental results obtained by Xu and Thomson[78] and also by Zeng et al [85]. This increase in flux can be explained from the chemical reaction taking place on the permeate side of the ITM which consumes the permeated oxygen, lowering the partial pressure on the permeate side leading to high oxygen driving force. It may also be explained from the oxygen surface exchange reactions and bulk diffusion that are improved at high temperatures. Hence separation of O_2 using an ITM along with a chemical reaction provides a favorable solution to enhance oxygen permeation flux. It gives conclusive remark that for a particular membrane surface, the amount of O_2 permeated with chemical reaction is higher compared to separation-only mode; thereby the length of the ITM reactor can be greatly reduced.

5.2.1 Effect of CO_2concentration on the oxygen permeation flux for reactive cases:

The effect of variation of concentration of CH_4/CO_2 in the fuel gas mixture on the permeation flux of oxygen through the ion transport membrane has been investigatedfor reactive cases. The mass flow rate of the fuel mixture is kept constant at 0.00075 kg/s while the mass fraction of CH_4/CO_2 has been varied. Figure 46shows the partial pressure on the feed and permeates side next to the surface of the ITM.Unlike non-reactive cases the partial pressure on the feed side also changes in reactive cases i.e. decreases with the increasing mass fraction of CH_4 in the fuel mixture.

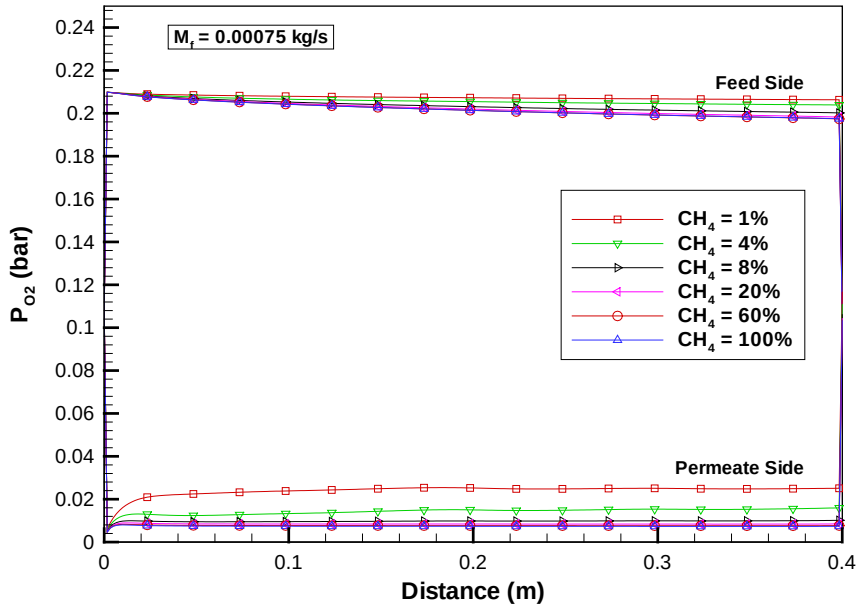

Figure 46: Partial pressures of O_2 on feed and permeate side of the ITMwith varying mass fraction of CH_4 for a constant mass flow rate of 0.00075 kg/s

In order to analyze the differences in partial pressure on the permeate side clearly, Figure 47 has been presented. It is clear from Figure 47 that with increase of CH_4 concentration in the fuel mixture the partial pressure of oxygen on the permeate side greatly reduces. There is approximately 77% of drop in the partial pressure of oxygen when CH_4 concentration is increased from 1% to 100%. Such high reduction in the partial pressure is due to the reaction taking place on the permeate side of the ITM.This reaction consumes the permeated oxygen causing the partial pressure to decrease. Figure 48 shows the corresponding permeation fluxes of O_2 along the length of the membrane for the same mass flow rate of 0.00075 kg/s of the fuel mixture for the reactive cases

(separation and combustion).When the oxygen molecules starts migrating to the permeate side, i.e. when desorption of oxygen ions takes place on the permeate side, the partial pressure on the permeate starts building up causing Δp to reduce along the length of the ITM and then becomes constant. As a result, the oxygen flux also becomes stable attaining a constant value throughout the length of the ITM.Along with the consumption of O_2 in the reaction, the decrease in mass fraction of CO_2 also contributes to the increase in the flux.About 57% of oxygen flux is increased when CH_4 in the fuel mixture increases from 1% to 100%. It is worth noting that the oxygen flux increases till CH_4 in the fuel mixture is increased to 60%. But further increasing CH_4 (or reducing CO_2) in the mixture does not increase the flux but rather remains constant.

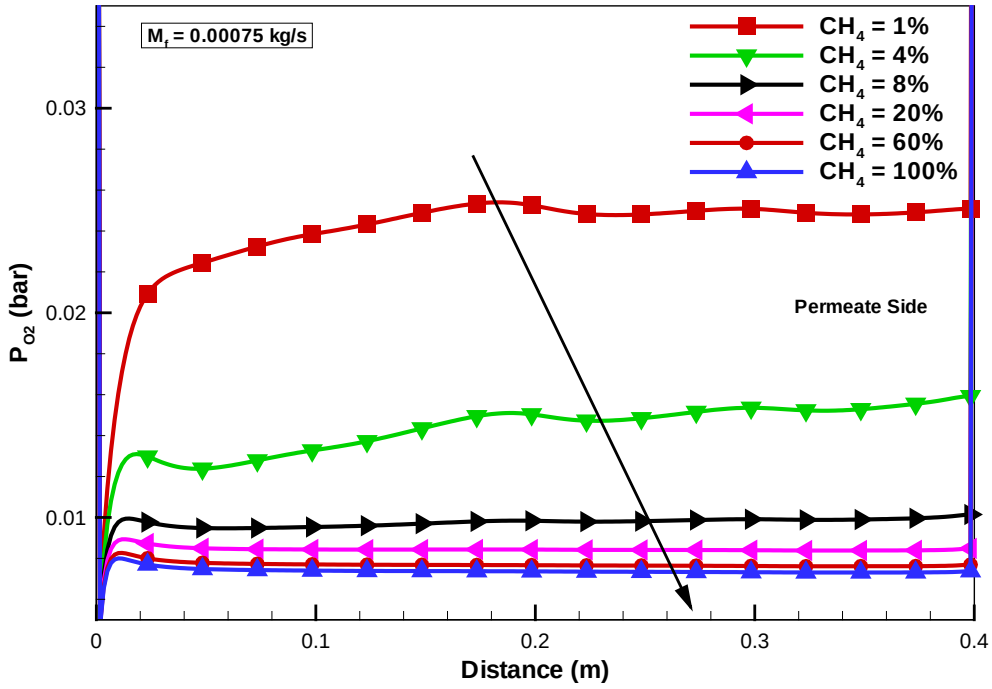

Figure 47: Partial pressure on the permeate side of ITMwith varying mass fraction of CH_4 for a constant mass flow rate of 0.00075 kg/s

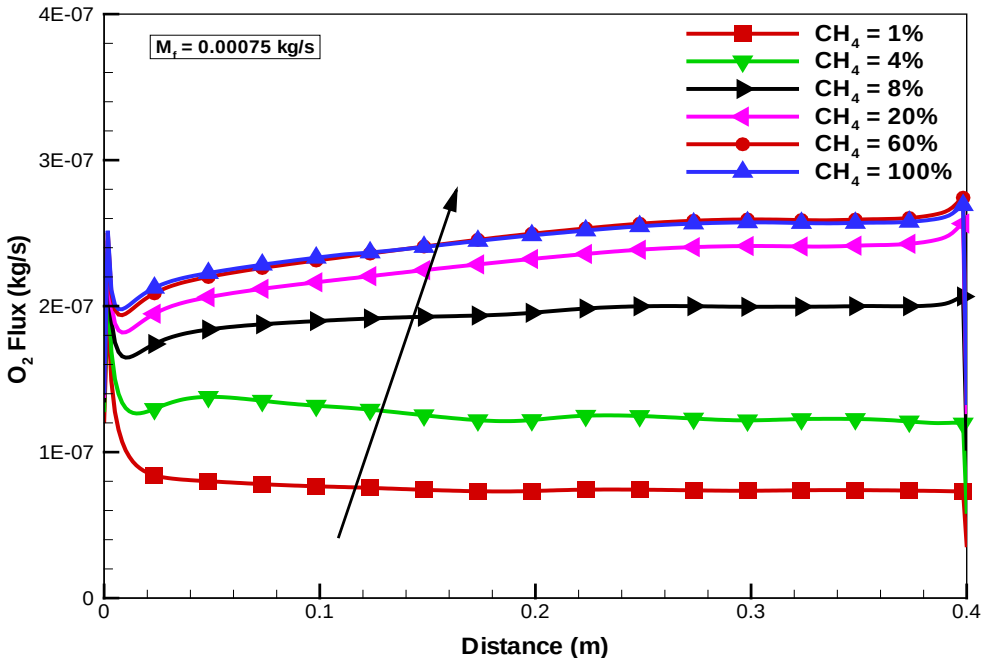

Figure 48: Oxygen flux on the permeate side of the ITMwith varying mass fraction of CH_4 for a constant mass flow rate of 0.00075 kg/s

In order to study the temperature and reaction kinetics for different mass flow rates of fuel mixture and compositions a parametric study is carried out for the conditions shown in Table 5.

5.2.2 Temperature characteristics in the present oxygen transport reactor:

Figure 49shows the normal distribution of the reaction ratesat a distance of 200mm from the entrance of the reactor. The profiles are presented for increasing CH_4/CO_2 mass fraction ratios for three different mass flow rates of the fuel mixture. Figure 50shows the corresponding temperature plots. It is observed that the reaction rate increases with increase in CH_4 mass fraction in the fuel mixture.It isalso shown that the reaction zone shifts towards the ITM. The corresponding temperature also increases as the CH_4%

increases. Howeveras the CH_4/CO_2percentageincreases beyond60/40 the temperature slightly reduces even though the reaction rate increases. Similar results are obtained with increasing mass flow rates where the temperature of the ITM reduces beyond 60% of CH_4 in the fuel mixture. This may be due to the conduction of heat through the ion transport membrane when the reaction zone is near to the ITM (for $\%CH_4$ range of 60 to 100). This has to be avoided because the reaction near to the ITM may degrade the membrane material and affect the performance of the membrane. Both effects were shown during the discussions of the temperature and reaction contours. Moreover as explained earlier that the reactions near to the membrane may give rise to surface exchange reactions where the material of ITM reacts with the gases and forms unwanted carbon compounds on the surface of the permeate side of the ITM limiting the desorption of oxygen ions leading to reduction in oxygen permeation flux.

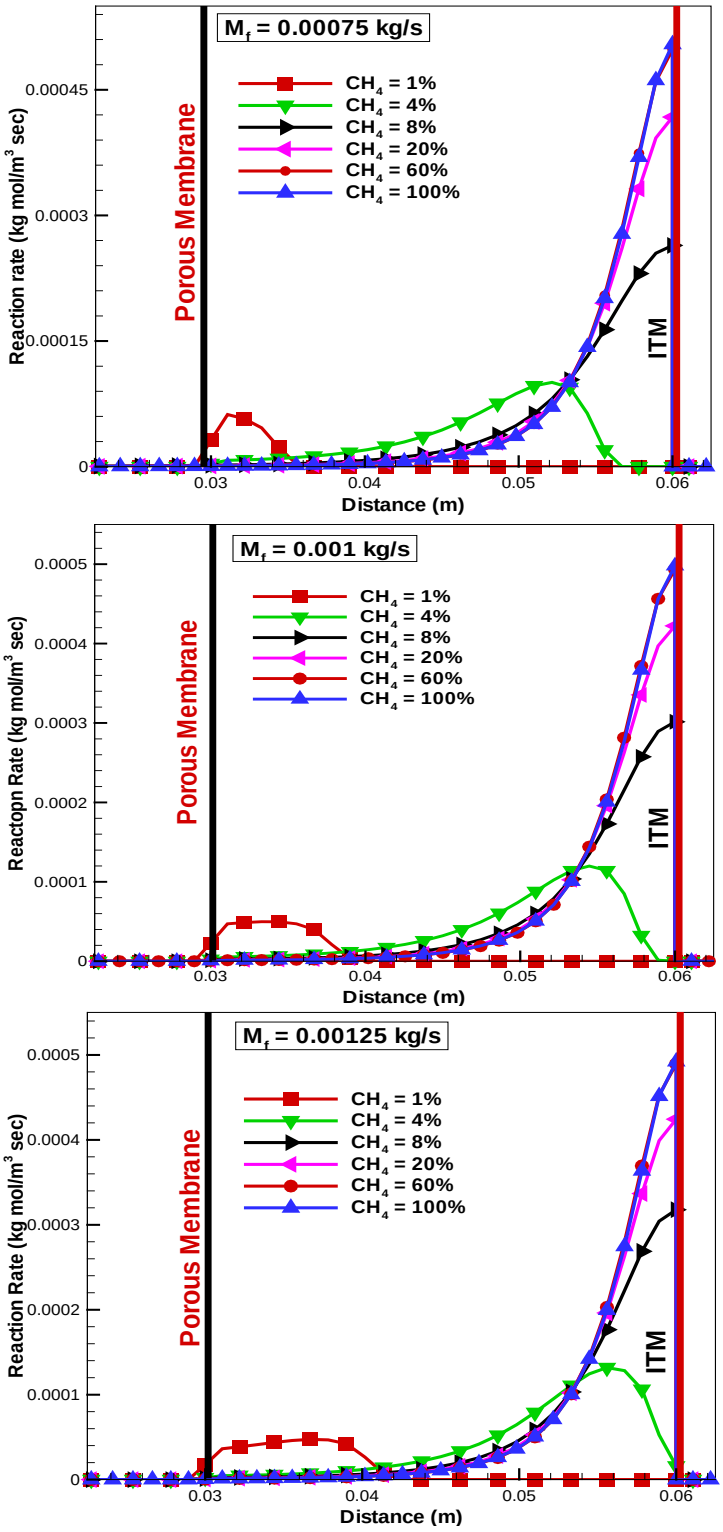

Figure 49: Reaction rate plots for increasing CH_4/CO_2 mass fraction ratios at a normal distance of 200mm from the entrance of the reactor

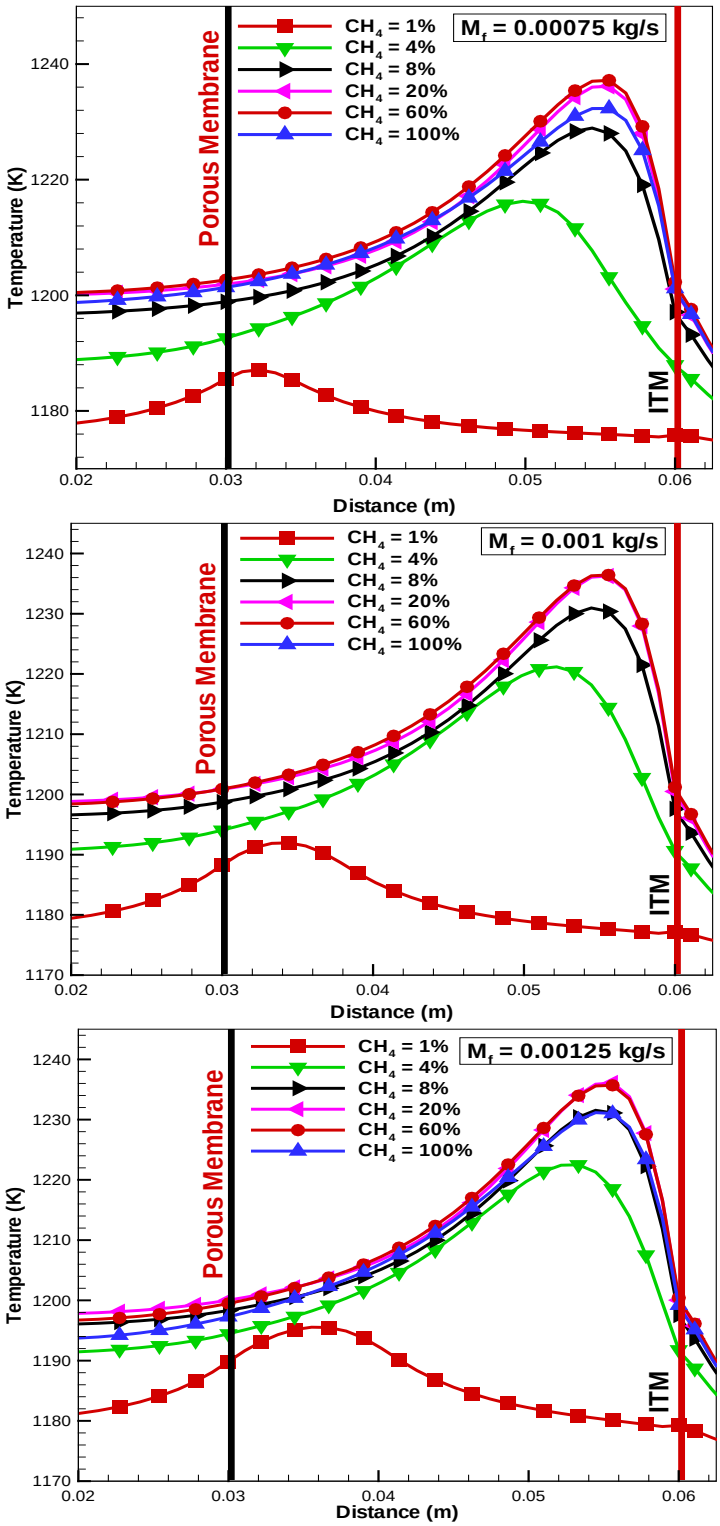

Figure 50: Temperature plots for increasing CH_4/CO_2 mass fraction ratios at a normal distance of 200mm from the entrance of the reactor

Figure 51 shows Mass fraction of CH_4 at a normal distance of 200mm from the entrance of the reactorfor different CH_4 percentages in the fuel mixture. The mass flow rate of the fuel mixture is 0.00075 kg/s. It is observed that with small amounts of CH_4 percentages in the fuel mixture gives 100% CH_4 conversions are obtained. It is also clear from Figure 51 that mass fraction of CH_4 decreases from the porous membrane towards the ITM indicating that it is being consumed in the reaction.

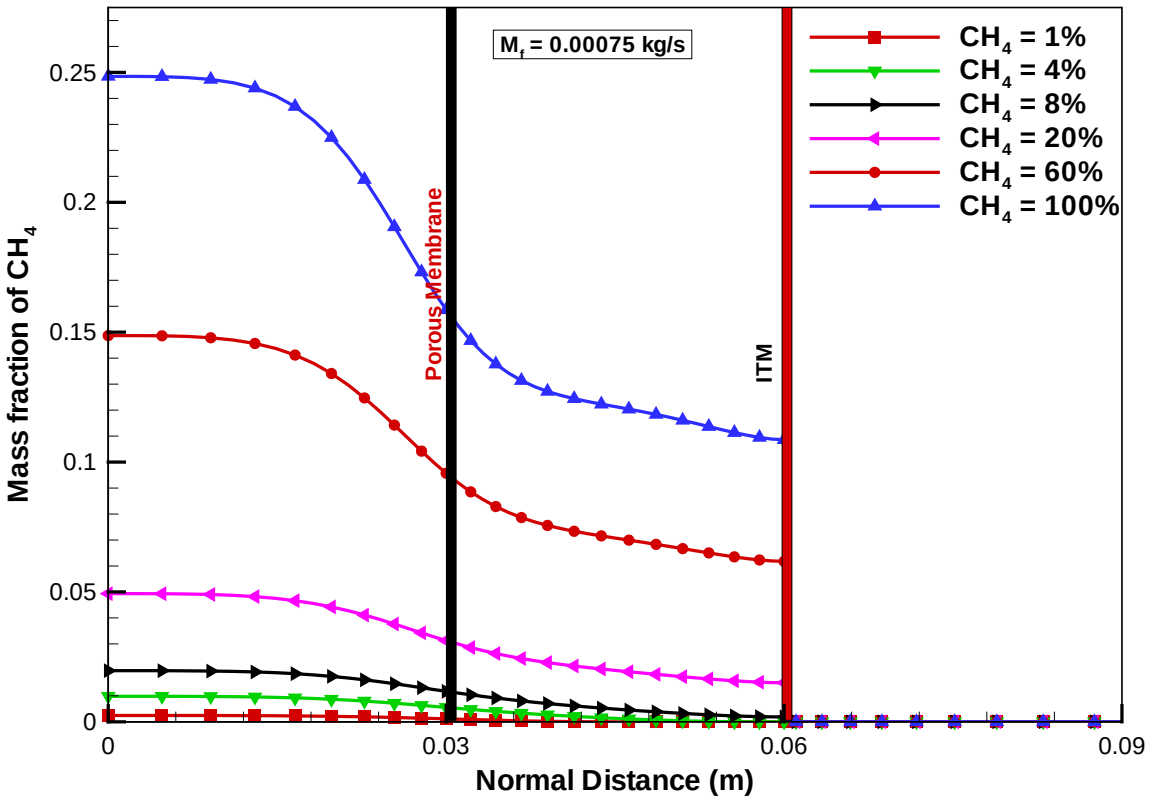

Figure 51: Normal profiles of mass fraction of CH_4 for different CH_4 percentages in the fuel mixture at a distance of 200mm from the entrance of the reactor

The Mass fraction of O_2 for different CH_4 percentages in the fuel mixture at a normal distance of 200mm from the entrance of the reactor is presented in Figure 52. It is clear that the mass fraction of O_2 decreases from the ITM towards the porous membrane

indicating that it is being consumed in the reaction. In order to have high O_2 conversions the amount of CH_4 has to be increased. But this is achieved at a penalty of some amount of unburned CH_4. From the above discussion, it can be concluded that with high CH_4percentages(or less diluent CO_2) at inlet, high maximum temperatures can be achieved for increasing mass flow rate. This is accompanied by a reduction in conversion percentage of CH_4. With split ITM reactor design, the problem of fuel conversion can be overcome with more uniform temperature along the reactor and complete combustion.

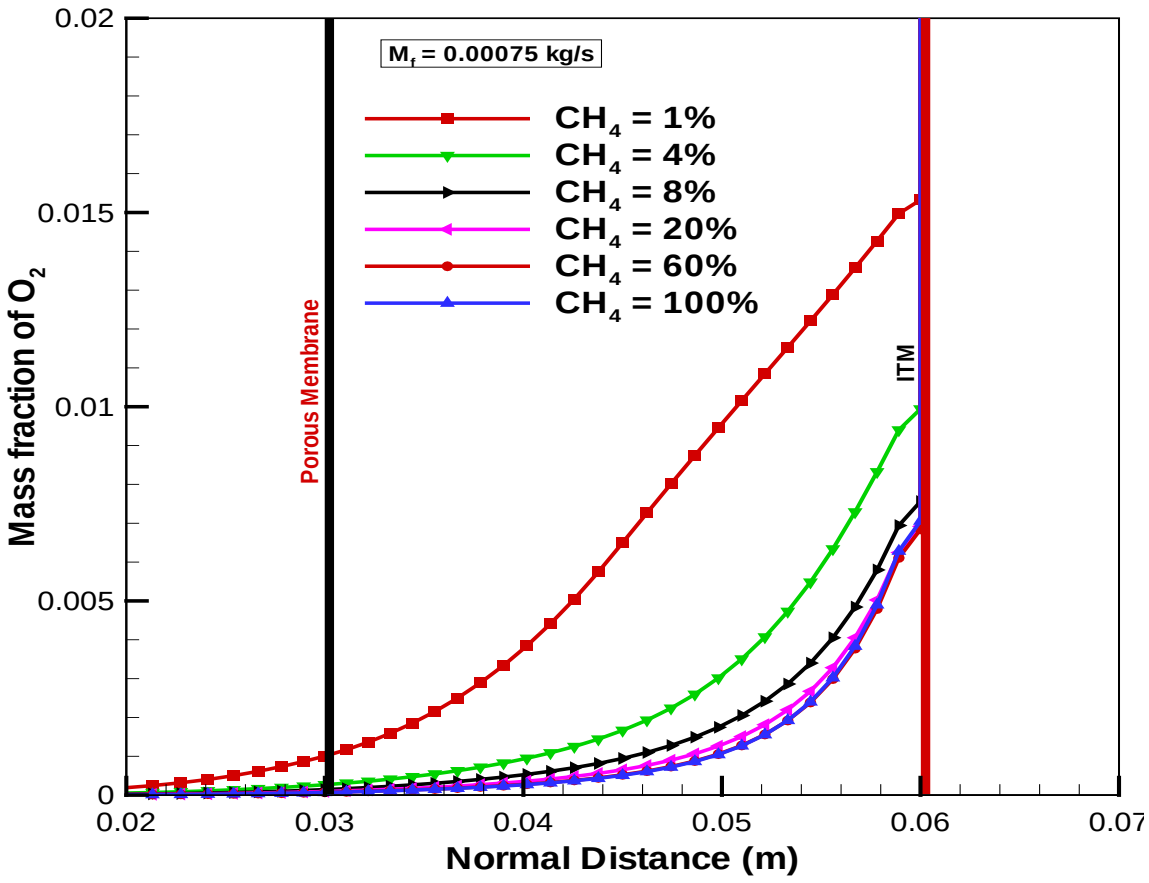

Figure 52: Normal profiles ofmass fraction of O_2 for different CH_4 percentages in the fuel mixture at a distance of 200mm from the entrance of the reactor

5.2.3 Effect of mass flow rates of fuel mixture on the combustion temperature:

Figure 53 shows the maximum temperature obtained in the reaction with increasing percentage of CH_4 and Figure 54 shows the average temperature of the reaction. From these figures it is clear that with increase in mass fraction of CH_4 the maximum temperature (shown in Figure 53) of the reaction increases and is consistent with the increase in the average temperatureat the exit of the reactor.At the same time we also notice that the corresponding reaction zone moves upwards, as indicated byFigure 56. Thus by adjusting the amount of CH_4 in the fuel mixture the reaction zone can be moved accordingly. Increasing the mass fraction ratio of CH_4/CO_2 beyond 60% CH_4 do not significantly increase the temperature but rather moves the reaction zone very near to the membrane. Allowing the reaction zone to occur near to the membrane may be advantageous to have higher oxygen flux with increase in the membrane temperature but it may degrade the membrane. The reaction zone near to the ITM may cause an increase in the surface reaction rate leading to deposition of unwanted carbon compounds that may reduce desorption of oxygen ions on the permeate side of the membrane. This may degrade the membrane as well as reduce the oxygen flux (due to decrease in desorption of oxygen ions by deposition of unwanted carbon compounds) with time. Xu and Thomson[78] found that more than 50% of the membrane surface on the permeate (methane) side was significantly etched when CH_4 was partially oxidized as compared to the fresh surface without reaction. Downstream locations exhibit higher temperature levels in the case of higher CH_4/CO_2 ratios. These effects are clearly seen in the temperature contours shown in Figure 55.

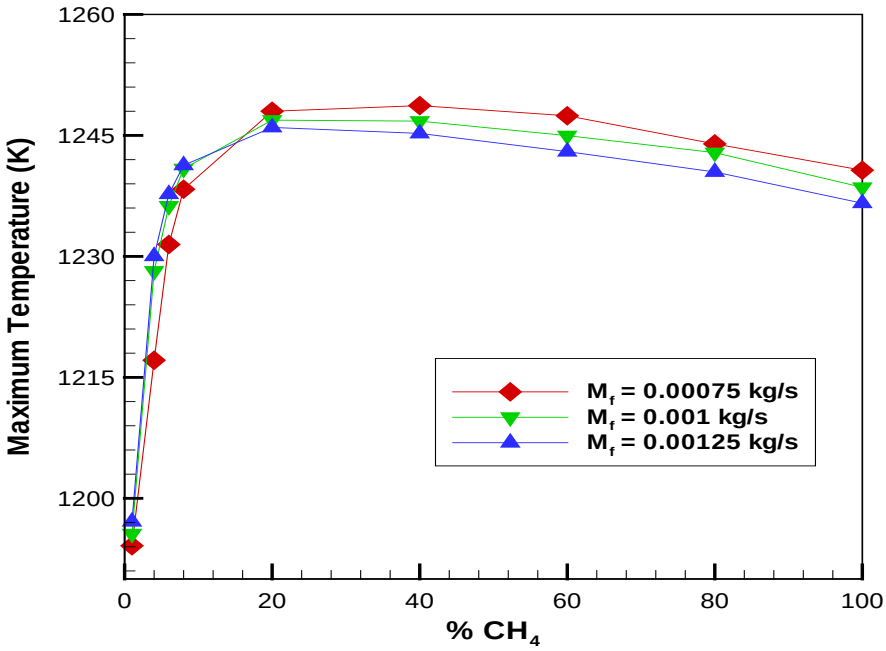

Figure 53: Maximum temperature obtained in the reaction with increasing percentage of CH_4 for three different flow rates of the fuel mixture

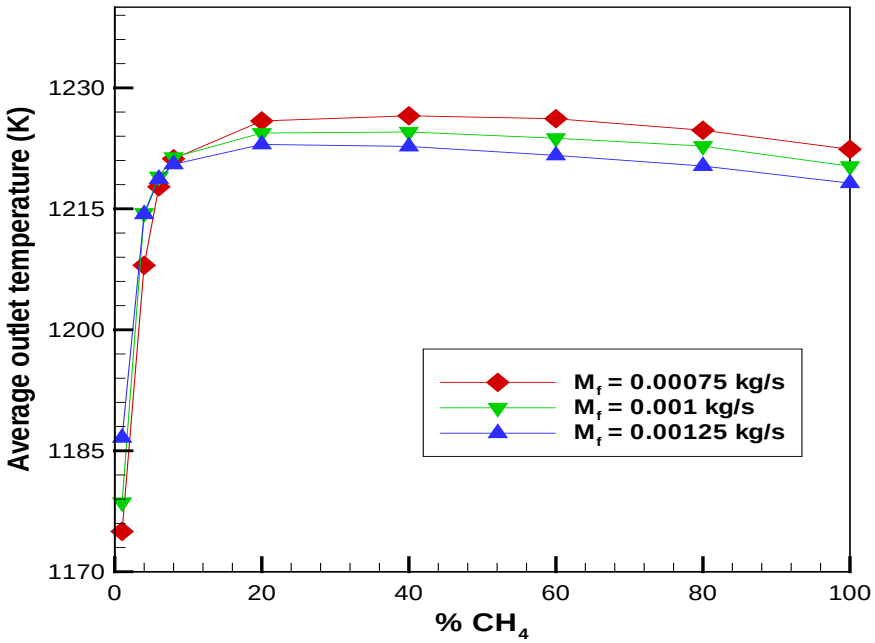

Figure 54: Average temperature of the reaction at the exit of the reactor with increasing percentage of CH_4 for three different mass flow rates of the fuel mixture

Figure 55shows temperature contours for four different mass fraction ratios of CH_4/CO_2 for a constant mass flow rate of fuel mixture of 0.00075 kg/s. It is important to mention that the contour levels are presented on the same scale and the color bar at the end of the last contour highlights the temperature variations. Integer values of the corresponding color are incorporated into the contour in order to have a better analysis of the variation of temperature. It is observed that the maximum value of temperature in the temperature contour with CH_4/CO_2 ratio of 0.01/0.99 i.e. 1% CH_4 is 1195 K. only 22K rise in temperature is observed and the reaction zone ends in the first half length of the reactor. This indicates that there is no enough CH_4 available for the complete combustion of oxygen permeated through the ITM. As the percentage of CH_4 is increased the maximum temperature of the reaction has also increased and the reaction zone occupies the whole length of the reactor.This is accompanied by a reduction in conversion percentage of CH_4. Figure 56 shows the reaction rate contours for different mass fraction ratios of CH_4/CO_2 for a constant mass flow rate of fuel mixture of 0.00075kg/s. It is important to mention that the reaction levels for different mass fraction of CH_4/CO_2 are presented on the same scale and the variation in the reaction rate is indicated on the color bar. Unlike temperature contoursthe reaction rate at different positions are indicated by aninteger and the corresponding reaction rate value is indicated under the integer in the color bar.

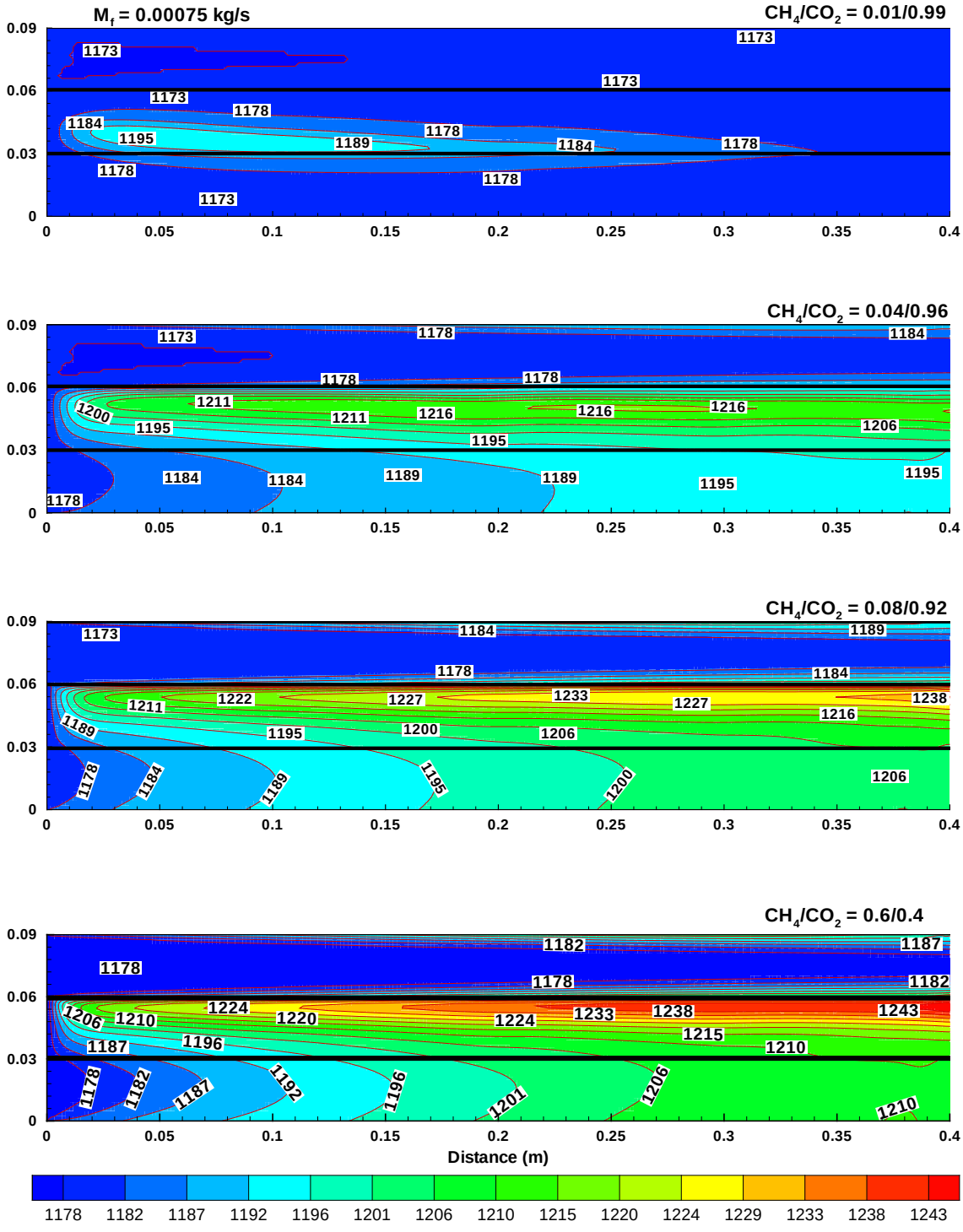

Figure 55: Temperature contours for increasing CH_4/CO_2 mass fraction ratio

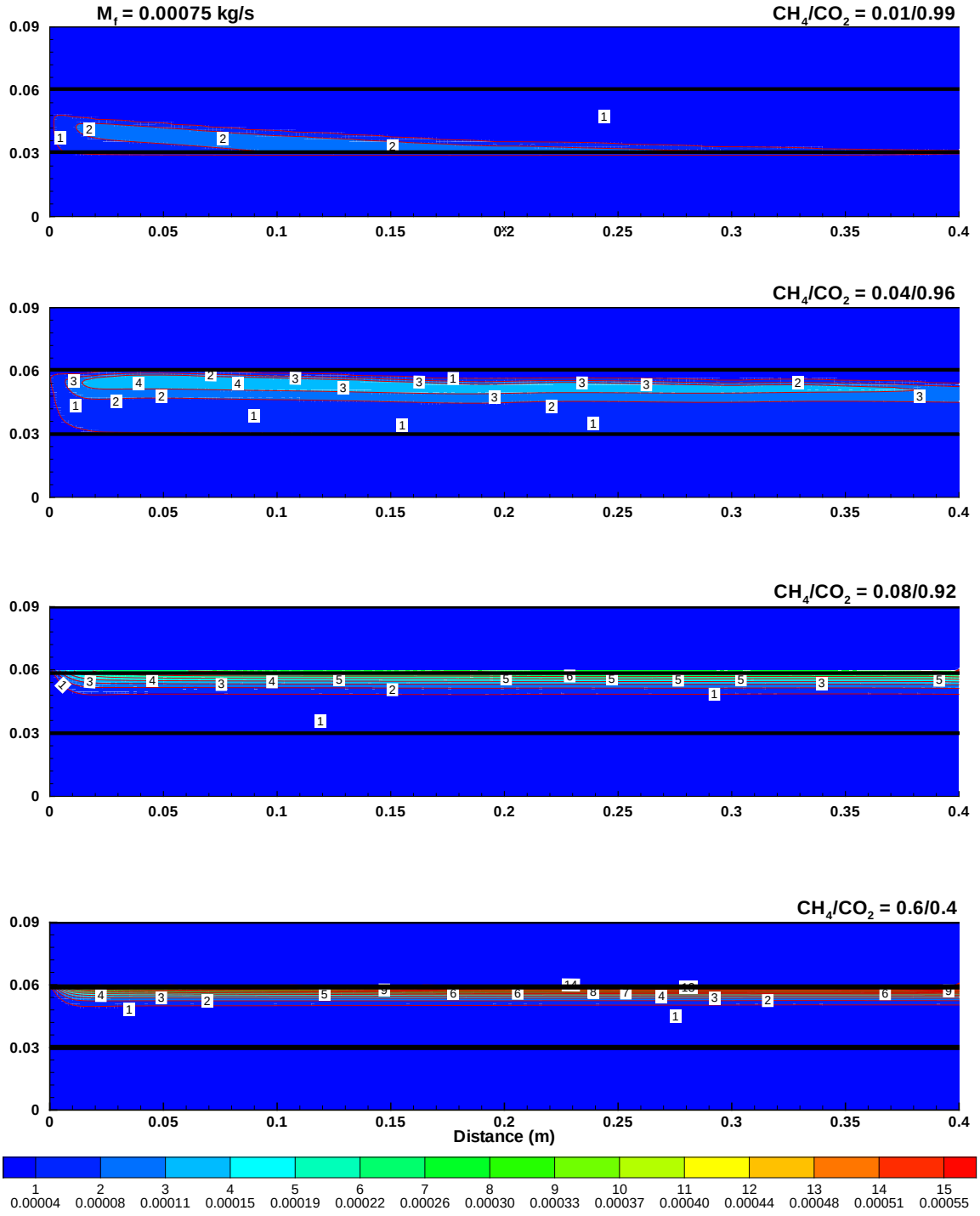

Figure 56: Reaction rate contours for increasing CH_4/CO_2 mass fraction ratios

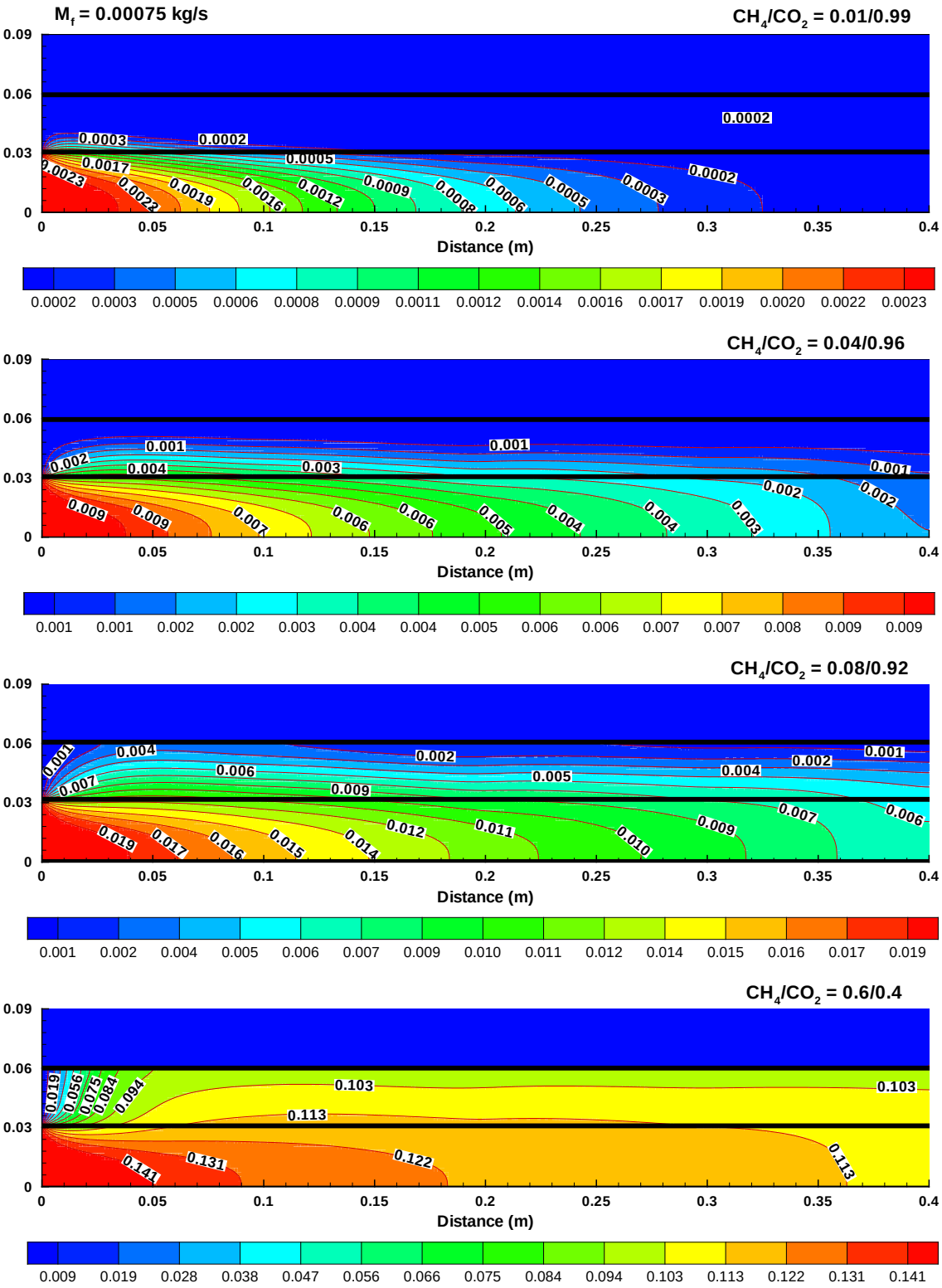

Figure 57: Mass fraction of CH_4 for increasing CH_4/CO_2 ratio

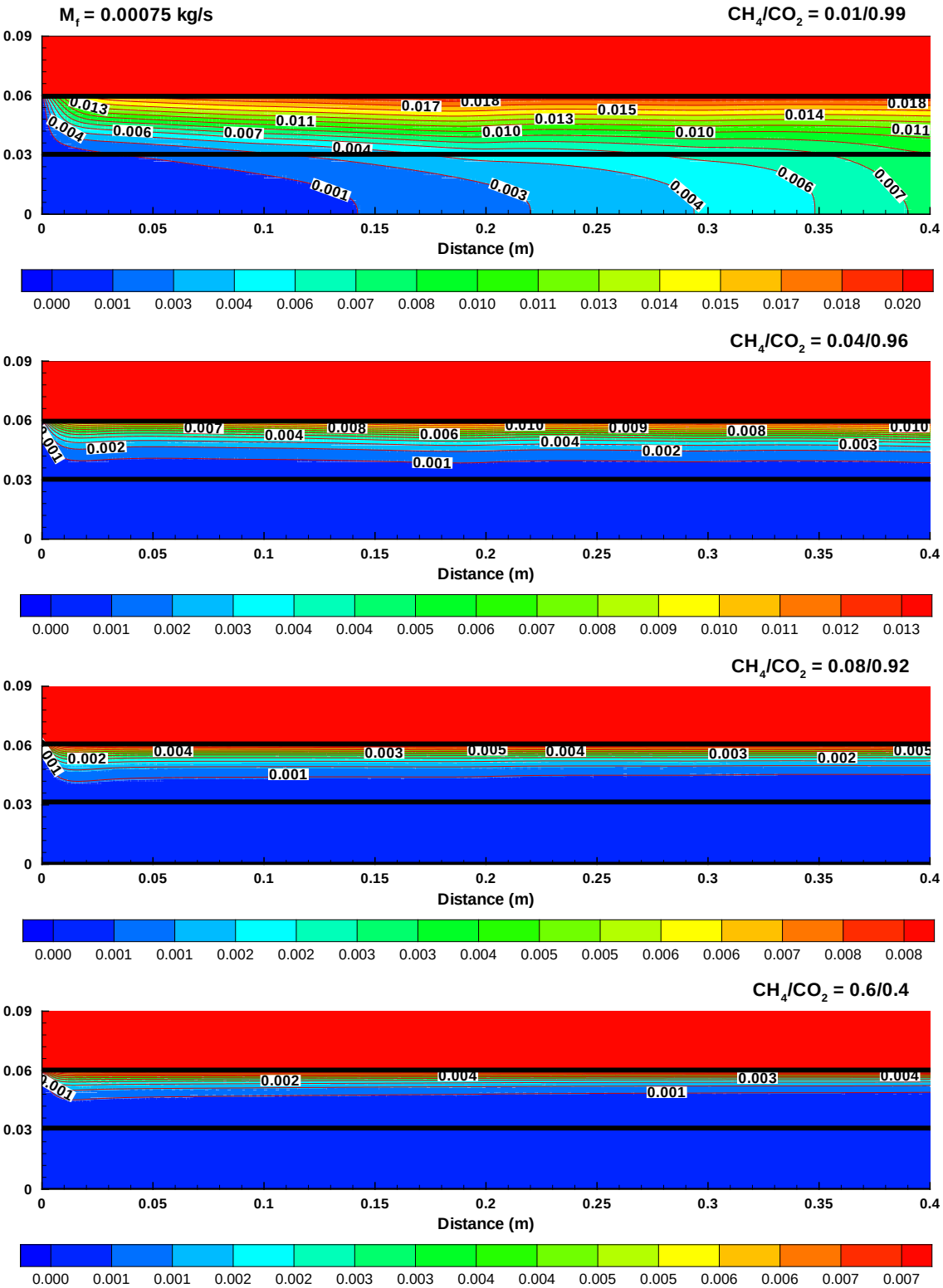

Figure 58: Mass fraction of O_2 for increasing CH_4/CO_2 ratio

5.2.4 Effect of mass flow rates on the temperature of ITM:

Figure 59 shows the temperature plot on the feed side and permeate side of the membrane. As the thickness of the membrane is very small i.e. 1 mm, the difference in temperatures is also small. The maximum difference in temperature along the length of the ITM is approximately 30K. Oxy-fuel combustion using ion transport membranes produces a longer ‘‘milder’’ flame distributed over much of the reactor length. This may be an advantage since the resulting heat flux is likely to be more uniform over a longer distance in the reactor. The uniform heat flux reduces the wall shear stresses that may arouse due to high temperature differences, thereby increasing the performance as well as life cycle of the membrane. The same effects are shown previously in the temperature contours, presented in Figure 55.

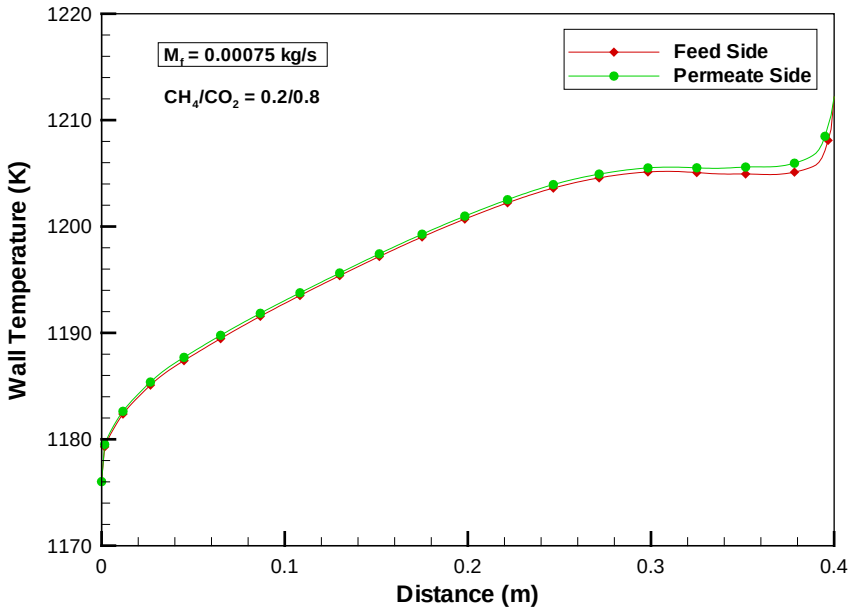

Figure 59: Wall temperature at air side and permeate side of ITM

Figure 60shows the temperature on the permeate side of the ion transport membrane for three different mass flow rates of fuel mixture. It is clear from this plot that with increase in mass fraction of CH_4 in the fuel mixture, the temperature of the ITM increases. This is because the reaction rate increases with increase in mass fraction of CH_4 in the fuel mixture. Moreover the reaction zone shifts towards the ITM, thereby increasing the temperature of the membrane. It is observed that the temperature of the ITM on the permeate side increases till the amount of CH_4in the fuel mixture reaches 60%. However beyond this value though the amount of CH_4 is increased, the temperature of the ITM is reduced slightly. This may be due to the heat transfer by conduction in the ITM and also by convection due to lower temperature air on the feed side.

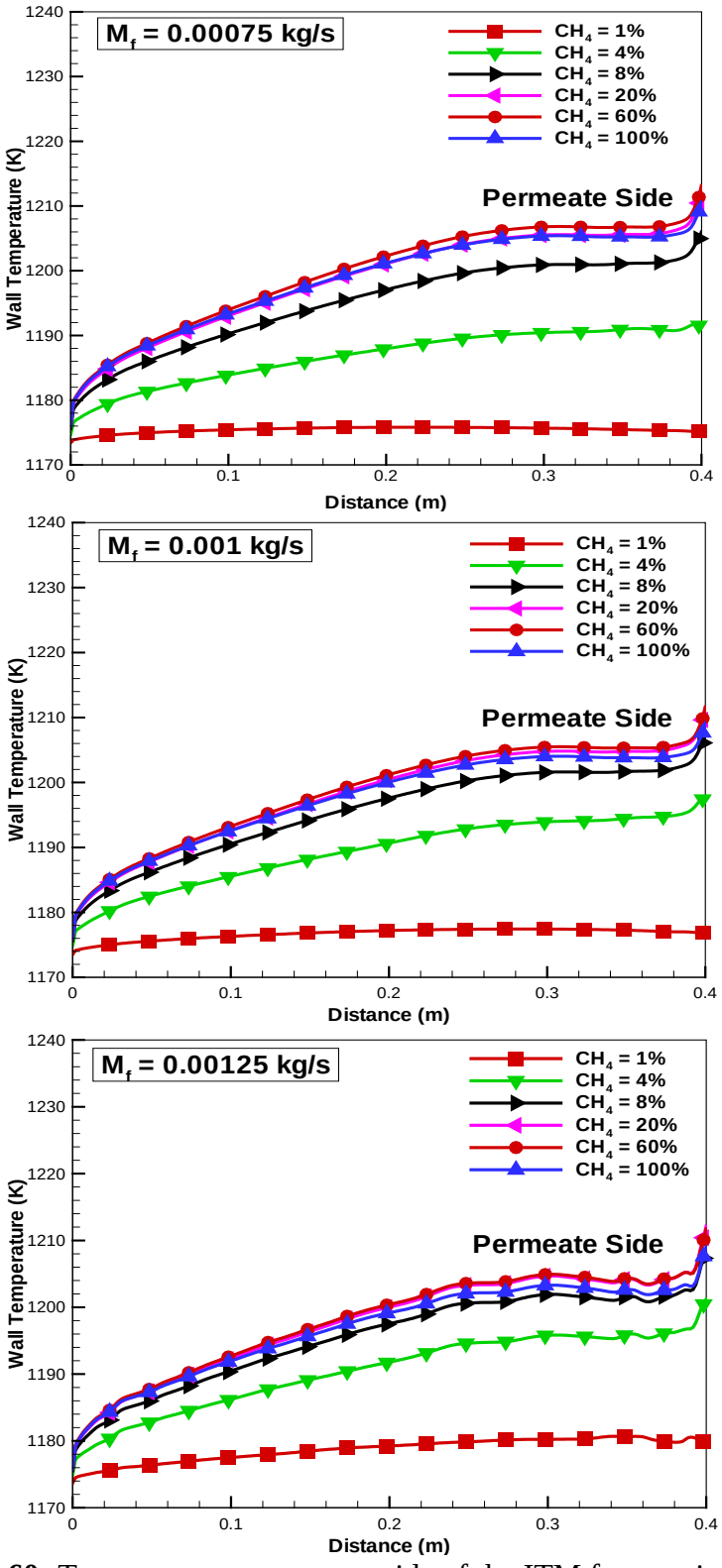

Figure 60: Temperature at permeate side of the ITM for reactive cases

5.2.5 Effect of mass flow rate of fuel mixture on the oxygen permeation rates:

Figure 61 shows the effect on oxygen permeation rates with increasing percentage of CH_4 for three different mass flow rates of the fuel mixture for the reactive cases. It is observed that for a constant mass flow rate of fuel, if the percentage of CO_2 is increased (or the percentage of CH_4 decreased) then the oxygen permeation rate decreases steadily up to 80% of CO_2 (or 20% of CH_4) but beyond this percentage the permeation rates decreases exponentially. This may be due to very low rate of reactions occurring at lower mass fraction ratios of CH_4/CO_2. Moreover decrease in the volume flow rate, as shown in Figure 62, also contributes to the decrease in oxygen permeation rates. This decrease in volume flow rate has already been explained in the previous sections. These results are confirmed from the work done by Wei et al[82]. On the other hand, with the increase in mass flow rate of fuel mixture there is no significant change in the oxygen permeation rates.

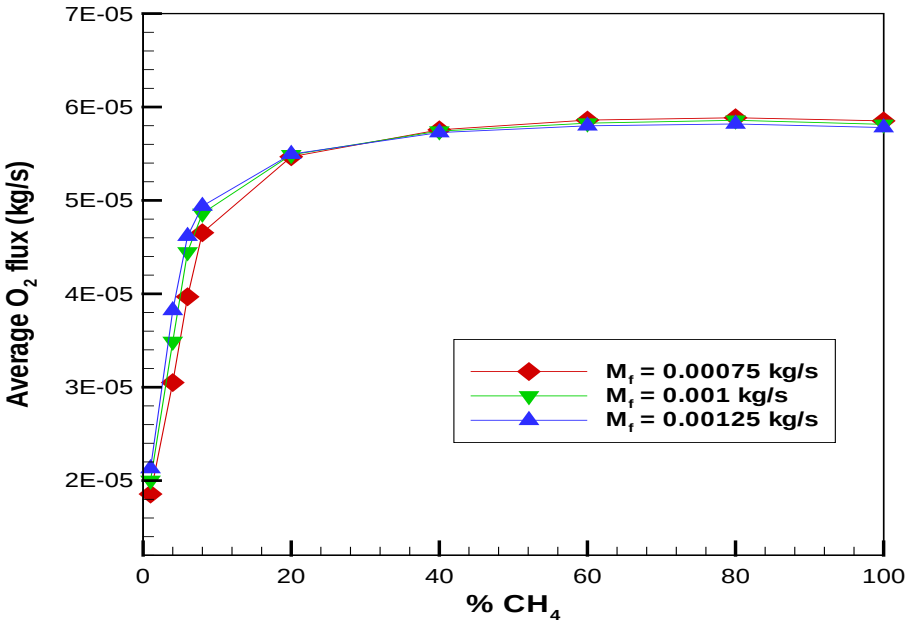

Figure 61: Effect of mass flow rate of fuel on the oxygen permeation flux with increasing percentage of CH_4 for reactive cases

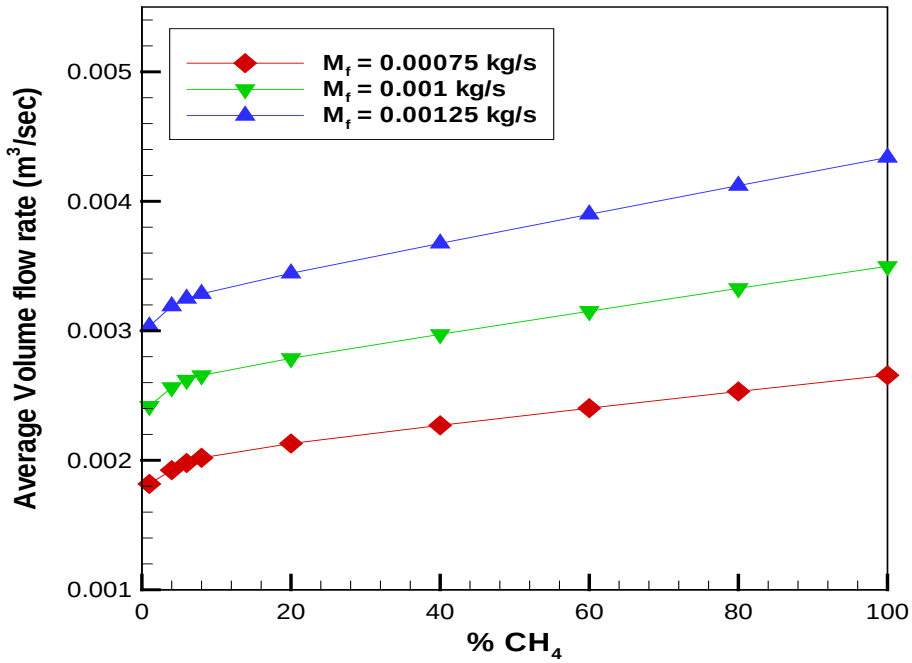

Figure 62: Volume flow rate for three different mass flow rates of fuel mixture with varying mass fraction of CO_2

Figure 63 shows the oxygen permeation rates for non-reactive (separation only) and reactive cases for the mass flow rate of 0.00075 kg/s. the amount of oxygen permeated through the ITM membrane for non-reactive (separation only) mode is 1.56 x 10^{-05} kg/s to 1.7 x 10^{-05} kg/s while for the reactive mode it is 1.85 x 10^{-05} kg/s to 5.85 x 10^{-05} kg/s for 1% to 100% of CH_4 in the fuel mixture.The oxygen permeation rate through the membrane is increases for 1% to 20% CH_4 at inlet and becomes almost constant for the increased CH_4 percentages. Oxygen permeation rate through ITM for combustion (reactive case) is very much higher compared to separation only mode and it is 15% to 70% higher for 1% to 100% increase in CH_4 at inlet.

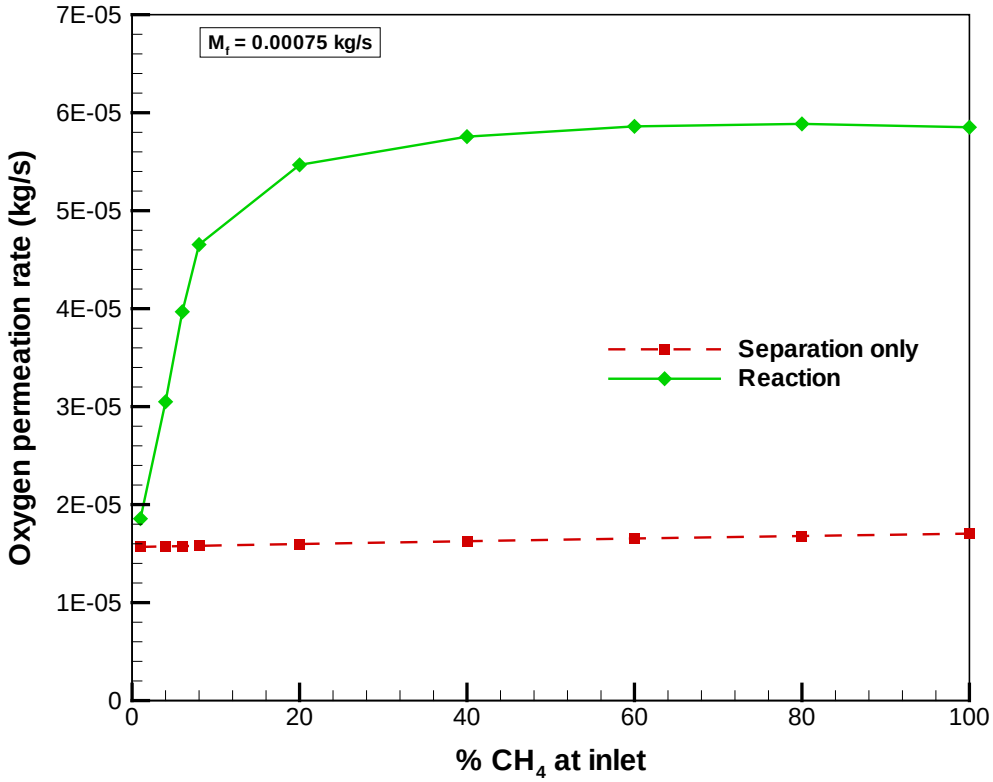

Figure 63: Comparison of O_2 permeation rates with and without reactions

5.2.6 Effect of CH_4/CO_2 mass fraction ratios on CH_4 and O_2 conversion:

In order to optimize the design of the present oxygen transport reactor for O_2 separation and fuel oxidation, the amount of CH_4 conversion is an important parameter that is affected by the diluents CO_2 concentration and O_2 permeation flux. Figure 64 shows the percentage conversion of CH_4 and O_2 with increase in the percentage of CH_4 in the fuel mixture for a constant mass flow rate of 0.00075 kg/s.

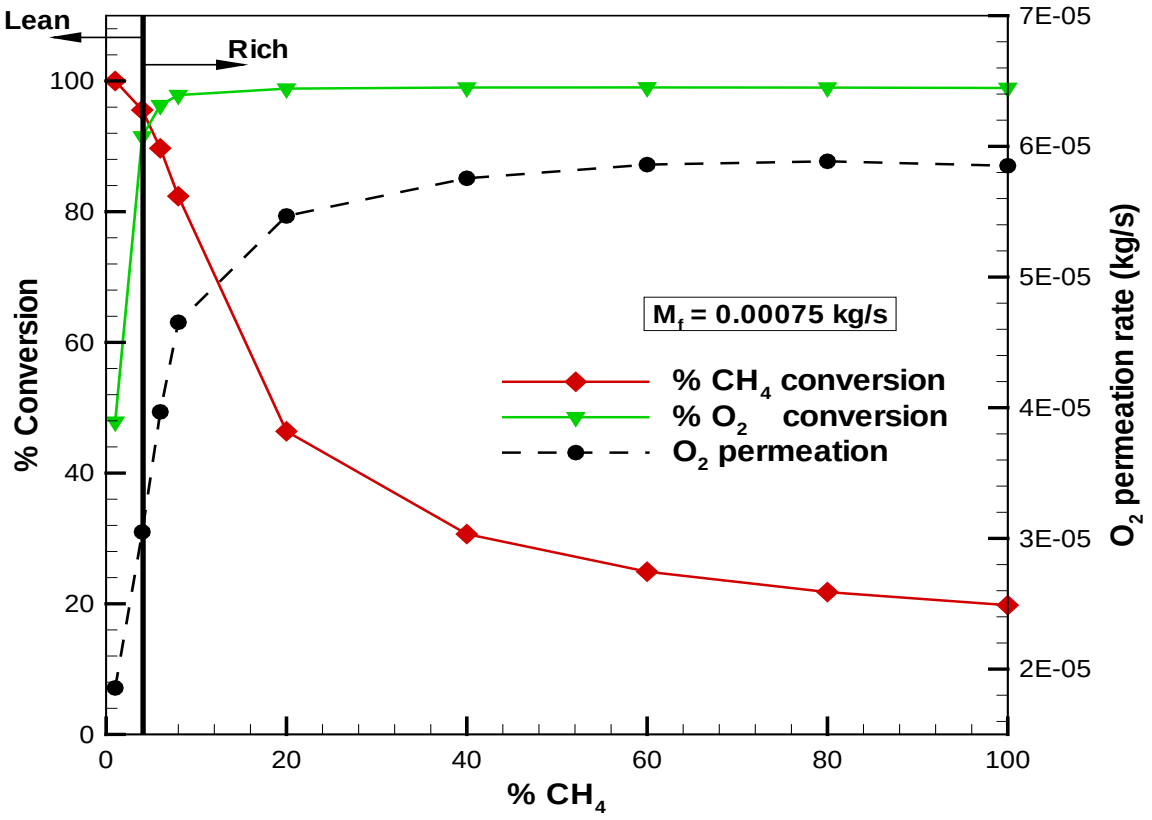

Figure 64: Conversion of CH_4 and O_2 with increase in the percentage of CH_4 in the fuel mixture

It is observed that with increase in the percentage of CH_4 in the fuel mixture the conversion percentage of O_2 increases.When CH_4 is 15% (relative percentage) in the fuel

mixture the % conversion of O_2reaches almost 100% while the % conversion of CH_4 decreases. It has been noted that approximately 4 to 15% of CH_4 in the fuel mixture gives maximum CH_4 and O_2percentage conversions. Similar profile for O_2 permeation rate and conversion of CH_4 and O_2 is obtained by Tan et al [33] for LSCF-ITM membrane.Similar conversion results were found when the mass flow rates of fuel mixture were increased to 0.001 kg/s and 0.00125 kg/s.O_2/CH_4 value is an important parameter to decide the region of flammability limit for combustion. Figure 65shows the representation of all the three mass flow rates with different CH_4% at inlet.

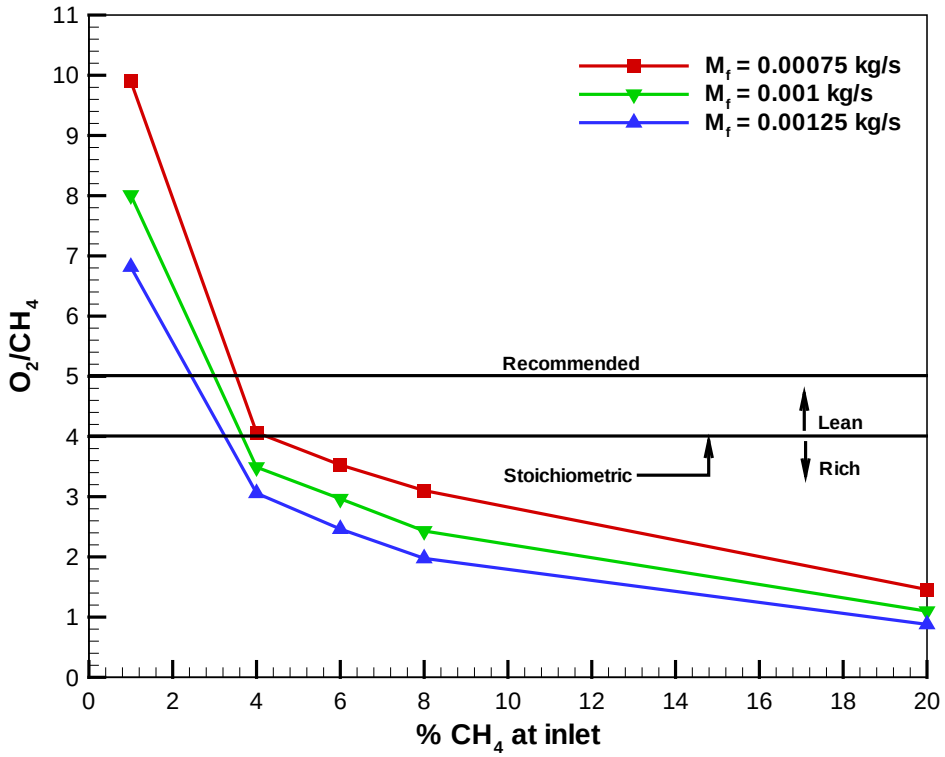

Figure 65: O_2/CH_4 ratio for three different mass flow rates of fuel

It can be seen that the fuel mixture containing only 3% to 4% of CH_4 fall in the recommended region.

5.2.7 Effect of mass flow rates of fuel mixture on CH_4 and O_2 conversion:

The results of % conversion of CH4 for increasing CH4 percentage at the fuel inlet for three different mass flow rates of fuel mixture are presented in Figure 66. It is evident that with increase in the mass flow rates of the fuel mixture the percentage conversion of CH_4 decreases. This also suggests that operating the reactor at low mass flow rates and low CH_4 percentages is advantageous in order to obtain maximum outputs.

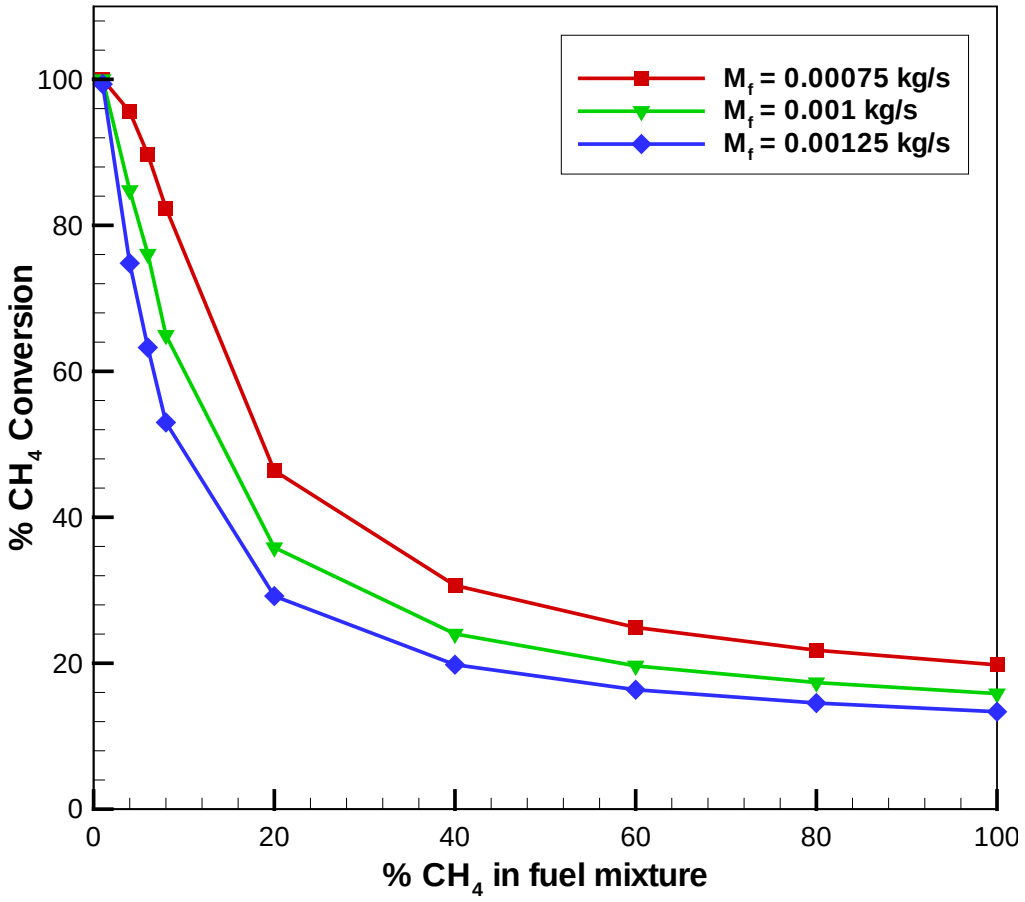

Figure 66: % Conversion of CH_4 for increasing CH_4 percentage in three different mass flow rates

5.2.8 Effect of mass flow rates of fuel mixture on the partial pressure and oxygen flux at permeate side of the ITM:

Figure 67shows the partial pressure of oxygen on the permeate side of the ITM for three different mass flow rates of the fuel mixture. The percentage of CH_4 has been varied from 1 to 100 for each mass flow rate. The results depicting the corresponding oxygen fluxes are presented in Figure 68. As discussed in the early sections, the partial pressure of oxygen decreases with increasing mass flow rates due to increased purging effects. Moreover the decrease in the percentages of CO_2 also contributes to the decrease thereby increasing the oxygen fluxes.

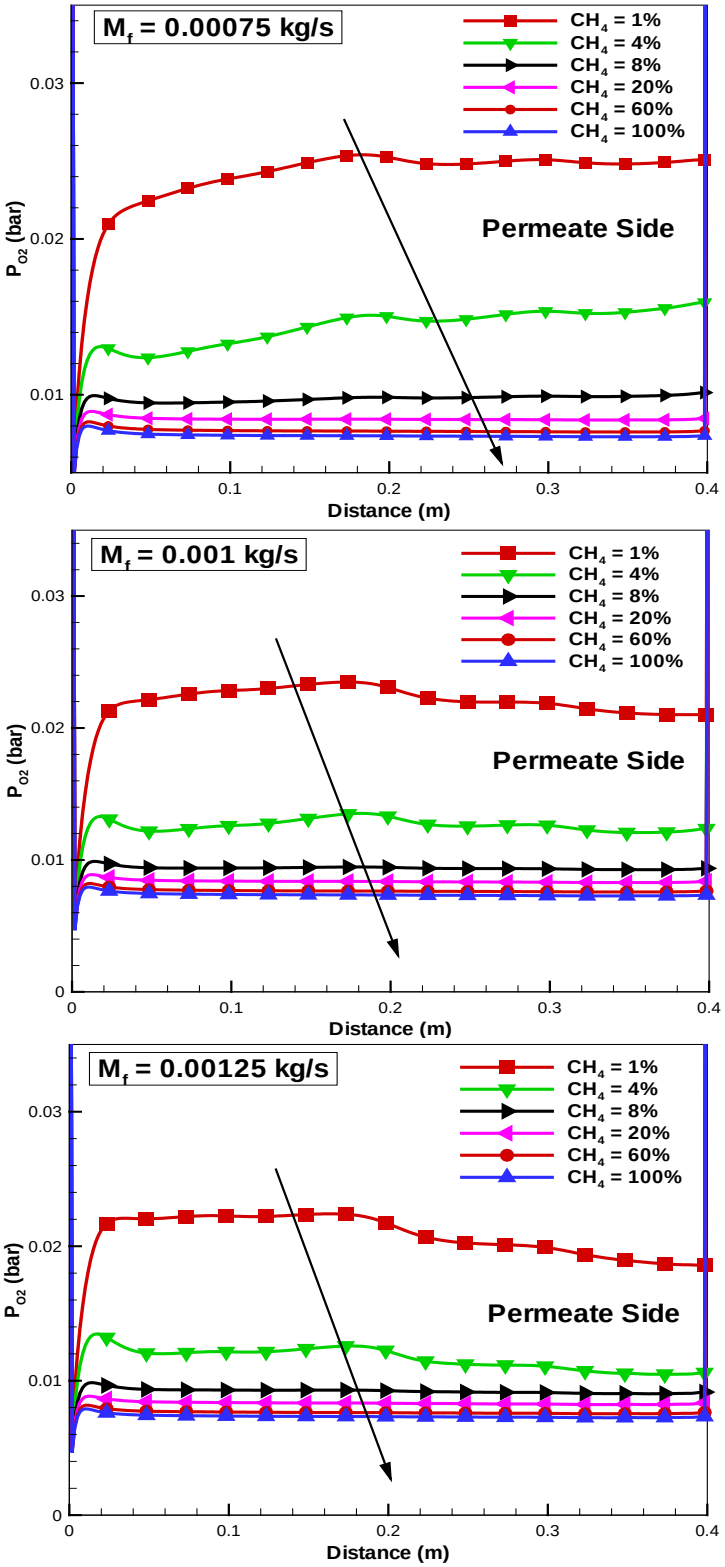

Figure 67: Partial pressure on the permeate side of ITM for reactive cases

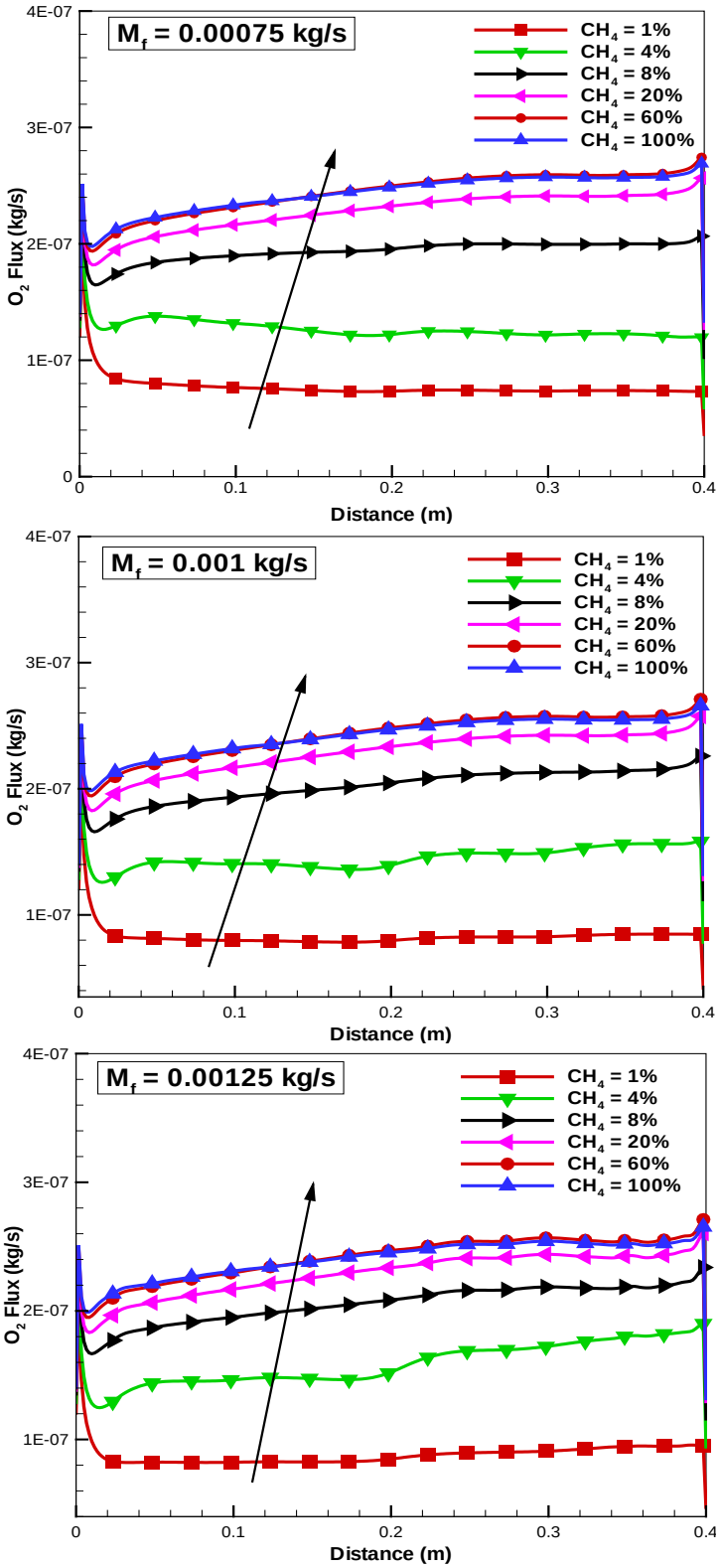

Figure 68: Oxygen permeation on permeate side of the membrane

In order to maximize the CH_4 conversion at high mass flow rates, use of ITMs with catalyst coatings at permeate side is suggested [80]. More work has to be done on material development and testing side before proceeding into the catalytic conversion of CH_4.

From the above discussion, it is clear that the present oxygen transport reactor has potential to be implemented in transforming a conventional combustion chamber to an ITM reactor in which separation and oxidation of fuel is done simultaneously. Moreover the results predict a more uniform temperature ITM reducing the strain induced due to high temperature gradients.

5.3 Advantages of the Present Model Reactor (Isothermal reactor)Over the Co-feed Reactor:

There are many advantages of isothermal reactor concept over co-feed reactor operations in terms of temperature homogeneity, uniform heat flux and in controlling the reaction zone. Some of them are discussed below.

Co-feed Reactor:

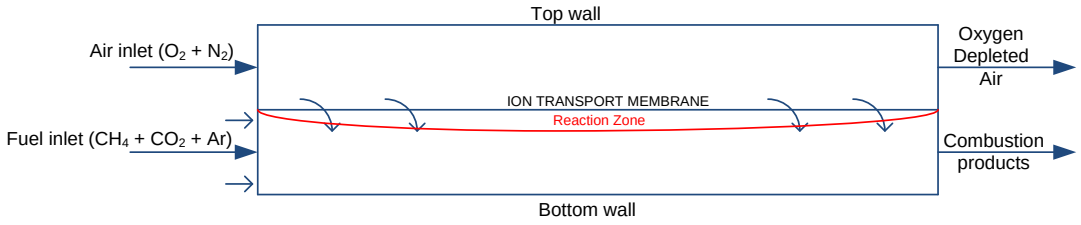

Figure 69: Line diagram of co-feed reactor

Isothermal Reactor:

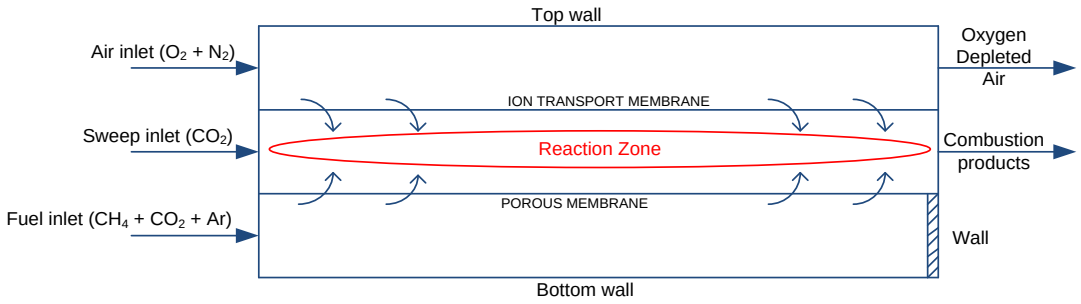

Figure 70: Line diagram of isothermal reactor

The comparison for Traditional co-feed reactor and isothermal reactor has been done for the below mentioned boundary conditions:

Mass flow rate of air (O_2 + N_2) = 0.03 kg/s

Mass flow rate of fuel mixture (CH_4 + CO_2 + Ar) = 0.00075 kg/s

Mass fraction of CH_4 in the fuel mixture = 0.01

Mass fraction of CO_2 in the fuel mixture = 0.24

Mass fraction of Argon = 0.75

Figure 71 shows the wall temperature on the permeate side of the ITM for co-feed and isothermal reactor cases. It is clear from the Figure 71that in case of an isothermal reactor concept the wall temperature is uniformly varying along the length of the ITM. This may be advantageous to achieve homogeneous temperature, uniform heat flux and to reduce wall shear stresses on the ion transport membrane, thus increasing the life cycle of the membrane.

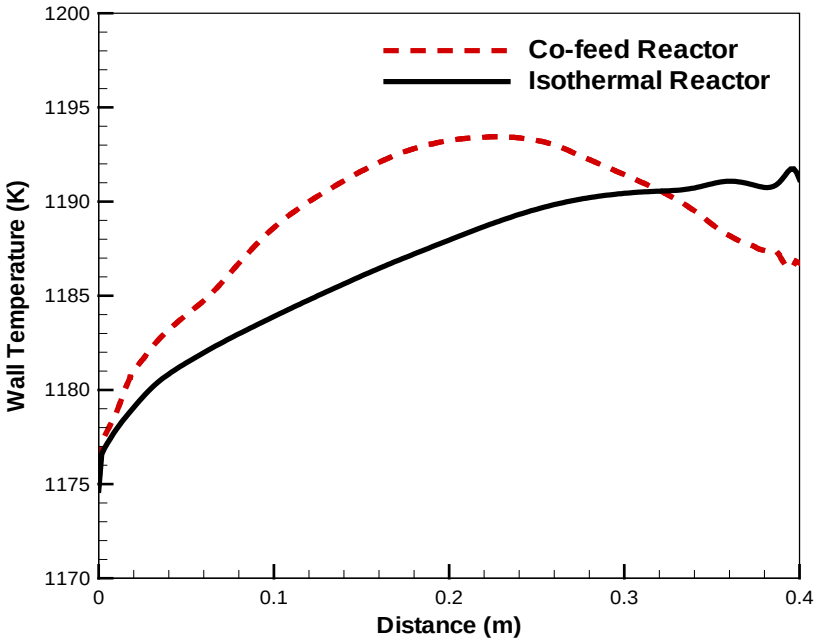

Figure 71: Comparison of wall temperature on the permeate side of the ITM for co-feed and isothermal reactors

Figure 72 shows the comparison of oxygen permeation flux for co-feed and isothermal reactor concepts. Comparison shows that the permeation flux in case of co-feed reactor is high in the first half region of the reactor and then it gradually decreases. This is because of the reaction zone near to the ITM which may be limiting factor for the stability and temperature homogeneity of the membrane. The same effects are shown again in reaction rate contours. The average permeation flux in case of co-feed reactor is only 30% (approximately) more than the isothermal reactor concept. But unlike Co-feed reactor the oxygen permeation flux in case of isothermal reactor is uniform all along the length of the ion transport membrane. This is useful in achieving uniform stoichiometric ratio (using porous membrane to feed fuel) in order to have uniform combustion all along the

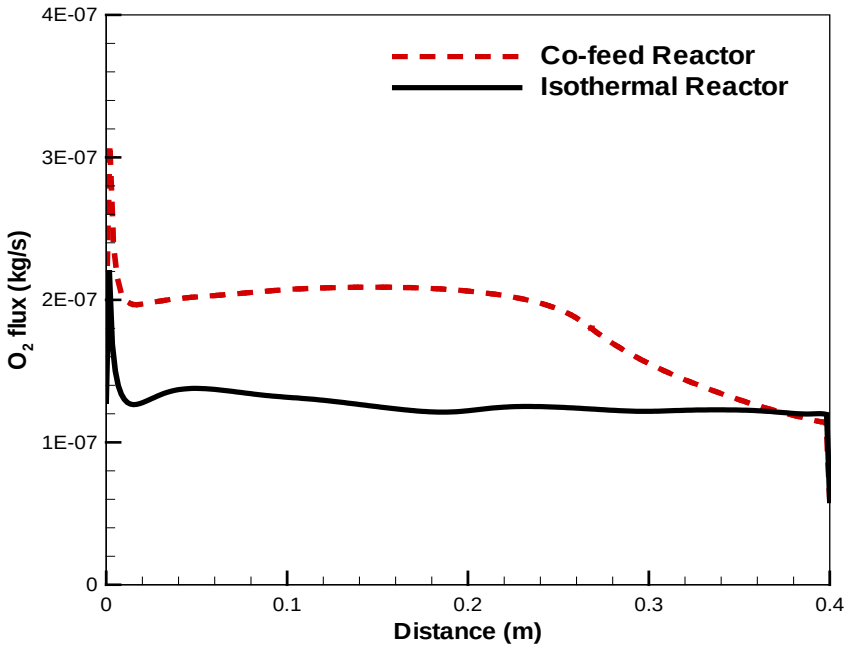

Figure 72: Comparison of oxygen permeation flux (on permeate side of the ITM) for co-feed and isothermal reactors

length of the membrane. Thus the isothermal reactor concept enables to achieve homogeneous temperature and uniform heat flux more easily than the co-feed reactor.

Figure 73 and Figure 74 shows the comparison of reaction rate and temperature plots respectively at a normal distance of 200mm from the entrance of both the co-feed and isothermal reactors. The comparison has been made in detail using the respective contours (Figure 75, Figure 76).

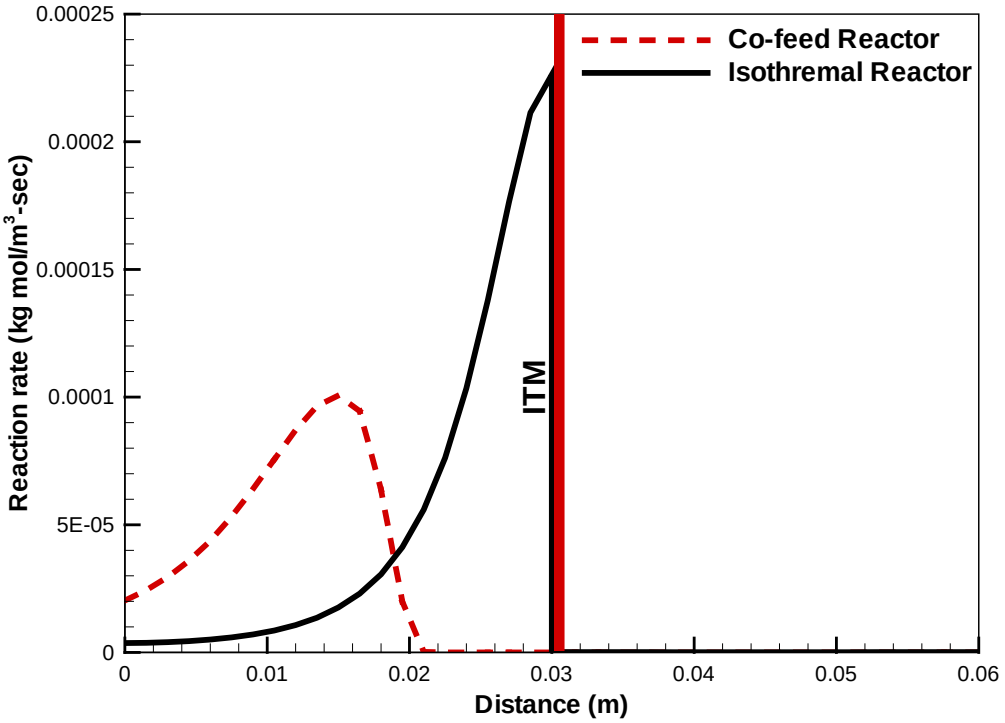

Figure 73: Comparison of normal profiles of reaction rates for co-feed and isothermal reactors

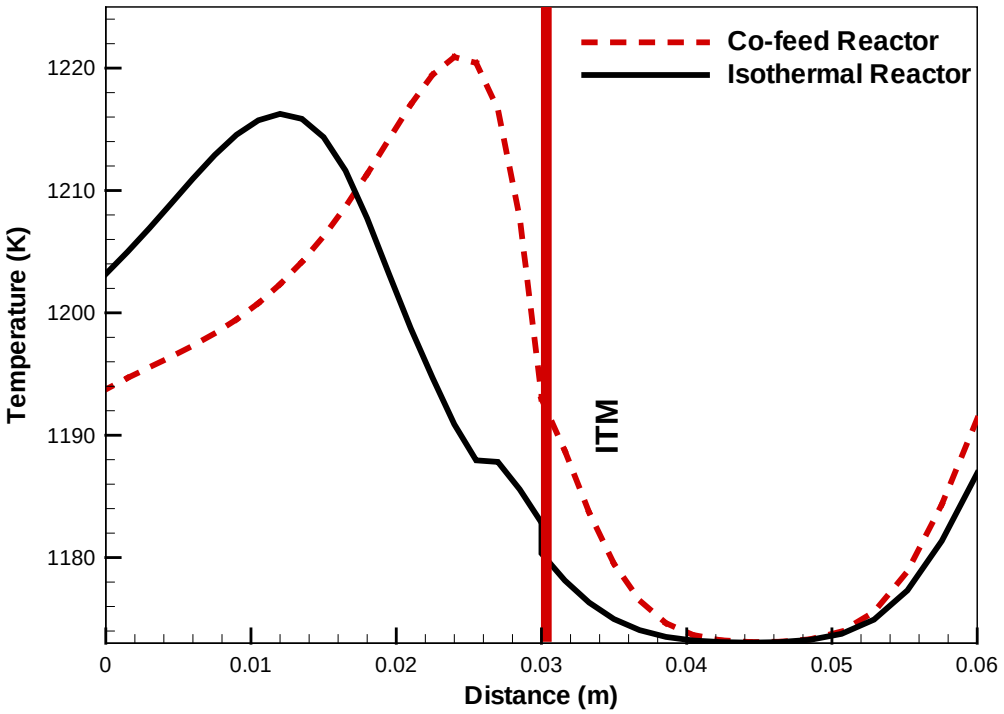

Figure 74: Comparison of normal profiles of temperatures for co-feed and isothermal reactors

Figure 75shows the reaction rate contours for co-feed and isothermal reactors. It is important to mention that the contour levels for both the cases are compared to the same scale and the color bar highlights the temperature variations. It is clear from the above reaction rate contours that in case of co-feed reactor the reaction takes place next to the ion transport membrane, which causes an increases in permeation flux in the first half of the reactor (as explained in the oxygen permeation flux plot), where as in the isothermal reactor concept the reaction zone can be shifted away from the ion transport membrane by adjusting the amount of CH_4 in the fuel mixture (fed through the porous membrane), thereby improving the performance of the ion transport membrane as well increasing its life cycle. The reaction near to the may also cause surface reactions between the gases

and the membrane material leading to formation of unwanted by-products that may deposit on the membrane, limiting desorption of oxygen on the permeate side.

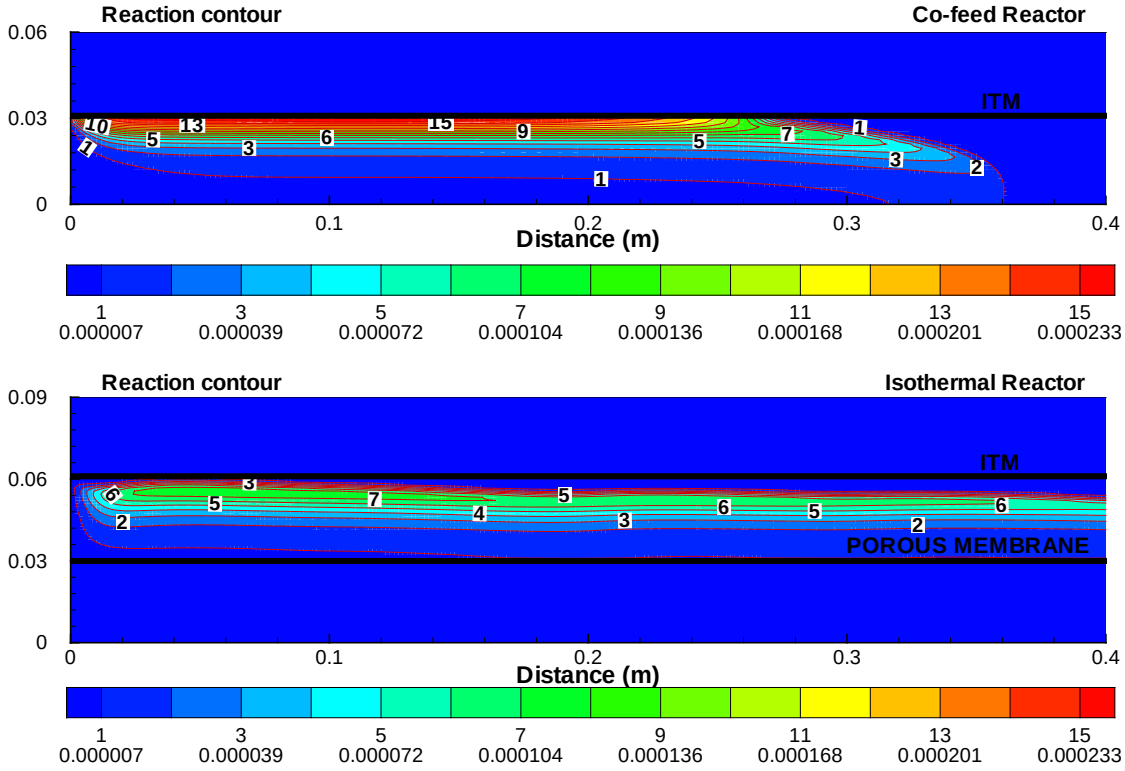

Figure 75: Comparison of reaction rate contours for co-feed and isothermal reactors

Figure 76 shows the temperature contours for both co-feed and isothermal reactors. These temperature contours show that in case of co-feed reactor the high temperature zone is concentrated where as the isothermal reactor produces a longer ‘‘milder’’ high temperature zone distributed (homogeneous) over much of the reactor length. This may be an advantage since the resulting heat flux, in case of isothermal reactor, is likely to be more uniform over a longer distance. Another advantage of the isothermal reactor over co-feed reactor is that the temperature at the exit of the isothermal reactor is high when

compared to the traditional co-feed reactor, which is useful in attaining high inlet temperatures (desirable) for the turbine.

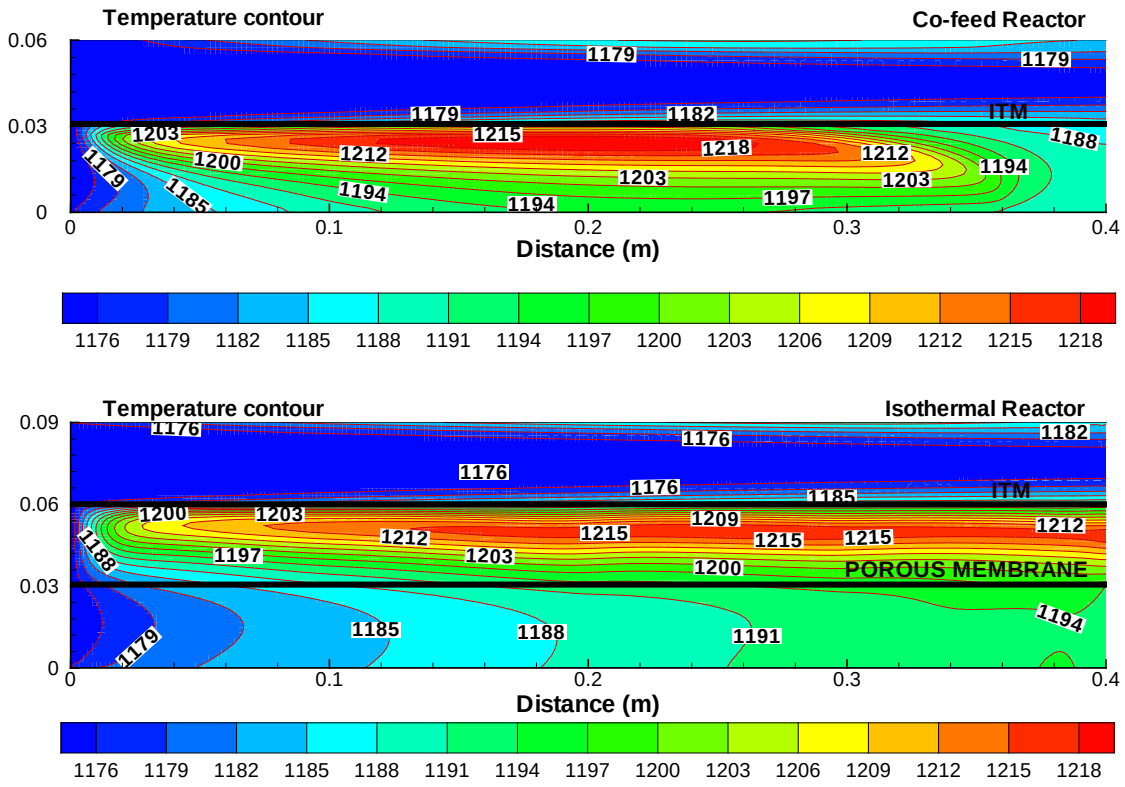

Figure 76: Comparison of temperature contours for co-feed and isothermal reactors

5.3.1 CH_4 and O_2conversions:

Isothermal reactor

CH_4 conversion = 95.6%

O_2 conversion = 91.5%

Co-feed Reactor

CH_4 conversion = 100%

O_2 conversion = 82%

The above conversion figures show that even though there is 100% methane conversion in case of co-feed reactor, the overall methane and oxygen conversion in isothermal reactor is much better. The co-feed reactor gives an approximately 10% less oxygen conversion i.e. 10% of the oxygen permeated is unused in the reaction. Therefore isothermal reactor offers many advantages over the co-feed reactor in terms of controlling the reaction zone and also to achieve uniform temperature all along the length of the ITM.

CHAPTER 6

CONCLUSIONS AND RECOMMENDATIONS

This chapter consists of three sections. The first two sections summarize the results presented in the previous sections and the third section presents some of the directions in which the present thesis work can be further extended.

In the present thesis work a two-dimensional, computational fluid dynamics (CFD) model has been developed to predict oxy-combustion characteristics in an oxygen transport reactor (nearly isothermal reactor). Details of temperature, flow, species distribution are predicted by the numerical solution of the conservation of mass, momentum, energy and species transport equations of two dimensional flows. The membrane (ITM) is modeled as a selective layer, which allows the permeation of oxygen as a function of temperature and the difference of partial pressures of oxygen in the feed side and the permeate side of the ITM. The porous layer is modeled as a function of permeability and thickness of the medium used. Validation for the models used has been performed against the experimental results available in the literature and were found to be in good agreement with the present work.

6.1 Separation Only Mode (Non-reactive Cases):

- The flow conditions at the permeate side influenced the performance of oxygen separation.
- It has been concluded that for a constant mass flow rate of the fuel mixture for the non-reactive environment (separation only cases), the oxygen permeation flux increases with increase in the CH_4 percentage.

6.2 Reactive Cases (Separation and Combustion):

The results of combustion in OTR for different composition of CH_4/CO_2 mixtures and for different mass flow rates have provided many important insights and conclusions.

- Firstly, the comparison between reactive and separation-only OTR units showed that combining reaction and separation increases significantly O_2 permeation rate to about 3 times under the assumptions given herein.
- Secondly, by using a porous membrane to introduce fuel mixture in the reactor (present model isothermal reactor) for combustion, a more uniform temperature along the length of the ITM has been obtained compared to the co-feed reactor.
- It has been observed that with increase in the percentage of CH_4 in the fuel mixture the conversion percentage of O_2 increases and reaches almost 100% when CH_4 is 15% (relative percentage of CH_4 and CO_2) in the fuel mixture but the % conversion of CH_4 decreases.

- It has been concluded that approximately 4% to 15% (relative percentage of CH_4 and CO_2) of CH_4 in the fuel mixture gives maximum CH_4 and O_2 percentage conversions.
- The present model isothermal reactor also provides the advantage of attaining higher exit temperatures that are essential for the inlet of the turbines.
- The reaction zone can also be controlled accordingly for the improved performance of the ITM.

6.3 Recommendations:

The use of ITM technology to capture CO_2in power cycles shows potential to retrofit or to use as an auxiliary system to separate O_2 for oxy-combustion. The O_2 permeation equation used in this work is based on experimental correlations. More work is needed to develop a more generalized equation which represents the membrane characteristics and operational conditions. Further, single-step chemistry is used in the present simulations for oxidation of methane into $CO_2$and H_2O, but in practice there will be other species such as CO, H_2, etc. Accordingly, detailed chemistry must be employed to study the impact and stability of such species on ITM. Other major issues related to the effect of carbon deposition and soot formation on the membrane characteristics needs detailed investigation. Continued modeling and simulation effort has to be made to predict the optimized dimensions of the reactor.

NOMENCLATURE

A_{cell}	Area of the cell [m^2]
A	Pre-exponential factor [-]
a	Absorption coefficient
C_p	Heat capacity [J/Kg-K]
C_i	Density of oxygen ions [mol/m^3]
$D_{i,m}$	Diffusion coefficient of mixture of species i [m^2/s]
D_s	Self-diffusivity [m^2/s]
D_v	Diffusion coefficient of oxygen vacancies [cm^2/s]
$D_{i,j}$	Binary mass diffusion coefficient of species i [m^2/s]
E_a	Activation energy [J/kg-mol]
F	Faraday's constant [c/mol]
I	Radiation intensity, which depends on position and direction
J_{O_2}	Oxygen permeation flux [mol/m^2-s]
K	Reaction rate constant [Kg-mol/m^3-s]

K_1	Geometric constant [-]
K_2	Constant depends on temperature [mol/m^2-s]
k_{io}	Surface exchange coefficient [m/s]
k_r	Surface-exchange reaction reverse-rate constant [mol $cm^{-2}s^{-1}$]
k_f	Surface-exchange reaction forward-rate constant [cm $atm^{-0.5}s^{-1}$]
L	Membrane thickness [m]
L_c	Characteristic membrane thickness [m]
M_i	Molecular weight of species i [Kg/Kmol]
$\dot{m}$	Mass flow rate [Kg/s]
n	Refractive index
p	Pressure [Pa]
P'_{O_2}, P_1	Partial pressure of oxygen at the feed side [atm]
P''_{O_2}, P_2	Partial pressure of oxygen at the permeate side [atm]
$P^0_{O_2}$, P_0	1 atm oxygen pressure

P1,P2,P3,P4	Face permeabilities of porous membranes 1,2,3,4 (equal lengths) [m^2]
$\Re$	Universal gas constant [J/mol-K]
R_1	Resistance to O_2 permeation at the inner membrane surface [$atm^{0.5}cm^2sec/mol$]
R_2	Resistance to O_2 permeation in the bulk region [$atm^{0.5}cm^2sec/mol$]
R_3	Resistance to O_2 permeation at the outer membrane surface [$atm^{0.5}cm^2sec/mol$]
r_1	Outer radius of the membrane tube [m]
r_2	Inner radius of the membrane tube [m]
$\vec{r}$	Position vector
S	Effective area of the membrane tube [m^2]
S_i, S_m	Source/sink term [Kg/m^3-s], mass source term [Kg/m^3-s]
$\vec{s}$, $\vec{s}'$	Direction vector, scattering direction vector
T	Temperature [K]
t_i	Ionic transference number [-]
t_e	Electronic transference number [-]

U, V	Superficial velocity [m s^{-1}]
V_m	Molar volume [m^3/mol]
$V_O^{\bullet\bullet}$	Oxygen vacancy [-]
V_{cell}	Volume of cell [m^3]
W	Effective length of the tube [m]
X_i	Mole fraction of species i [-]
Y_i	Mass fraction of species i [-]
$\varphi_{i,j}$	Mixture rule constant for species i in species j [-]
ϕ	Phase function
Ω	Solid angle
ρ	Density [Kg m^{-3}]
μ	Dynamic viscosity [N s m^{-2}]
μ_{O_2}	Oxygen vacancy potential [J/mol]
σ_i	Ionic conductivity [S/m]
σ_e	Electronic conductivity [S/m]
σ_s	Scattering coefficient

σ	Stefan-Boltzmann constant (5.669×10^{-08} W/m^2 – K^4)
β_1	Bulk-diffusion step constant [-]
λ_i	Thermal conductivity of species i [W/m/K]
ε	Bed porosity

REFERENCES

[1] J. Armor, "Addressing the CO_2 dilemma," *Catalysis Letters,* vol. 114, pp. 115-121, 2007.

[2] W. Terry F., "Combustion processes for carbon capture," *Proceedings of the Combustion Institute,* vol. 31, pp. 31-47, 2007.

[3] J. D. Figueroa, T. Fout, S. Plasynski, H. McIlvried, and R. D. Srivastava, "Advances in CO_2 capture technology ”The U.S. Department of Energy's Carbon Sequestration Program," *International Journal of Greenhouse Gas Control,* vol. 2, pp. 9-20, 2008.

[4] S. D. Gillian M. Bond, Ning Liu, Teri Dunn, Thomas Villanova, Christa Hockensmith, Brian J. McPherson, John Stringer, "Effective use of brine for CO_2 sequestration," *Proceedings of Fourth Annual Conference on Carbon Sequestration,* May 2-5 2005.

[5] K. F. a. E. Yantovski, "Fuel-Fired Zero Emissions Power Plant Cycles with Oxygen Ion Transport Membranes (History and State-of-the-Art)," *Proceedings of Fifth Annual Conference on Carbon Sequestration,* May 8-11. 2006.

[6] M. A. Habib, H. M. Badr, S. F. Ahmed, R. Ben-Mansour, K. Mezghani, S. Imashuku, G. J. la O', Y. Shao-Horn, N. D. Mancini, A. Mitsos, P. Kirchen, and A. F.

Ghoneim, "A review of recent developments in carbon capture utilizing oxy-fuel combustion in conventional and ion transport membrane systems," *International Journal of Energy Research,* vol. 35, pp. 741-764, 2011.

[7] N. D. Mancini and A. Mitsos, "Ion transport membrane reactors for oxy-combustion“ Part I: intermediate-fidelity modeling," *Energy PRES 2010,* vol. 36, pp. 4701-4720, 2011.

[8] R. M. Fristrom and A. A. Westenberg, *Flame structure* vol. 276: McGraw-Hill New York, 1965.

[9] C. K. Westbrook and F. L. Dryer, "Comprehensive Mechanism for Methanol Oxidation," *Combustion Science and Technology,* vol. 20, pp. 125-140, 1979.

[10] I. Glassman, *Combustion*. California 92101- 4495, USA: Academic Press, 1996.

[11] A. P. Simpson and A. J. Simon, "Second law comparison of oxy-fuel combustion and post-combustion carbon dioxide separation," *Energy Conversion and Management,* vol. 48, pp. 3034-3045, 2007.

[12] R. Steeneveldt, B. Berger, and T. A. Torp, "CO_2 Capture and Storage: Closing the Knowing–Doing Gap," *Chemical Engineering Research and Design,* vol. 84, pp. 739-763, 2006.

[13] P. Bernardo, E. Drioli, and G. Golemme, "Membrane gas separation: a review/state of the art," *Industrial & Engineering Chemistry Research,* vol. 48, pp. 4638-4663, 2009.

[14] M. Bernal, J. Coronas, M. Menendez, and J. Santamaria, "Separation of CO_2/N_2 mixtures using MFI-type zeolite membranes," *AIChE journal,* vol. 50, pp. 127-135, 2004.

[15] P. J. Gellings and H. Bouwmeester, *The CRC handbook of solid state electrochemistry*. USA: CRC press, 1997.

[16] J. Sunarso, S. Baumann, J. M. Serra, W. A. Meulenberg, S. Liu, Y. S. Lin, and J. C. Diniz da Costa, "Mixed ionic“electronic conducting (MIEC) ceramic-based membranes for oxygen separation," *Journal of Membrane Science,* vol. 320, pp. 13-41, 2008.

[17] R. J. Allam, "Improved oxygen production technologies," *Energy Procedia,* vol. 1, pp. 461-470, 2009.

[18] C. Press and P. Gellings, "The CRC handbook of solid state electrochemistry," 1997.

[19] S. J. Xu and W. J. Thomson, "Oxygen permeation rates through ion-conducting perovskite membranes," *Chemical Engineering Science,* vol. 54, pp. 3839-3850, 1999.

[20] U. Balachandran, B. Ma, P. S. Maiya, R. L. Mieville, J. T. Dusek, J. J. Picciolo, J. Guan, S. E. Dorris, and M. Liu, "Development of mixed-conducting oxides for gas separation," *Solid State Ionics,* vol. 108, pp. 363-370, 1998.

[21] K. Foy and J. McGovern, "Comparison of ion transport membranes," in *Proc. 4th Annual Conference on Carbon Capture and Sequestration*, 2005, pp. 2-5.

[22] B. J. P. Buhre, L. K. Elliott, C. D. Sheng, R. P. Gupta, and T. F. Wall, "Oxy-fuel combustion technology for coal-fired power generation," *Progress in Energy and Combustion Science,* vol. 31, pp. 283-307, 2005.

[23] J.-C. Chen, Z.-S. Liu, and J.-S. Huang, "Emission characteristics of coal combustion in different O_2/N_2, O_2/CO_2 and O_2/RFG atmosphere," *Journal of Hazardous Materials,* vol. 142, pp. 266-271, 2007.

[24] J.-C. Chen and J.-S. Huang, "Combustion Efficiency and CO_2 Emission from O_2/N_2, O_2/CO_2, and O_2/RFG Coal Combustion Processes," *Environmental Engineering Science,* vol. 24, pp. 353-362, 2007.

[25] Y. Tan, E. Croiset, M. A. Douglas, and K. V. Thambimuthu, "Combustion characteristics of coal in a mixture of oxygen and recycled flue gas," *Fuel,* vol. 85, pp. 507-512, 2006.

[26] K. Andersson and F. Johnsson, "Flame and radiation characteristics of gas-fired O_2/CO_2 combustion," *Fuel,* vol. 86, pp. 656-668, 2007.

[27] E. Kakaras, A. Koumanakos, A. Doukelis, D. Giannakopoulos, and I. Vorrias, "Oxyfuel boiler design in a lignite-fired power plant," *Fuel,* vol. 86, pp. 2144-2150, 2007.

[28] M. Anheden, J. Yan, and G. De Smedt, "Capture par oxy-combustion," *Oil & Gas Science and Technology - Rev. IFP,* vol. 60, pp. 485-495, 2005.

[29] F. Châtel-Pélage, R. Varagani, P. Pranda, N. Perrin, H. Farzan, S. J. Vecci, L. Yongqi, S. Chen, M. Rostam-Abadi, and A. C. Bose, "Applications of oxygen for NO_x control and CO_2 capture in coal-fired power plants," *Thermal Science,* vol. 10, pp. 119-142, 2006.

[30] H. Liu, R. Zailani, and B. M. Gibbs, "Comparisons of pulverized coal combustion in air and in mixtures of O_2/CO_2," *Fuel,* vol. 84, pp. 833-840, 2005.

[31] C. K. Hermsdorf, A.; Klostermann, M.; Mieske, K., "Oxyfuel Process for Hard Coal with CO_2 Capture: First results," *Fourth Nordic Minisymposium on Carbon Dioxide Capture and Storage, Otaniemi, Espoo (FI),* 2005.

[32] D. Singh, E. Croiset, P. L. Douglas, and M. A. Douglas, "Techno-economic study of CO_2 capture from an existing coal-fired power plant: MEA scrubbing vs. O_2/CO_2 recycle combustion," *Energy Conversion and Management,* vol. 44, pp. 3073-3091, 2003.

[33] X. Tan, K. Li, A. Thursfield, and I. S. Metcalfe, "Oxyfuel combustion using a catalytic ceramic membrane reactor," *Catalysis Today,* vol. 131, pp. 292-304, 2008.

[34] H. Wang, Y. Cong, and W. Yang, "Oxygen permeation study in a tubular $Ba_{0.5}Sr_{0.5}Co_{0.8}Fe_{0.2}O_{3-\hat{I}'}$ oxygen permeable membrane," *Journal of Membrane Science*, vol. 210, pp. 259-271, 2002.

[35] M. Guillodo, J. Fouletier, L. Dessemond, and P. Del Gallo, "Oxygen permeation through dense $Bi_2V_{0.9}Cu_{0.1}O_{5.35}$ ceramic membranes," *Journal of the Electrochemical Society*, vol. 149, pp. J93-J99, 2002.

[36] Z. Taheri, K. Nazari, N. Seyed-Matin, A. Safekordi, B. Ghanbari, S. Zarrinpashne, and R. Ahmadi, "Comparison of oxygen permeation through some perovskite membranes synthesized with EDTNAD," *Reaction Kinetics, Mechanisms and Catalysis*, vol. 100, pp. 459-469, 2010.

[37] X. Zhu, S. Sun, Y. Cong, and W. Yang, "Operation of perovskite membrane under vacuum and elevated pressures for high-purity oxygen production," *Journal of Membrane Science*, vol. 345, pp. 47-52, 2009.

[38] J. Xuan, M. K. H. Leung, D. Y. C. Leung, and M. Ni, "Integrating chemical kinetics with CFD modeling for autothermal reforming of biogas," *International Journal of Hydrogen Energy*, vol. 34, pp. 9076-9086, 2009.

[39] M. Coroneo, G. Montante, and A. Paglianti, "Numerical and Experimental Fluid-Dynamic Analysis To Improve the Mass Transfer Performances of Pd–Ag Membrane Modules for Hydrogen Purification," *Industrial & Engineering Chemistry Research*, vol. 49, pp. 9300-9309, 2010.

[40] S. Goto, S. Assabumrungrat, T. Tagawa, and P. Praserthdam, "The effect of direction of hydrogen permeation on the rate through a composite palladium membrane," *Journal of Membrane Science,* vol. 175, pp. 19-24, 2000.

[41] M. Coroneo, G. Montante, M. Giacinti Baschetti, and A. Paglianti, "CFD modelling of inorganic membrane modules for gas mixture separation," *Chemical Engineering Science,* vol. 64, pp. 1085-1094, 2009.

[42] v. H. Bart A, "Oxygen transfer across composite oxygen transport membranes," *Solid State Ionics,* vol. 174, pp. 253-260, 2004.

[43] W. Zhong, G. Tao, X. Li, K. Kawashima, and T. Kagawa, "Determination of flow rate characteristics of porous media using charge method," *Flow Measurement and Instrumentation,* vol. 22, pp. 201-207, 2011.

[44] L. Martínez, F. J. Florido-Díaz, A. Hernández, and P. Prádanos, "Characterisation of three hydrophobic porous membranes used in membrane distillation: Modelling and evaluation of their water vapour permeabilities," *Journal of Membrane Science,* vol. 203, pp. 15-27, 2002.

[45] E. L. Cussler, *Diffusion: Mass transfer in fluid systems*: Cambridge Univ Pr, 1997.

[46] Z. Li-Zhi, "A fractal model for gas permeation through porous membranes," *International Journal of Heat and Mass Transfer,* vol. 51, pp. 5288-5295, 2008.

[47] A. B. Shelekhin, A. G. Dixon, and Y. H. Ma, "Adsorption, permeation, and diffusion of gases in microporous membranes. II. Permeation of gases in microporous glass membranes," *Journal of Membrane Science*, vol. 75, pp. 233-244, 1992.

[48] M. L. Sawley, P. W. Cleary, and J. Ha, "Modelling of flow in porous media and resin transfer moulding using smoothed particle hydrodynamics," in *Second International Conference on CFD in the Minerals and Process Industries*, 1999, pp. 473 - 478.

[49] Q. Hou, B. Guo, L. Li, and A. Yu, "Numerical Simulation Of Gas Flow in an Electrostatic Precipitator," Dec 9-11 2009.

[50] S. Sunquist, H. Eklund, and T. Griffin, "AZEP–an EC-funded Project for Development of a CCGT Power Plant without CO_2 Emissions," 2004.

[51] S. G. Sundkvist, A. Klang, M. Sjödin, K. Wilhelmsen, K. Åsen, A. Tintinelli, S. McCahey, and H. Ye, "AZEP Gas Turbine Combined Cycle Power Plants–Thermal Optimisation and LCA Analysis," 2004.

[52] M. Simmonds, I. Miracca, and K. Gerdes, "Oxyfuel technologies for CO_2 capture: a techno-economic overview," *Proceedings of GHGT*, vol. 7, pp. 5-9, 2004.

[53] F. Beggel, S. Engels, M. Modigell, and N. Nauels, "Oxyfuel combustion by means of high temperature membranes for air separation," 2009.

[54] H. Stadler, F. Beggel, M. Habermehl, B. Persigehl, R. Kneer, M. Modigell, and P. Jeschke, "Oxyfuel coal combustion by efficient integration of oxygen transport membranes," *International Journal of Greenhouse Gas Control*, vol. 5, pp. 7-15, 2011.

[55] E. Yantovski, J. Gorski, B. Smyth, and J. ten Elshof, "Zero-emission fuel-fired power plants with ion transport membrane," *Energy*, vol. 29, pp. 2077-2088, 2004.

[56] K. Foy, "Investigation into the possible use of an oxygen ion transport membrane combustion unit in an oxyfired power plant," *Doctoral*, p. 7, 2007.

[57] S. V. Patankar, *Numerical heat transfer and fluid flow*: Hemisphere Pub, 1980.

[58] F. U. Guide, "Fluent," *Inc. Lebanon, NH*, 2007.

[59] G. Cao, "Electrical conductivity and oxygen semipermeability of terbia and yttria stabilized zirconia," *Journal of applied electrochemistry*, vol. 24, pp. 1222-1227, 1994.

[60] Y. S. Lin, W. Wang, and J. Han, "Oxygen permeation through thin mixed-conducting solid oxide membranes," *AIChE journal*, vol. 40, pp. 786-798, 1994.

[61] E. Capoen, M. C. Steil, G. Nowogrocki, M. Malys, C. Pirovano, A. Löfberg, E. Bordes-Richard, J. C. Boivin, G. Mairesse, and R. N. Vannier, "Oxygen permeation in bismuth-based materials. Part I: Sintering and oxygen permeation fluxes," *Solid State Ionics*, vol. 177, pp. 483-488, 2006.

[62] H. J. M. Bouwmeester, H. Kruidhof, A. J. Burggraaf, and P. J. Gellings, "Oxygen semipermeability of erbia-stabilized bismuth oxide," *Solid State Ionics*, vol. 53-56, Part 1, pp. 460-468, 1992.

[63] D. P. Fagg, I. P. Marozau, A. L. Shaula, V. V. Kharton, and J. R. Frade, "Oxygen permeability, thermal expansion and mixed conductivity of $Gd_xCe_{0.8-x}Pr_{0.2}O_{2-\delta}$, x=0, 0.15, 0.2," *Journal of Solid State Chemistry*, vol. 179, pp. 3347-3356, 2006.

[64] Y. Zeng and Y. S. Lin, "Oxygen permeation and oxidative coupling of methane in yttria doped bismuth oxide membrane reactor," *Journal of Catalysis*, vol. 193, pp. 58-64, 2000.

[65] J. Kim and Y. S. Lin, "Synthesis and oxygen permeation properties of ceramic-metal dual-phase membranes," *Journal of Membrane Science*, vol. 167, pp. 123-133, 2000.

[66] J. Han, Y. Zeng, and Y. S. Lin, "Oxygen permeation through fluorite-type bismuth-yttrium-copper oxide membranes," *Journal of Membrane Science*, vol. 132, pp. 235-243, 1997.

[67] Y. Nigara, J. Mizusaki, and M. Ishigame, "Measurement of oxygen permeability in CeO_2 doped CSZ," *Solid State Ionics*, vol. 79, pp. 208-211, 1995.

[68] S. Dou, C. R. Masson, and P. D. Pacey, "Mechanism of Oxygen Permeation Through Lime-Stabilized Zirconia," *Journal of the Electrochemical Society*, vol. 132, pp. 1843-1849, 1985.

[69] R. M. Thorogood, R. Srinivasan, T. F. Yee, and M. P. Drake, "Composite mixed conductor membranes for producing oxygen," ed: Google Patents, 1993.

[70] H. J. M. Bouwmeester, H. Kruidhof, and A. J. Burggraaf, "Importance of the surface exchange kinetics as rate limiting step in oxygen permeation through mixed-conducting oxides," *Solid State Ionics,* vol. 72, Part 2, pp. 185-194, 1994.

[71] J. E. ten Elshof, H. J. M. Bouwmeester, and H. Verweij, "Oxidative coupling of methane in a mixed-conducting perovskite membrane reactor," *Applied Catalysis A, General,* vol. 130, pp. 195-212, 1995.

[72] S. Kim, Y. Yang, A. Jacobson, and B. Abeles, "Oxygen Surface Exchange in Mixed Ionic Electronic Conductors," pp. pp. 31-36, 1999.

[73] S. Liu, X. Tan, Z. Shao, and J. C. Diniz da Costa, "$Ba_{0.5}Sr_{0.5}Co_{0.8}Fe_{0.2}O_{3-\delta}$ ceramic hollow-fiber membranes for oxygen permeation," *AIChE journal,* vol. 52, pp. 3452-3461, 2006.

[74] X. Tan and K. Li, "Modeling of air separation in a LSCF hollow fiber membrane module," *AIChE journal,* vol. 48, pp. 1469-1477, 2002.

[75] M. Staudacher, M. Harasek, T. Brinkmann, W. Hilgendorff, and A. Friedl, "CFD-simulation of mass transfer effects in gas and vapour permeation modules," *Desalination,* vol. 146, pp. 237-241, 2002.

[76] H. A. McGee, *Molecular engineering / Henry A. McGee, Jr.* New York :: McGraw Hill, 1991.

[77] H. Kusaba, Y. Shibata, K. Sasaki, and Y. Teraoka, "Surface effect on oxygen permeation through dense membrane of mixed-conductive LSCF perovskite-type oxide," *Solid State Ionics Solid State Ionics 15: Proceedings of the 15th International Conference on Solid State Ionics, Part II,* vol. 177, pp. 2249-2253, 2006.

[78] S. J. Xu and W. J. Thomson, "Stability of $La_{0.6}Sr_{0.4}Co_{0.2}Fe_{0.8}O_{3-\hat{I}'}$ Perovskite Membranes in Reducing and Nonreducing Environments," *Industrial & Engineering Chemistry Research Ind. Eng. Chem. Res.,* vol. 37, pp. 1290-1299, 1998.

[79] L. Mota, M. G. da Silva, V. P. de Souza, H. Vargas, V. F. Guimarães, and H. R. Paes Júnior, "On the use of photoacoustic technique for monitoring the thermal properties of lanthanum strontium cobalt ferrite–yttria stabilized zirconia two-layer systems," *Thin Solid Films,* vol. 519, pp. 938-942, 2010.

[80] H. Mei, C. Li, H. Liu, and S. Ji, "Simulation of catalytic combustion of methane in a monolith honeycomb reactor," *Chinese Journal of Chemical Engineering,* vol. 14, pp. 56-64, 2006.

[81] M. A. Habib, R. Ben-Mansour, H. M. Badr, S. F. Ahmed, and A. F. Ghoniem, "Computational fluid dynamic simulation of oxyfuel combustion in gas-fired water tube boilers," *Computers & Fluids,* vol. 56, pp. 152-165, 2012.

[82] Y. Wei, J. Tang, L. Zhou, J. Xue, Z. Li, and H. Wang, "Oxygen separation through U-shaped hollow fiber membrane using pure CO_2 as sweep gas," *AIChE journal*, 2011.

[83] A. Petric, P. Huang, and F. Tietz, "Evaluation of La–Sr–Co–Fe–O perovskites for solid oxide fuel cells and gas separation membranes," *Solid State Ionics,* vol. 135, pp. 719-725, 2000.

[84] S. Li, W. Jin, N. Xu, and J. Shi, "Synthesis and oxygen permeation properties of $La_{0.2}Sr_{0.8}Co_{0.2}Fe_{0.8}O_{3-\hat{I}'}$ membranes," *Solid State Ionics,* vol. 124, pp. 161-170, 1999.

[85] Y. Zeng, Y. S. Lin, and S. L. Swartz, "Perovskite-type ceramic membrane: synthesis, oxygen permeation and membrane reactor performance for oxidative coupling of methane," *Journal of Membrane Science,* vol. 150, pp. 87-98, 1998.

VITAE

Name	:	Shaik Pervez Ahmed
Address	:	H.No. 1-1-1002, Rayeespet, Bodhan,
		Nizamabad (District), A.P., India
Telephone	:	+966-561668791
Date of Birth	:	09-08-1987
Nationality	:	Indian
Languages known	:	English, Urdu, Hindi, Telugu and Arabic (Basic)
Contact Address	:	King Fahd University of Petroleum and Minerals
		P.O.BOX-8650, Dhahran-31261, Kingdom of Saudi Arabia
Email	:	pervez.ahmed0617@gmail.com,
		pervezahmed@kfupm.edu.sa

Education :

Master of Science (M.S.) May 2012

Mechanical Engineering Department

King Fahd University of Petroleum and Minerals, Dhahran, Saudi Arabia

Bachelor of Engineering (B.E.) May 2008

Mechanical Engineering Department

Osmania University, Hyderabad, India in 2008.